Dear Helen,

please find our revised version of the manuscript. Based on the reviewers comments we have primarily reworked the:

- histograms and the related text
- conclusion section
- method comparison section

With kind regards

Stefan on behalf of all authors

Response to the Comments

Color code:

comments of the reviewer
response by the authors
proposed changes in the manuscript

General comment:

This is an impressive and important paper and it must have been a huge task to get all the information and data together. However, the huge dimension of the task is reflected in the length of the paper and thus it is very hard to read. It is not only the length that gives a hard reading, it is also the surprisingly difficult interpretation of "relative bias" and the listing of a very large number of single features of curves that might sometimes be simply noise. Thus there is potential to shorten the paper. I will explain that in more detail below.

Otherwise, I recommend the paper for publication after consideration of the following comments.

Major comment #1:

The reader easily gets lost in all the details that the paper provides. Although the conclusion section gives a kind of summary, it is still hard to get an overview for a potential user on which data to use for which purpose. The conclusion section, however, is a good start for this. I suggest to either make lists of bullet points in the last section where information is easier to be found than in the running text, or, even better, a table mentioning advantages and disadvantages for each of the datasets, with respect to both bias and drift issues. If you dare to give recommendations, these would be welcome.

Major response #1:

A certain level of detail is clearly intended, primarily for the sake of transparency. Since we are part of an assessment we really like our results to be easily reproduced.

For an overview which data set to use we prefer the summary. In the earlier sections specific results can be only presented for one or two data sets. Which data set is considered varies. This is an attempt to give as many as possible data sets some visibility (across the different papers) and to avoid promotion of a specific data set. In the summary our approach has been to mention data sets if there is something noteworthy about them. If not, they are simply not mentioned. In that sense we clearly prefer a bullet list over a table.

The data set specific results in the summary are provided in a more structured way using bullet lists.

Major comment #2:

Isn’t there a lot of averaging in the calculation of biases, for instance? An example where I note this is Fig. 4. Coincidences are found and averaged over all seasons and over the whole latitude band that is available, sometimes 20°. Doesn’t this averaging make the results appear much better than they actually are? A good place to discuss this is in the 2nd paragraph of section 4.1.

Major response #2:

In our work we provide mean biases (see Eq. 6) to obtain general results for different combinations of time periods and latitude bands. As described in Sect. 3.3 we require at least 20 coincidences to provide reasonable estimates (other choices could be made). In that sense, yes, there is a lot of averaging involved. But to say that the results appear much better than they actually are is rather odd. Obviously individual comparisons will show smaller biases while other will exhibit larger biases. Individual comparisons are not our interest, but the combination of a bulk of them. Interesting of are course variations among the different time periods and latitude bands as presented in Fig. 9 and Fig. S8.

Major comment #3:

I understand your point that none of the two compared datasets should be ennobled as reference. But with your definition of relative bias you get some non-intuitive results that should be mentioned. First, a relative bias undershooting –100% does not imply that x_1 is negative. Instead we have

$$x_1 = \frac{2+b}{2-b} \cdot x_2$$

which unfortunately is a quite non-linear function. For instance we get $x_1 = x_2/3$ at a bias of –100%, $x_1 = x_2/2$ at $b = -2/3$, and $x_1 = 3 \cdot x_2$ at a bias of +100%. In effect, the fair comparison comes at the price of a non-linear and not easily comprehensible relative bias measure. To my impression, all the relative biases given in the paper easily mislead the reader (and perhaps the authors as well). For instance, in line 8 on page 16 you say "biases ... even exceed ... ±100% in some occasions", which implies that x_1 either undershoots $x_2/3$ or exceeds $3 \cdot x_2$. Is this really what you have intended to say?

Major response #3:

In fact, this was not our thinking or mind set. If you do an evaluation for single data set then often the data set itself is used as reference. Here we compare a whole matrix of data set combinations. For the relative bias we had multiple options what to be used as reference. For example it could be always the first data set in a comparison, the second data set or the mean among the data sets. We decided to use the mean among the data sets. Besides avoiding any preference of a reference data set this has also practical advantages:

(a) we do not need to know which data set is used as reference in a specific comparison

(b) we do not need to deal with questions regarding the reference when comparing A vs. B or B vs. A (with possible asymmetries)

Given our choice the relative bias is only comprehensible for what it is, i.e. a difference of two data sets about their mean, not data set #1 nor data set #2.

Trying to relating it to data set #1 or data set #2 seems not meaningful nor appropriate. Of course the results for the other reference choices could be calculated. This is however a major effort at this point, let alone integrating the results side by side.

We further motivate our choice and note the non-linearity aspect that was brought up here.

Major comment #4:

Page 16, lines 9 to 33: There is a quite detailed description of minor wiggles, local maxima and minima, of the summary bias curves (rhs of Figure 5). Are you sure that these wiggles are physically significant? That is, is there a physical argument that, for instance, the 50% percentile profile minimises at 60 hPa, or isn't this rather incidentally given the sensors that you have in your comparison data base. The non-aggregated line displays different wiggles and it seems to me that you describe noise.

Major response #4:

It will always be a combination of the data sets involved and physics. The relative importance of these aspects will vary depending on the considered percentile. For the 95% percentile the specific set of data sets considered will certainly have a larger importance than physics.

To provide a more quantitative statement how these percentiles vary we have applied a jackknife approach. Randomly we leave out five data sets and recalculate the percentiles. We repeat this until every data set has been left out at least once. For a given percentile we have then a set of different realisations (typically 25 for the non-aggregated data and a dozen for the aggregated data) from which a standard deviation can calculated. One result is shown in the figure below.

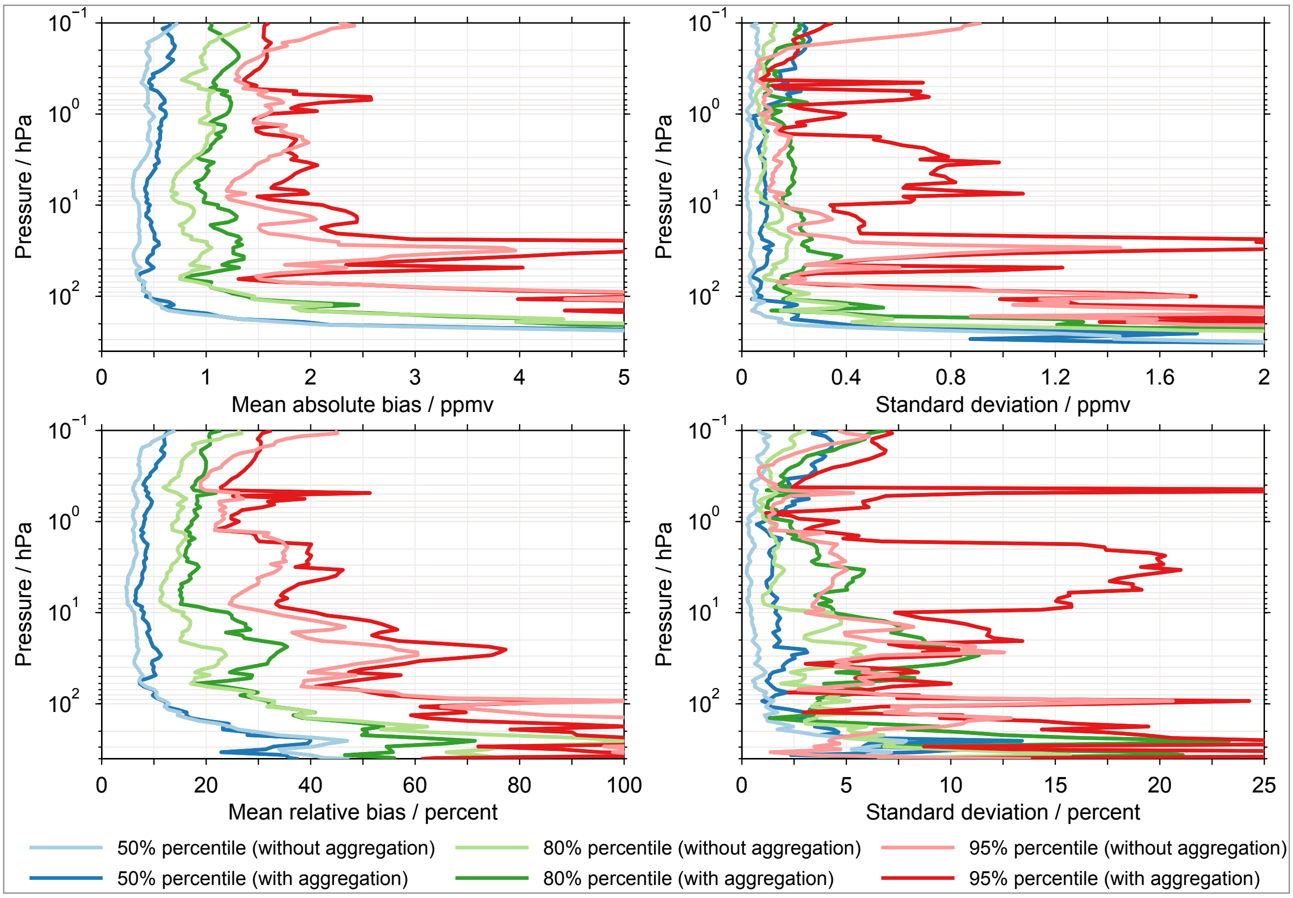

For the 50% percentile the standard deviations are around 0.05 ppmv (1%) without the aggregation of the MIPAS results. With this aggregation the standard deviations are typically twice as large in the stratosphere. Close to 0.1 hPa standard deviations around 0.25 ppmv (4%) are observed. For the 80% percentile the standard deviations amount roughly to 0.1 ppmv (1% - 5%) and 0.2 ppmv (2% - 10%) without and with the aggregation of the MIPAS results, respectively. For the 95% percentile the standard deviations vary typically between 0.05 ppmv and 0.5 ppmv (2% - 10%) when no aggregation of the MIPAS results is considered. If the aggregation is taken account a larger variation is observed with peak values exceeding 1 ppmv (20%). Given the random approach many realisations are possible. The general picture is very similar. The largest variations are visible for 95% percentile.

The results presented here are briefly noted in the manuscript.

Major comment #5:

Histograms: I doubt that showing and discussing these histograms is of any value. The reader generally wants to know whether a certain data set can be used for an application, that is, whether it has a small bias and low drift in a given altitude (and latitude etc.) region. Perhaps it is important then to have more than one dataset at hand for estimates of uncertainties. But it is not clear to me which purpose the knowledge of these histograms should serve. What, in a concrete situation as sketched, is the gain one has from knowing that the distribution of drift values over 33 data sets peaks in a certain bin? I find this discussion unnecessary and it can be removed without any intellectual loss to the paper.

Furthermore, there are technical issues with the histograms. For instance, the histogram of figure 12 contains about 60 bins which is not ideal. There are several rules for an optimal number of bins, and the result in this case is of the order 15. Consequently there is much noise in the curves and it is not clear whether a single peak as the one described in line 4 on page 22 is real or just noise. A similar comment applies to figure 7, but the curves are much smoother there.

Deleting the histograms and the corresponding text would also have the advantage of getting rid of the unnecessary speculation whether these look Gaussian or not. My impression is, they do not, but my feeling is also that this an irrelevant point. Whether these distributions are Gaussian or not is not used anywhere in the paper as the basis of an argument.

Major response #5:

The histograms are presented in a section that focuses on general results. Employing here arguments that emphasise specific data set characteristics does not feel appropriate. We simply had no preconception how such histograms would look like. Also, we wanted to provide another representation of the biases that exist in the observational database, especially comparing the occurrence rate of a given bias as function of latitude band. This is clearly something that is interesting for other multi-data set comparisons, may it be among satellite data sets, model simulations or a combination of both. We definitely strongly argue against their removal.

In terms of the technical comments we agree the number of bins that used can be reduced. We estimated the number of bins with several rules, i.e. Rice's rule, Scott's rule, Freedman and Diaconis's rule as well as Doane's rule. This was not ultimately helpful. For the bias data (Fig. 7) we found range between 10 to 50 bins depending on rule, number of data points as well the standard deviation or interquartile range of the data. We decided for 0.1 ppmv (0.05 ppmv before) bins for the absolute bias and 2% (1% before) for the relative bias. For the drift data (Fig. 12) the different rules yield a similar picture. In this case we decided for 0.1 ppmv/decade bin (0.05 ppmv/decade before).

There is not so much speculation whether these histograms are Gaussian or not. We fitted a Gaussian function to the histograms, but decided not to show these results to keep number of lines to a reasonable level. Arguably the fits are better at larger biases/drifts than at lower values. We decided to remove this argumentation.

The histograms are recalculated and all related text is adapted. The argumentation on the Gaussian shape of the histograms is removed.

Major comment #6:

Section 5.4: While it is certainly necessary to compare the methods of drift determination between the current paper and that of Khosrawi et al., I doubt whether it is useful to spend so many lines of text to it and to dwell on so many details. Looking at the corresponding figures, it is evident that the two methods yield essentially consistent results. There are only a handful of exceptions with drift estimates exceeding 2σ. Instead of quoting all the boring numbers (e.g. σ is not much larger than 2, namely 2.01) it would be more useful to think about the possible reasons why the two methods differ for certain data set combinations more than for others. A more fundamental question is whether such differences are generally expected at all and whether a significant deviation is a surprise or not. To my opinion, this section should be rewritten or drastically shortened.

Major response #6:

Also in this case we had no real preconceptions how similar or how different the drift estimates derived from the two approaches would be. It was probably a surprise that so few statistically significant differences exist. We agree to reduce the amount of detail that has been spent on describing the figures. In addition, we performed more analyses, trying to find any prominent behaviour. The differences among the drift estimates from the two approaches are on average largest for comparisons among sparse data sets (i.e. ACE-FTS, GOMOS, HALOE MAESTRO, POAM, SAGE, SCIAMACHY occultation and SOFIE) and smallest for comparisons among dense data sets (HIRDLS, MIPAS, MLS, SCIAMACHY limb, SMR). At the same time the percentage of significant differences in the drift estimates is smallest for comparisons between sparse data sets and largest for comparisons between dense data sets. Comparisons between dense and sparse data sets yield statistics in the middle. This behaviour is intuitive, but the numbers also support this relation in reality.

The detailed description of Figs. 15 and 16 is shortened. The results from the additional analyses described here shortly will be added.

Minor issue #1:

It is a problem that a paper by Walker and Stiller is quite often quoted, which is still in preparation. The reader has no possibility to consult it and does not know when and in which Journal this will eventually become possible. Are there perhaps other "grey" sources of information that may at least partly replace the "in preparation" paper?

Minor response #1:

Within the WAVAS-II activity is was decided to have such data set overview paper to avoid describing the data set all over again and to have a central reference. Critically, we have to admit that this should have been one of the first papers, but it will be one of the last instead. The following publications (certainly not a complete list) are of relevance:

(1) Azam et al. (2012)

(2) Carleer et al. (2008)

(3) Dinelli et al. (2010)

(4) Eriksson et al. (2014)

(5) Gille et al. (2013)

(6) Griesfeller et al. (2008)

(7) Hegglin et al. (2013)

(8) Kley et al. (2000)

(9) Livesey et al. (2015)

(10) Lumpe et al. (2006)

(11) Montoux et al. (2009)

(12) Noël et al. (2010)

(13) Raspollini et al. (2013)

(14) Rong et al. (2010)

(15) Sioris et al. (2016)

(16) Taha et al. (2004)

(17) Thomason et al. (2010)

(18) von Clarmann et al. (2009)

(19) Weigel et al. (2016)

(20) Urban et al. (2007)

The full references are provided at the end of this document.

Minor issue #2:

Page 3, lines 6-14: it would be nice to have an indication of the relative contribution of each pathway to WV transport into the tropical stratosphere. The sentence "about 3.5 ppmv to 4.0 ppmv of water vapour enter the stratosphere" is not understandable. I expect to read something like "per year a total mass of x kilogram of water vapour enters the stratosphere".

Minor response #2:

Currently we cannot give exact numbers on the relative importance of the different pathways contributing to the transport of water vapour from the troposphere to the stratosphere. This is an important topic of ongoing research. Slow ascent certainly plays the most important role and the relative importance will vary throughout the year.

The 3.5 ppmv to 4.0 ppmv describe the typical entry mixing ratio of water vapour in the tropical stratosphere (averaged over a year). This is a common notion. Of course we could provide a total mass in kilogramme, however this would quite unusual in this context and especially when it comes to satellite observations.

The text is changed to: “Overall, the stratospheric entry mixing ratios typically amount to 3.5 ppmv to 4.0 ppmv, on an annual average (Kley et al., 2000).”

Minor issue #3:

Page 6, line 16: I am surprised that mixing ratios between –20 and zero are not excluded. Please explain.

Minor response #3:

Negative volume mixing ratios can occur due to noise in the observations which propagates through the retrievals. As such, this is an important information that should not be removed. In addition, screening these negative values can create biases that are not correct.

Minor issue #4:

Page 7, lines 16 ff: I have only a vague feeling why comparing A to B might give coincidences different from comparing B to A. Perhaps this can be explained a bit clearer. I assume that the "lower half of the comparison matrix" contains just the coincidences of A to B. What then do you mean with "we used those results for the upper half of the matrix"? What does this upper half contain if not the B to A coincidences and in which way can the A to B results be used for the B to A comparisons? And finally, what are the "lower boundaries of the comparisons"?

Minor response #4:

The sketch below provides a simple example of different coincidences for comparisons A vs. B and B vs. A. As described in the manuscript the data sets sorted chronologically. For the comparison A vs. B we go through the individual observations of A (here described by the subscripts 1 to 4) and try to find observations of B that fulfil the coincidence criteria. For observation A_1 only one coincidence is found, namely B_1 (marked by the solid arrow). Next in line is observation A_2. In this case three coincident observations of B are found. In this case we chose the observations closest in space as coincidence, which is here B_3. For the observations A_3 and A_4 no coincident observations of B are found. Overall, we find two coincidences for this simple comparison: A_1 vs. B_1 and A_2 vs. B_3. When B vs. A is compared the observations B_1 and A_1 are coincident again. For observation B_2 only A_2 is found as coincidence. Next is observation B_3. In this case also observation A_2 fulfils the coincidence criteria. However since A_2 was already considered as a coincidence (to B_2) it is not further considered (marked by the dotted line). This is what we denote in the manuscript as the unique coincidence approach (i.e. no observation is used twice in a comparison). For observation B_4 there is the same situation as for B_3. Overall, we also find two coincidences for the comparison B vs. A: B_1 vs. A_1 and B_2 vs. A_2. However, they are different than for A vs. B. In general, not only the exact coincidences can be different, but also their absolute number.

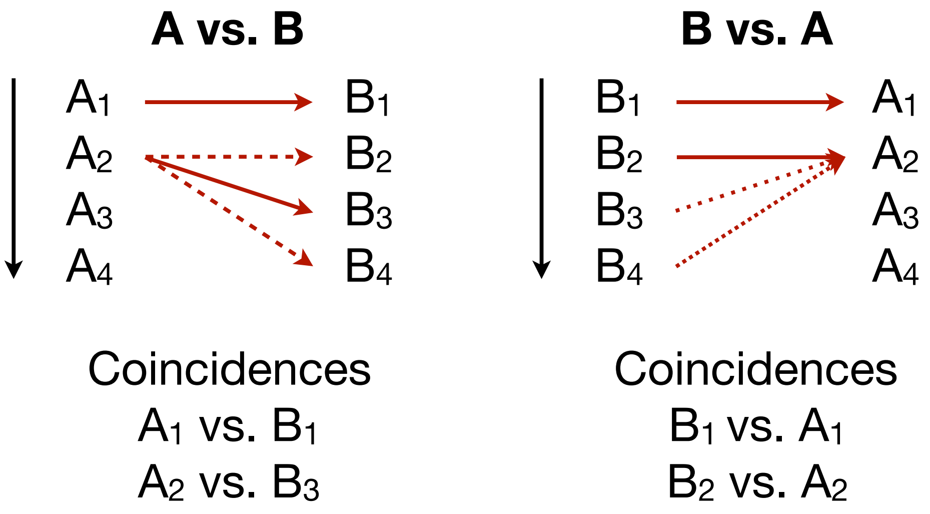

Regarding the lower and upper half of the comparison matrix an example is given below considering four data sets A, B, C and D. We have only performed comparison in the lower half of matrix, here marked in blue. For the upper half, here marked in red, we used the results from the lower half, but of course with the opposite sign.

x	A	B	C	D
A	**x**	-(A - B)	-(A - C)	-(A - D)
B	A - B	**x**	-(B - C)	-(B - D)
C	A - C	B - C	**x**	-(C - D)
D	A - D	B - D	C - D	**x**

The term “lower boundaries of the comparisons” is supposed to described the lowermost altitudes where comparisons were possible.

The text is changed to: “Larger deviations were mostly found at the lower altitude limits of the comparisons.”

Minor issue #5:

Page 8, line 1: in which respect is the coverage of the hygropause limited? I don’t understand what you mean.

Minor response #5:

The data sets in question have all their lower altitude limit (where reasonable retrievals are possible) close to the hygropause. In that sense the observational coverage is meant. Some retrieved profiles will cover the hygropause, others not.

The text is changed to: “In the table columns some data sets have been marked by an asterisk, indicating that these data sets have a limited observational coverage of the hygropause. Some retrieved profiles will include the hygropause, others not. Hence, some comparisons to these data sets may not necessarily need the consideration of differences in the vertical resolution in this altitude range.”

Minor issue #6:

Eq. 1: I wonder why the vectors x_{high} and x_{apriori} have the same number of components although x_{high} refers to high resolution (i.e. more values) while x_{apriori} refers to low resolution (less values).

Minor response #6:

The relation that is indicated here does not need to exist. Results with low vertical resolution can be retrieved on a fine grid (corresponding to more values). Prominent examples are the MIPAS data sets retrieved with the IMKIAA processor. The retrieval uses a fixed 1 km grid through most of the stratosphere while the vertical resolution varies between 3 km and 5 km. As described by Eqs. 1 and 2 the convolution is performed on the grid of the lower resolved data set. Regridding the high resolved data set to the grid of the lower resolved data set follows the work of Stiller et al. (2012).

The approach to regrid the high resolved data set to the grid of the lower resolved data is mentioned.

Minor issue #7:

Page 9, line 25: the following is not an equation, please replace "equation" with "quantity".

Minor response #7:

Okay.

The text is changed accordingly.

Minor issue #8:

Eq. 5: Why do you need the factor 4 ln(2) under the exp?

Minor response #8:

The starting point is the basic Gauss function:

$$\mathbf{G(x,\mu,\sigma) = \exp\left\{-\frac{[x-\mu]^2}{2\cdot\sigma^2}\right\}}$$

In our case we have substituted the vector $\mathbf{x}$ with the altitude vector $\mathbf{z}$. The average μ is used as the specific altitude for which the kernel is created, i.e. $\mathbf{z}(j)$. Furthermore we consider the altitude resolution $\mathbf{dz}(j)$ (i.e. full width at half maximum) at the specific altitude instead of the standard deviation σ. This gives:

$$\mathbf{G}[\mathbf{z},\mathbf{z}(j),\sigma] = \exp\left\{-\frac{[\mathbf{z}-\mathbf{z}(j)]^2}{2\cdot\sigma^2}\right\} \quad \text{with}$$

$$\sigma = \frac{\mathbf{dz}(j)}{2\cdot\sqrt{2\cdot ln(2)}} \quad \text{or} \quad \sigma^2 = \frac{\mathbf{dz}(j)^2}{8\cdot ln(2)} \quad \text{yields}$$

$$\mathbf{G}[\mathbf{z},\mathbf{z}(j),\mathbf{dz}(j)] = \exp\left\{-\frac{4\cdot\ln(2)\cdot[\mathbf{z}-\mathbf{z}(j)]^2}{\mathbf{dz}(j)^2}\right\}$$

Minor issue #9:

Page 10, beginning of section 3.3: I suggest to write "time period" instead of "time" and "latitude band" instead of "latitude". I was puzzled by assuming that t is a point in time and ϕ is a certain latitude and then reading in Eq. 6 that there can be more than one, namely $n_c(t,\phi,z)$measurements for this point. Later it gets clear, but it is better if it is clear right from the beginning.

Minor response #9:

We agree.

The text is adapted accordingly.

Minor issue #10:

Section 3.4: you say f(...) is the regressed bias time series. Before, we had b(...) as the bias between two data sets. Unfortunately, it is not very clear to me what the relation is between f(...) and b(...). Probably there is one and it would be good to know it.

Minor response #10:

$f(t,\phi,z)$ and $\overline{b}(t,\phi,z)$ are of course related. $f(t,\phi,z)$ represents the fit of regressed time series of $\overline{b}(t,\phi,z)$, however in this case t describes not a specific season or the entire year but all months which the data sets compared have sufficient overlap (i.e. at least 5 coincidences, see Sect. 3.4). We do not want to change the regression equation as it has been used in different WAVAS publications, avoiding the creation of any unnecessary inconsistency.

The text is changed to: "In the equation $f(t,\phi,z)$ represents the fit of the regressed bias time series $\overline{b}(t,\phi,z)$, however here t describes all months where the data sets that are compared have sufficient overlap (i.e. 5 coincidences, see above)."

Minor issue #11:

Page 13, line 16: "comparison results ... are not considered any further". Is this really meant or rather "... are not used for other calculations"? To me, it sounds useless to compute something that is not considered further.

Minor response #11:

The comparison results among the MIPAS data sets are only used the non-aggregated results. For the aggregated results they are not used, as the aggregation treats the MIPAS data sets as if they were only one data set. Accordingly, the comparisons among them are not relevant.

The text is changed to: "comparison results between different MIPAS data sets are not considered (in the calculation of the aggregated quantities)".

Minor issue #12:

Page 13, line 27: figures (plural).

Minor response #12:

Thanks!

The text is changed accordingly.

Minor issue #13:

Page 14, line 8: "this has not further been pursued".

Minor response #13:

Done.

The text is changed accordingly.

Minor issue #14:

Page 16, line 11/12: This is not surprising, as this variation is controlled by a smaller and smaller number of outliers.

Minor response #14:

We totally agree, it just describes the observation.

Minor issue #15:

Page 17, line 11: "within a small altitude range". Actually, this may be a small range in pressure, but certainly quite a large distance in altitude. Please correct.

Minor response #15:

Yes, this could be misleading.

The phrase is removed.

Minor issue #16:

Fig. 7, right panel: Note that 1% bins are of unequal size in terms of actual differences between x_1 and x_2. This results from the non-linear character of your bias definition, cf. comment above.

Minor response #16:

Please see our major response #3.

Minor issue #17:

Page 18, line 25: "in the right columns”.

Minor response #17:

Okay.

The word “right” is added and “columns” is corrected to “column”.

Minor issue #18:

Page 18, line 27: "contributing to" and "results are based on the aggregation".

Okay.

The first part is changed accordingly. The second part is added but just with parentheses.

Minor issue #19:

Figure 10: Please provide for the sake of completeness the mathematical definition of σ. How is it computed for the present application? This should fit after eq. 9.

Minor response #19:

Okay.

The equation is provided at the end of section 3.4.

Minor issue #20:

Figure 11: I wonder why the smaller (blue lines) drifts are statistically significant whereas the larger (grey) ones are not.

Minor response #20:

These cases can actually be attributed to specific data sets. Throughout the stratosphere this concerns comparisons to the GOMOS data set. This data set exhibits a low precision, resulting both in large drift and associated uncertainty estimates. In the lower stratosphere, such behaviour occurs in a significantly increased manner also in comparisons to the HIRDLS, MAESTRO and SMR 544 GHz data sets. All three data sets have their upper vertical limit in this altitude region where they exhibit increased uncertainties.

Minor issue #21:

Page 24, line 25: is this really from top to bottom? The figure (15) says the opposite. Please check.

Minor response #21:

This is a typo. Thank you for spotting!

The text is corrected.

Minor issue #22:

Page 27, line 9: please rewrite the sentence. The impression of drifting data sets is surely not what is intended here.

Minor response #22:

This is certainly an unfortunate expression.

It is removed in the rework of the conclusion as described in the major response #1.

References

Azam, F., Bramstedt, K., Rozanov, A., Weigel, K., Bovensmann, H., Stiller, G. P., and Burrows, J. P.: SCIAMACHY lunar occultation water vapor measurements: retrieval and validation results, Atmospheric Measurement Techniques, 5, 2499 – 2513, https://doi.org/10.5194/amt-5-2499-2012, 2012.

Carleer, M. R., Boone, C. D., Walker, K. A., Bernath, P. F., Strong, K., Sica, R. J., Randall, C. E., Vömel, H., Kar, J., Höpfner, M., Milz, M., von Clarmann, T., Kivi, R., Valverde-Canossa, J., Sioris, C. E., Izawa, M. R. M., Dupuy, E., McElroy, C. T., Drummond, J. R., Nowlan, C. R., Zou, J., Nichitiu, F., Lossow, S., Urban, J., Murtagh, D. P., and Dufour, D. G.: Validation of water vapour profiles from the Atmospheric Chemistry Experiment (ACE), Atmospheric Chemistry & Physics Discussions, 8, 4499 – 4559, 2008.

Dinelli, B. M., Arnone, E., Brizzi, G., Carlotti, M., Castelli, E., Magnani, L., Papandrea, E., Prevedelli, M., and Ridolfi, M.: The MIPAS2D database of MIPAS/ENVISAT measurements retrieved with a multi-target 2-dimensional tomographic approach, Atmospheric Measurement Techniques, 3, 355 – 374, 2010.

Eriksson, P., Rydberg, B., Sagawa, H., Johnston, M. S., and Kasai, Y.: Overview and sample applications of SMILES and Odin-SMR retrievals of upper tropospheric humidity and cloud ice mass, Atmospheric Chemistry & Physics, 14, 12613 – 12629, https://doi.org/10.5194/acp-14-12613-2014, 2014.

Gille, J., Grey, L., Cavanaugh, C., Coffey, M., Dean, V., Halvorson, C., Karol, S., Khosravi, R., Kinnison, D., Massie, S., Nardi, B., Rivas, M. B., , Smith, L., Torpy, B., Waterfall, A., and Wright, C.: HIRDLS data description and quality version 7, http://docserver.gesdisc.eosdis.nasa.gov/repository/Mission/HIRDLS/3.3_Product_Documentation/3.3.5_Product_Quality/HIRDLS-DQD_V7.pdf, Last access: 17 January 2018, 2013.

Griesfeller, A., von Clarmann, T., Griesfeller, J., Höpfner, M., Milz, M., Nakajima, H., Steck, T., Sugita, T., Tanaka, T., and Yokota, T.: Intercomparison of ILAS-II version 1.4 and version 2 target parameters with MIPAS-Envisat measurements, Atmospheric Chemistry & Physics, 8, 825 – 843, 2008.

Hegglin, M. I., Tegtmeier, S., Anderson, J., Froidevaux, L., Fuller, R., Funke, B., Jones, A., Lingenfelser, G., Lumpe, J., Pendlebury, D., Remsberg, E., Rozanov, A., Toohey, M., Urban, J., Clarmann, T., Walker, K. A., Wang, R., and Weigel, K.: SPARC Data Initiative: Comparison of water vapor climatologies from international satellite limb sounders, Journal of Geophysical Research, 118, 11 824, https://doi.org/10.1002/jgrd. 50752, 2013.

Kley, D., Russell, J. M., and Philips, C.: Stratospheric Processes and their Role in Climate (SPARC) - Assessment of upper tropospheric and stratospheric water vapour, SPARC Report 2, WMO/ICSU/IOC World Climate Research Programme, Geneva, 2000.

Livesey, N. J., Read, W. J., Wagner, P. A., Froidevaux, L., Lambert, A., Manney, G. L., Millan, L. F., Pumphrey, H. C., Santee, M. L., Schwartz, M. J., Wang, S., Fuller, R. A., Jarnot, R. F., Knosp, B. W., , and Martinez, E.: Aura/MLS version 4.2x level 2 data quality and description document, http://mls.jpl.nasa.gov/data/v4-2_data_ quality_document.pdf, Last access: 18 August 2017, 2015.

Lumpe, J., Bevilacqua, R., Randall, C., Nedoluha, G., Hoppel, K., Russell, J. M., Harvey, V. L., Schiller, C., Sen, B., Taha, G., Toon, G., and Vömel, H.: Validation of Polar Ozone and Aerosol Measurement (POAM) III version 4 stratospheric water vapor, Journal of Geophysical Research, 111, 11 301, https://doi.org/10.1029/2005JD006763, 2006.

Montoux, N., Hauchecorne, A., Pommereau, J.-P., Lefêvre, F., Durry, G., Jones, R. L., Rozanov, A., Dhomse, S., Burrows, J. P., Morel, B., and Bencherif, H.: Evaluation of balloon and satellite water vapour measurements in the Southern tropical and subtropical UTLS during the HIBISCUS campaign, Atmospheric Chemistry & Physics, 9, 5299 – 5319, 2009.

No¨el, S., Bramstedt, K., Rozanov, A., Bovensmann, H., and Burrows, J. P.: Water vapour profiles from SCIAMACHY solar occultation measurements derived with an onion peeling approach, Atmospheric Measurement Techniques, 3, 523 – 535, 2010.

Raspollini, P., Carli, B., Carlotti, M., Ceccherini, S., Dehn, A., Dinelli, B. M., Dudhia, A., Flaud, J.-M., López-Puertas, M., Niro, F., Remedios, J. J., Ridolfi, M., Sembhi, H., Sgheri, L., and von Clarmann, T.: Ten years of MIPAS measurements with ESA Level 2 processor V6 - Part 1: Retrieval algorithm and diagnostics of the products, Atmospheric Measurement Techniques, 6, 2419 – 2439, https://doi.org/10.5194/amt-6-2419-2013, 2013.

Rong, P., Russell, J. M., Gordley, L. L., Hervig, M. E., Deaver, L., Bernath, P. F., and Walker, K. A.: Validation of v1.022 mesospheric water vapor observed by the SOFIE instrument on the AIM Satellite, Journal of Geophysical Research, 115, D16 209, https://doi.org/10.1029/2010JD013852, 2010.

Sioris, C. E., Zou, J., Plummer, D. A., Boone, C. D., McElroy, C. T., Sheese, P. E., Moeini, O., and Bernath, P. F.: Upper tropospheric water vapour variability at high latitudes - Part 1: Influence of the annular modes, Atmospheric Chemistry & Physics, 16, 3265 – 3278, https://doi.org/10.5194/acp-16-3265-2016, 2016.

Stiller, G. P., Kiefer, M., Eckert, E., von Clarmann, T., Kellmann, S., García-Comas, M., Funke, B., Leblanc, T., Fetzer, E., Froidevaux, L., Gomez, M., Hall, E., Hurst, D., Jordan, A., Kämpfer, N., Lambert, A., McDermid, I. S., McGee, T., Miloshevich, L., Nedoluha, G., Read, W., Schneider, M., Schwartz, M., Straub, C., Toon, G., Twigg, L. W., Walker, K., and Whiteman, D. N.: Validation of MIPAS IMK/IAA temperature, water vapor, and ozone profiles with MOHAVE-2009 campaign measurements, Atmospheric Measurement Techniques, 5, 289 – 320, https://doi.org/ 10.5194/amt-5-289-2012, 2012.

Taha, G., Thomason, L. W., and Burton, S. P.: Comparison of Stratospheric Aerosol and Gas Experiment (SAGE) II version 6.2 water vapor with balloon-borne and space- based instruments, Journal of Geophysical Research, 109, D18313, https://doi.org/ 10.1029/2004JD004859, 2004.

Thomason, L. W., Moore, J. R., Pitts, M. C., Zawodny, J. M., and Chiou, E. W.: An evaluation of the SAGE III version 4 aerosol extinction coefficient and water vapor data products, Atmospheric Chemistry & Physics, 10, 2159 – 2173, 2010.

Urban, J., Lautie, N., Murtagh, D. P., Eriksson, P., Kasai, Y., Lossow, S., Dupuy, E., de La Nöe, J., Frisk, U., Olberg, M., Le Flochmöen, E., and Ricaud, P.: Global observations of middle atmospheric water vapour by the Odin satellite: An overview, Planetary and Space Science, 55, 1093 – 1102, https://doi.org/ 10.1016/j.pss.2006.11.021, 2007.

von Clarmann, T., Höpfner, M., Kellmann, S., Linden, A., Chauhan, S., Funke, B., Grabowski, U., Glatthor, N., Kiefer, M., Schieferdecker, T., Stiller, G. P., and Versick, S.: Retrieval of temperature, H_2O, O_3, HNO_3, CH_4, N_2O, $ClONO_2$ and ClO from MIPAS reduced resolution nominal mode limb emission measurements, Atmospheric Measurement Techniques, 2, 159 – 175, 2009.

Weigel, K., Rozanov, A., Azam, F., Bramstedt, K., Damadeo, R., Eichmann, K.-U., Gebhardt, C., Hurst, D., Kraemer, M., Lossow, S., Read, W., Spelten, N., Stiller, G. P., Walker, K. A., Weber, M., Bovensmann, H., and Burrows, J. P.: UTLS water vapour from SCIAMACHY limb measurements V3.01 (2002-2012), Atmospheric Measurement Techniques, 9, 133 – 158, https://doi.org/10.5194/ amt-9-133-2016, 2016.

Response to the Comments

Color code:

comments of the reviewer
response by the authors
proposed changes in the manuscript

General comment:

The paper has an impressive author list and I am sure that the results are worthwhile to publish. But in my mind the pdf-format is not a best way to publish figures including an impenetrable jungle of line plots. You would need a shorter summary in pdf and then an interactive web-page where you could extract detailed results.

General response:

Certainly interactive figures would be a better way to present the data. There are even technologies to include interactive features in PDF files, e.g. U3D (see https://en.wikipedia.org/wiki/Universal_3D). However, since Copernicus does not support such interactive PDF files this is no solution. To set up a website with interactive figures can be achieved with reasonable effort. But, also such a website cannot act as an official part of a Copernicus publication. It can only be a supplement, not a replacement.

A shorter summary is very difficult to achieve. We attempt to do justice to 33 data sets, resulting not only literally in a million figures. How to condense all this information into a sustainable amount has been part of many and quite sustained discussions within the WAVAS-II core team. We are always open to new ideas. Since the critique here is rather vague we opt to work with the comments that the other reviewer provided on this topic.

Shortening of Sect. 5.4.

The SPARC water vapour assessment II: Profile-to-profile comparisons of stratospheric and lower mesospheric water vapour data sets obtained from satellites

Stefan Lossow[1], Farahnaz Khosrawi[1], Michael Kiefer[1], Kaley A. Walker[2], Jean-Loup Bertaux[3], Laurent Blanot[4], James M. Russell[5], Ellis E. Remsberg[6], John C. Gille[7,8], Takafumi Sugita[9], Christopher E. Sioris[10], Bianca M. Dinelli[11], Enzo Papandrea[11,12], Piera Raspollini[13], Maya García-Comas[14], Gabriele P. Stiller[1], Thomas von Clarmann[1], Anu Dudhia[15], William G. Read[16], Gerald E. Nedoluha[17], Robert P. Damadeo[6], Joseph M. Zawodny[6], Katja Weigel[18], Alexei Rozanov[18], Faiza Azam[18], Klaus Bramstedt[18], Stefan Noël[18], John P. Burrows[18], Hideo Sagawa[19], Yasuko Kasai[20], Joachim Urban[21†], Patrick Eriksson[21], Donal P. Murtagh[21], Mark E. Hervig[22], Charlotta Högberg[23], Dale F. Hurst[24], and Karen H. Rosenlof[24]

[1]Karlsruhe Institute of Technology, Institute of Meteorology and Climate Research, Hermann-von-Helmholtz-Platz 1, 76344 Leopoldshafen, Germany.
[2]University of Toronto, Department of Physics, 60 St. George Street, Toronto, ON M5S 1A7, Canada.
[3]LATMOS, CNRS/UVSQ/IPSL, Quartier des Garennes, 11 Boulevard d'Alembert, 78280 Guyancourt, France.
[4]ACRI-ST, 260 Route du Pin Montard, 06904 Sophia-Antipolis Cedex, France.
[5]Hampton University, Center for Atmospheric Sciences, 23 Tyler Street, Hampton, VA 23669, USA.
[6]NASA Langley Research Center, 21 Langley Boulevard, Hampton, VA 23681, USA.
[7]National Center for Atmospheric Research, Atmospheric Chemistry Observations & Modeling Laboratory, P.O. Box 3000, Boulder, CO 80307-3000, USA.
[8] University of Colorado, Atmospheric and Oceanic Sciences, Boulder, CO 80309-0311, USA.
[9]National Institute for Environmental Studies, Center for Global Environmental Research, 16-2 Onogawa, Tsukuba, Ibaraki 305-8506, Japan.
[10]Environment and Climate Change Canada, 4905 Dufferin Street, Toronto, ON M3H 5T4, Canada.
[11]Istituto di Scienze dell'Atmosfera e del Clima del Consiglio Nazionale delle Ricerche (ISAC-CNR), Via Gobetti, 101, 40129 Bologna, Italy.
[12]Serco SpA, Via Sciadonna, 24–26, 00044 Frascati, Italy.
[13]Istituto di Fisica Applicata del Consiglio Nazionale delle Ricerche (IFAC-CNR), Via Madonna del Piano, 10, 50019 Sesto Fiorentino, Italy.
[14]Instituto de Astrofísica de Andalucía (IAA-CSIC), Glorieta de la Astronomía, 18008 Granada, Spain.
[15]University of Oxford, Atmospheric Physics, Clarendon Laboratory, Parks Road, Oxford OX1 3PU, United Kingdom of Great Britain and Northern Ireland.
[16]Jet Propulsion Laboratory, 4800 Oak Grove Drive, Pasadena, CA 91109, USA.
[17]Naval Research Laboratory, Remote Sensing Division, 4555 Overlook Avenue Southwest, Washington, DC 20375, USA.
[18]University of Bremen, Institute of Environmental Physics, Otto-Hahn-Allee 1, 28334 Bremen, Germany.
[19]Kyoto Sangyo University, Faculty of Science, Motoyama, Kamigamo, Kita-ku, Kyoto 603-8555, Japan.
[20]National Institute of Information and Communications Technology (NICT), 20 THz Research Center, 4-2-1 Nukui-kita, Koganei, Tokyo 184-8795, Japan.
[21]Chalmers University of Technology, Department of Space, Earth and Environment, Hörsalsvägen 11, 41296 Göteborg, Sweden.
[22]GATS Inc., 65 South Main Street #5, Driggs, ID 83442, USA.
[23]Stockholm University, Department of Physical Geography, Svante-Arrhenius-väg 8, 10691 Stockholm, Sweden.

[24]NOAA Earth System Research Laboratory, Global Monitoring Division, 325 Broadway, Boulder, CO 80305, USA.
[†]deceased on 14 August 2014

Correspondence: Stefan Lossow (stefan.lossow@kit.edu)

Version: Saturday 9th March, 2019 13:30 CET

Abstract. Within the framework of the second SPARC (Stratosphere-troposphere Processes And their Role in Climate) water vapour assessment (WAVAS-II), profile-to-profile comparisons of stratospheric and lower mesospheric water vapour were performed considering 33 data sets derived from satellite observations of 15 different instruments. These comparisons aimed to provide a picture of the typical biases and drifts in the observational database and to identify data set specific problems. The observational database typically exhibits the largest biases below 70 hPa, both in absolute and relative terms. The smallest biases are often found between 50 hPa and 5 hPa. Typically, they range from 0.25 ppmv to 0.5 ppmv (5% to 10%) in this altitude region, based on the 50% percentile over the different comparison results. Higher up, the biases are overall increasing with altitude but this general behaviour is accompanied by considerable variations. Characteristic values vary between 0.3 ppmv and 1 ppmv (4% to 20%). Obvious data set specific bias issues are found for a number of data sets. In our work we performed a drift analysis for data sets overlapping for a period of at least 36 months. This assessment shows a wide range of drifts among the different data sets that are statistically significant at the 2σ uncertainty level. In general, the smallest drifts are found in the altitude range between about 30 hPa to 10 hPa. Histograms considering results from all altitudes indicate the largest occurrence for drifts between 0.05 $\mathrm{ppmv} \cdot \mathrm{decade}^{-1}$ and 0.3 $\mathrm{ppmv} \cdot \mathrm{decade}^{-1}$. Comparisons of our drift estimates to those derived from comparisons of zonal mean time series only exhibit statistically significant differences in slightly more than 3% of the comparisons. Hence, drift estimates from profile-to-profile and zonal mean time series comparisons are largely interchangeable. As for the biases, a number of data sets exhibit prominent drift issues. In our analyses we found that the large number of MIPAS data sets included in the assessment affects our general results as well as the bias summaries we provide for the individual data sets. This is because these data sets exhibit a relative similarity with respect to the remaining data sets, despite that the fact that they are based on different measurement modes and different processors implementing different retrieval choices. Because of that, we have by default considered an aggregation of the comparison results obtained from MIPAS data sets. Results without this aggregation are provided on multiple occasions to characterise the effects due to the numerous MIPAS data sets. Among other effects, they cause a reduction of the typical biases in the observational database.

1 Introduction

Water vapour in the stratosphere and lower mesosphere is important for a number of reasons. In the lower stratosphere water vapour is the most important greenhouse gas. As such it strongly affects global warming at the Earth's surface (Riese et al., 2012; Dessler et al., 2013). In addition, water vapour plays a decisive role for ozone chemistry (e.g. Solomon, 1999; Brasseur and Solomon, 2005). On one hand, water vapour is an essential component of polar stratospheric clouds (PSCs). The heterogenous chemistry occurring on the surfaces of the cloud particles causes the severe ozone depletion in the lower stratosphere during winter- and springtime. On the other hand, water vapour is the primary source of hydrogen radicals (i.e. OH, H, HO_2). These radicals destroy ozone within auto-catalytic cycles and dominate the ozone budget in the lower stratosphere and above about 1 hPa. Beyond that, water vapour is a particularly suitable trace gas to diagnose dynamical processes in the stratosphere such as the Brewer-Dobson circulation and the overturning circulation in the mesosphere (e.g. Brewer, 1949; Remsberg et al., 1984; Mote et al., 1996; Pumphrey and Harwood, 1997; Seele and Hartogh, 1999).

In the stratosphere and lower mesosphere water vapour has two major sources. One is the transport of water vapour from the troposphere into the stratosphere, for which several pathways exist (Holton et al., 1995; Moyer et al., 1996; Fueglistaler et al., 2009; Sioris et al., 2016). The primary pathway is the slow ascent through the cold tropical tropopause layer, typically accompanied by large horizontal motions. The cold point temperature along the air parcel trajectories controls the amount of water vapour entering the stratosphere. Another pathway is the convective lofting of ice. Once the ice particles reach the stratosphere they evaporate and correspondingly increase the amount of water vapour. A third pathway is the transport along isentropic surfaces that span both the troposphere and stratosphere. Occasionally water vapour is directly injected into the stratosphere by volcanic eruptions. Overall, ~~about~~ the stratospheric entry mixing ratios typically amount to 3.5 ppmv to 4.0 ppmv~~of water vapour enter the stratosphere .~~, on an annual average (Kley et al., 2000). The other major source is the in situ oxidation of methane. The importance of this process for the water vapour budget increases with altitude and typically maximises in the upper stratosphere (Le Texier et al., 1988; Frank et al., 2018). In the lower mesosphere the methane abundances are small, so that its oxidation can no longer contribute significantly to the water vapour production. Above that, the oxidation of molecular hydrogen is a minor source of water vapour in the upper stratosphere and lower mesosphere (Sonnemann et al., 2005; Wrotny et al., 2010). The major sink of water vapour in the stratosphere is the reaction with $O(^1D)$. With increasing altitude photodissociation becomes increasingly important as a sink and plays the dominant role in the mesosphere. Dehydration, the permanent removal of water due to the sedimentation of PSC particles in the polar vortices, is another sink, however its importance is limited in space and time (Kelly et al., 1989; Fahey et al., 1990). Leaving this last sink process aside, the volume mixing ratio of water vapour generally increases with altitude in the stratosphere due to the dominant role of methane oxidation. Usually, around the stratopause a maximum in the vertical distribution is found. Higher up, the volume mixing ratio of water vapour typically decreases since a major source is missing.

Satellite observations of water vapour in the stratosphere and lower mesosphere were performed since the second half of the1970s, with a few gaps. First sensible results could be derived from observations of the LIMS (Limb Infrared Monitor of the Stratosphere; Remsberg et al., 1984) and SAMS (Stratospheric and Mesospheric Sounder; Munro and Rodgers, 1994) instruments. Both were deployed on the Nimbus-7 satellite that was launched in October 1978. The LIMS observations of stratospheric water vapour lasted until May 1979 while the SAMS observations yielded results in the upper half of the stratosphere and lower mesosphere from 1979 to 1981. In the 1980s observations of the SAGE II (Stratospheric Aerosol and Gas Experiment II; Rind et al., 1993; Taha et al., 2004) and the ATMOS (Atmospheric Trace Molecule Spectroscopy; Gunson et al., 1990) instruments provided stratospheric water vapour information. The SAGE II instrument was carried by the Earth Radiation Budget Satellite (ERBS) and operated for almost 21 years from October 1984 to August 2005. In contrast, the first ATMOS observations covered only a short period of time from late April to early May in 1985. The instrument was part of the European Space Agency's (ESA) Spacelab 3 laboratory module carried by the Space Shuttle. In September 1991 the Upper Atmosphere Research Satellite (UARS) was launched. It carried four instruments that measured water vapour in the stratosphere and lower mesosphere, i.e. CLAES (Cryogenic Limb Array Etalon Spectrometer; Roche et al., 1993), HALOE (Halogen Occultation Experiment, Harries et al., 1996 or Kley et al., 2000), ISAMS (Improved Stratospheric and Mesospheric Sounder; Goss-Custard et al., 1996) and MLS (Microwave Limb Sounder; Lahoz et al., 1994). The HALOE observations lasted until November 2005, providing many new insights on stratospheric and mesospheric water vapour. The observations of the other instruments were much more short-lived. The CLAES and ISAMS observations ceased May 1993 and July 1992, respectively. The MLS instrument operated longer, however the water vapour channel already ceased functioning in April 1993. In March/April 1992, April 1993 and November 1994 the ATMOS instrument performed more measurements, again aboard the Space Shuttle. During all these three missions, the MAS (Millimeter-wave Atmospheric Sounder; Bevilacqua et al., 1996) instrument also obtained information on stratospheric and lower mesospheric water vapour. In addition, on the last of these three Space Shuttle flights water vapour observations by the CRISTA (Cryogenic Infrared Spectrometers and Telescopes for the Atmosphere; Offermann et al., 2002) and the MARSHI (Middle Atmosphere High Resolution Spectrograph Investigation; Summers et al., 2001) instruments were also carried out. In August 1997 CRISTA and MARSHI were put on a second Space Shuttle mission. From October 1996 to June 1997 the Improved Limb Atmospheric Sounder (ILAS; Kanzawa et al., 2002) aboard the Advanced Earth Observing Satellite (ADEOS) performed observations of stratospheric water vapour at high latitudes. Similar coverage was obtained by the POAM III (Polar Ozone and Aerosol Measurement III; Nedoluha et al., 2002) instrument that was carried by the French SPOT 4 (Satellite Pour l'Observation de la Terre). The satellite was launched in March 1998 and POAM III delivered data until December 2005.

In 2000, within the framework of the first SPARC water vapour assessment (Kley et al., 2000), many of these satellite data sets (i.e. LIMS, SAGE II, ATMOS, HALOE, MLS, MAS, ILAS, POAM III) were evaluated. The comparisons indicated a reasonable degree of consistency among the data sets in the stratosphere. On average, the majority of them showed biases of less than ± 10% (see Sect. 2.4, Fig. 2.72 and Tabs. 2.5 to 2.7 of Kley et al., 2000) relative to the HALOE data set, which was used as reference. The differences were typically larger in the altitude range between 100 hPa and 60 hPa than in the stratosphere higher up.

Since this first assessment a wealth of new satellite data sets focusing on stratospheric and lower mesospheric water vapour has been obtained. In 2001 the Odin, TIMED (Thermosphere-Ionosphere-Mesosphere Energetics and Dynamics) and Meteor-3M satellites were launched. Aboard they carried the SMR (Sub-Millimetre Radiometer; Urban et al., 2007), the SABER (Sounding of the Atmosphere using Broadband Emission Radiometry; Feofilov et al., 2009) and the SAGE III (Thomason et al., 2010) instruments, respectively. While the SMR and SABER instruments still perform observations of stratospheric and mesospheric water vapour to this day, the SAGE III observations in the stratosphere ceased like those of POAM III in December 2005. In March 2002 Envisat (Environmental Satellite) was launched carrying three instruments performing water vapour observations in the stratosphere and lower mesosphere, namely GOMOS (Global Ozone Monitoring by Occultation of Stars; Montoux et al., 2009), MIPAS (Michelson Interferometer for Passive Atmospheric Sounding; Payne et al., 2007; Wetzel et al., 2013 and von Clarmann et al., 2009) and SCIAMACHY (Scanning Imaging Absorption Spectrometer for Atmospheric

Chartography, Noël et al., 2010; Azam et al., 2012; Weigel et al., 2016). The observation of all three instruments ceased in April 2012 when contact with the satellite was lost. Aboard ADEOS-II the successor of ILAS, i.e. ILAS II (Griesfeller et al., 2008), was also sent into orbit in 2002. As for ILAS, the observations were short-lived, effectively covering the time period from April to October 2003. The same year the Canadian SCISAT (or SCISAT-1) was launched. The satellite carries the ACE-FTS (Atmospheric Chemistry Experiment - Fourier Transform Spectrometer; Nassar et al., 2005) and MAESTRO (Measurement of Aerosol Extinction in the Stratosphere and Troposphere Retrieved by Occultation; Sioris et al., 2010) instruments that perform observations to the present day. The ACE-FTS observations yield water vapour information in the stratosphere and mesosphere while those by MAESTRO cover the lower stratosphere. To this day also a new version of the MLS instrument performs observations of water vapour in the stratosphere and mesosphere (Waters et al., 2006). The instrument is deployed on the Aura satellite that was launched in July 2004. Aboard Aura there is a second instrument that was capable of observing water vapour in the lower stratosphere, i.e. HIRDLS (High Resolution Dynamics Limb Sounder; Gille et al., 2013). Its operations ceased in March 2008 after an instrumental failure. Since April 2007 the SOFIE (Solar Occultation for Ice Experiment; Rong et al., 2010) instrument carried by the AIM (Aeronomy of Ice in the Mesosphere) satellite performs observations focusing on high latitudes. The penultimate addition to the observational database regarding lower stratospheric water vapour came from the SMILES (Superconducting SubMillimeter-Wave Limb-Emission Sounder; Baron et al., 2011) instrument that was mounted on the International Space Station (ISS) in 2009. The observations by this instrument lasted until April 2010. Finally, in February 2017 an almost exact replica of the SAGE III instrument flown on the Meteor-3M satellite was carried to the ISS from where this new instrument performs observations of stratospheric water vapour.

Many of the satellite water vapour data sets obtained since the new millennium have been validated individually in the last years. Prominent examples can be found in the works of Carleer et al. (2008); Milz et al. (2009); Noël et al. (2010); Rong et al. (2010); Sioris et al. (2010); Thomason et al. (2010); Azam et al. (2012) and Weigel et al. (2016). Within the framework of the second SPARC water vapour assessment (WAVAS-II) satellite observations of stratospheric and lower mesospheric water vapour obtained between 2000 and 2014 are collectively evaluated with respect to a multitude of parameters, like biases, drifts or variability characteristics (Lossow et al., 2017; Nedoluha et al., 2017; Khosrawi et al., 2018). This aims to gain a contemporary overview of the typical uncertainties in the observational database. As part of this programme we present here profile-to-profile comparisons of more than 30 satellite data sets of stratospheric and lower mesospheric water vapour. The advantage of this approach is that it reduces the sampling error relative to comparisons of binned data sets, e.g. zonal or monthly means as used in the works of Hegglin et al. (2013); Lossow et al. (2017) and Khosrawi et al. (2018). Unlike the first SPARC water vapour assessment, we do not invoke a specific reference data set (which was HALOE) but compare all possible combinations of data sets. Besides biases we also focus on drifts among the data sets. The aim of this work is two-fold. On one hand we want to provide a general overview of the typical biases and drifts in the observational database. On the other hand we also want to give an account of data set specific characteristics that could be valuable in the analysis of individual data sets. The outline of this work is as follows. In the next section we provide a very brief overview of the data sets considered and their handling. The comparison approach is described in detail in Sect. 3. The results are presented in Sects. 4 and 5. The former section focuses on biases and the latter section on drifts between the different data sets. Conclusions from this work are provided in Sect. 6. Additional results are presented in the Supplement, complementing those of the main manuscript.

2 Data sets

In the present comparisons overall 33 data sets from 15 individual satellite instruments are considered. Table 1 lists them alphabetically with respect to the instrument name. In case of multiple data sets from one instrument, the data sets have been sorted either alphabetically (e.g. MIPAS-Bologna data sets before MIPAS-ESA data sets) or chronologically (e.g. ACE-FTS v2.2 before ACE-FTS v3.5) or a combination of both. The table also lists the corresponding data set labels and numbers that are used in the figures. In addition, Fig. 1 provides a visual overview of the temporal coverage of the individual data sets to give an indication when coincident observations between two data sets were possible. A complete description of the individual data sets is provided in the WAVAS-II data set overview paper by Walker and Stiller (in preparation). The focus of the present comparisons is on observations that were acquired since the previous millennium as a follow-up to the last WAVAS report in 2000 (Kley et al., 2000). HALOE, POAM III and SAGE II have provided data in the old millennium but correspondingly those were not considered here. While the SABER observations cover almost the entire time period considered in the assessment no data set has become available and thus they are not part of WAVAS-II. Also, the SAGE III observations from the ISS are not considered as they only commenced in 2017.

In a first step we screened the data sets according to the recommendations provided by the individual data set teams. Those screening criteria are listed in full detail in the WAVAS-II data set overview paper (Walker and Stiller, in preparation). In addition, we excluded profiles from the comparison that exhibited volume mixing ratios below $-20\,\mathrm{ppmv}$ or above $50\,\mathrm{ppmv}$ anywhere at altitudes above $70\,\mathrm{hPa}$. This wide interval was chosen to reject obvious outliers that might influence the comparisons in an undesirable way and that were not removed by the earlier screening. For many data sets this affected only a handful profiles. In absolute numbers most profiles were affected for the GOMOS, HIRDLS, MIPAS-Bologna V5R NOM, MIPAS-Oxford and SMR 544 GHz data sets. For the GOMOS data set this meant that about 3.5% of the profiles were discarded, for the other data sets the percentage was in the per mille range. As a last step we sorted the individual observations of a given data set chronologically.

3 Approach

3.1 Determination of coincident observations

Principally, we have considered observations from two data sets as coincident when the following criteria were satisfied:

- a maximum temporal separation of 24 h
- a maximum spatial separation of $1000\,\mathrm{km}$
- a maximum latitude separation of 5°

- a maximum equivalent latitude separation of 5°

When different versions of the ACE-FTS, MIPAS, SCIAMACHY solar occultation and the SMILES data sets were compared with each other these coincidence criteria were not invoked. In these cases the exact same observations were compared. For SMR the different data sets are obtained on different measurement days, so that this exception does not apply. The same is true for MIPAS observations in the nominal mode (NOM) and the middle atmosphere (MA) mode. Also, the different SCIAMACHY observation geometries did not provide simultaneous measurements among them.

To apply the equivalent latitude criterion a scalar value has been assigned to every observation. This value was based on an average of equivalent latitudes within the altitude range from 425 K to 2000 K potential temperature, which essentially covers the entire stratosphere. The equivalent latitude information was derived from MERRA (Modern Era Retrospective-Analysis for Research and Applications, Rienecker et al., 2011) reanalysis data of potential vorticity.

To determine the coincidences we went through the individual observations of the first data set and determined the observations of the second data set that fulfilled the coincidence criteria. If multiple coincidences were found we chose the coincidence closest in spatial distance. This choice is optimised for the stratosphere where the diurnal variation is small (Haefele et al., 2008). Close to the tropopause and towards the middle mesosphere the diurnal variation in water vapour becomes more relevant. Once an observation of the second data set was determined as a coincidence it was not considered any further as a possible coincidence for other observations of the first data set. Inherent in this approach is that the final coincidence pairs are dependent on the choice of the first data set, i.e. comparing ACE-FTS vs. HALOE for example can result in different coincidences than comparing HALOE vs. ACE-FTS. To avoid inconsistent results based on this aspect, we derived only coincidences for the lower half of the data set comparison matrix and used those results for the upper half of that matrix. According to the sorting of the data sets in Tab. 1 the ACE-FTS v2.2 data set has been used as first data set in all comparisons. The SMR 489 GHz data set was considered as first data set only in the comparison to the SOFIE data set while the latter never served as the first data set. We investigated the influence of the first data set choice based on test comparisons to the HALOE, ACE-FTS v2.2 and MIPAS-IMKIAA V5H data sets. Typically the differences in the biases were smaller than 0.05 ppmv or 1% in absolute and relative terms, respectively. Larger deviations were mostly found at the lower ~~boundaries~~ altitude limits of the comparisons.

3.2 Consideration of different vertical resolutions

The data sets considered in our comparisons have different vertical resolutions. A summary figure and a description how the resolutions have been estimated is provided in the data set overview paper by Walker and Stiller (in preparation). Differences in the vertical resolution only play a role for the comparisons at altitudes where the vertical distribution exhibits distinct structures, elsewhere the data sets can be compared directly regardless of the resolution differences. In our work this concerns first and foremost the hygropause region in the lowermost stratosphere. To decide in which comparisons a consideration of differences in the vertical resolution is necessary we categorised the data sets into various classes according to their vertical resolution dz around the hygropause, using some reasonably selected resolution intervals. These classes are given by the first four columns in Tab. 2. The lower the class number the better the vertical resolution of the data sets around the hygropause. The differences in the vertical resolution were considered in those comparisons where the two data sets were in different classes. The data set in the lower class was degraded to the vertical resolution of the data set in the higher class. In the table columns some data sets have been marked by an asterisk, indicating that these data sets have a limited observational coverage of the hygropause. ~~Hence,~~ Some retrieved profiles will include the hygropause, others not. Hence, some comparisons to these data sets may not necessarily need the consideration of differences in the vertical resolution in this altitude range. Yet, they have been taken into account for completeness.

The water vapour maximum in the vicinity of the stratopause is relatively broad and can be accordingly considered less problematic. Yet, some data sets exhibit a strong degradation of their vertical resolution in this altitude region, in particular in the lower mesosphere. To check any influence of this degradation we considered a fifth convolution class that includes data sets whose vertical resolution exceeds $6\,\mathrm{km}$ anywhere above $1\,\mathrm{hPa}$ in the resolution summary figure presented by Walker and Stiller (in preparation). The differences in the vertical resolution are considered in the comparisons to those data sets that are not part of this convolution class and which cover altitudes up to at least $1\,\mathrm{hPa}$. The GOMOS, HIRDLS, MAESTRO, SCIAMACHY limb, SMILES-NICT band A, SMILES-NICT band B and SMR $544\,\mathrm{GHz}$ data sets do not fulfil the latter criterion.

Due to the focus on differences in the vertical resolution in two different altitude regions, hybrid cases are possible, i.e. comparisons between data sets where one data set is better vertically resolved around the hygropause but worse than the other data set at high altitudes and vice versa. In total there have been 19 such cases in which we performed two comparisons considering individually the differences around the hygropause and at high altitudes. The results will be presented later as a combination of these two comparisons. Up to $10\,\mathrm{hPa}$ data from the comparison considering the differences in the vertical resolution around the hygropause are taken into account, above the results from the comparison focusing on the resolution differences at the stratopause and the lower mesosphere are used.

The degradation of the higher vertically resolved data sets followed the approach by Connor et al. (1994). Using the averaging kernel $\mathbf{A}$ and the a priori profile $\boldsymbol{x}_{\mathrm{a\ priori}}$ of the lower resolved profile, which we denote collectively as convolution data, the degradation of the higher resolved profile $\boldsymbol{x}_{\mathrm{high}}$ can be achieved as follows:

$$\boldsymbol{x}_{\mathrm{deg}} = \boldsymbol{x}_{\mathrm{a\ priori}} + \mathbf{A} \cdot (\boldsymbol{x}_{\mathrm{high}} - \boldsymbol{x}_{\mathrm{a\ priori}}). \tag{1}$$

The degraded profile $\boldsymbol{x}_{\mathrm{deg}}$ can then be compared directly to the lower vertically resolved data set. According to the equation the degradation is performed on the grid of the lower resolved profile. The regridding of the higher resolved to this grid follows the work of Stiller et al. (2012a). For some data sets the averaging kernel considers the log space, i.e. $\mathbf{A} = \mathbf{A}_{\mathrm{ln}}$, based on a different retrieval approach. In these cases Eq. 1 has to be adapted to (e.g. Stiller et al., 2012a):

$$\boldsymbol{x}_{\mathrm{deg}} = \exp\{\ln(\boldsymbol{x}_{\mathrm{a\ priori}}) + \mathbf{A}_{\mathrm{ln}} \cdot [\ln(\boldsymbol{x}_{\mathrm{high}}) - \ln(\boldsymbol{x}_{\mathrm{a\ priori}})]\}\,. \tag{2}$$

The third column of Tab. 3, which lists the sources and characteristics of the convolution data employed in our comparisons, indicates the data sets for which this aspect had to be considered. Please note, that this is specific to the convolution data employed here. For example, the retrievals of the MIPAS-Oxford V5H and V5R MA data sets are performed in log space. But for these data sets we had to generate the convolution data ourselves (as described below, see the second column of Tab. 3) which simply assumed a linear space. The degradation of the vertically higher resolved data sets has been performed in the natural domain of the lower resolved data sets, as specified in the fourth column of Tab. 3. Most data sets have volume mixing ratio as natural domain, only some SCIAMACHY data sets use number density. Again this is specific to the convolution data used in this work. The retrievals of the GOMOS and SCIAMACHY solar Onion data sets for example use number density as natural domain, but once more we needed to generate the corresponding convolution data which assumed volume mixing ratio as the natural domain. Temperature and pressure data for the conversion between volume mixing ratio and number density have been provided by all data set teams, either retrieved from the same set of measurements or from an auxiliary data source as reanalysis. Walker and Stiller (in preparation) provide a comprehensive summary on the retrieval spaces and domains of the individual data sets as well as the sources of the additional temperature and pressure information.

Another aspect is, that the convolution data often exceed the altitude range covered by the particular profile to be degraded. This can be handled by either reducing the altitude range of the convolution data or by extending the altitude range of the profile to be degraded. For that a priori or other climatological data as well as model simulations can be employed. In practice the latter approach is often the better choice, leading to more reasonable results at the vertical boundaries of the degraded profile. After the degradation the extension data is removed again. Here we utilised offset-corrected, climatological data from HAMMONIA (Hamburg Model of the Neutral and Ionized Atmosphere, Schmidt et al., 2006) as function of month and latitude.

The second column of Tab. 3 lists the sources of the convolution data that have been employed in the comparisons. For most MIPAS data sets and the SCIAMACHY limb data set the complete set of averaging kernels and the corresponding a priori data were available. A single characteristic averaging kernel and observation-dependent a priori data were provided for the MLS, SCIAMACHY lunar and solar OEM data sets. For the MIPAS-Oxford V5R NOM data set and both SMR data sets collections of characteristic averaging kernels were supplied. They are dependent on time and latitude band. For the SMR 544 GHz data set there is also a dependency on the tropopause altitude. This data set only covers the upper troposphere and lower stratosphere and the tropopause altitude is the main source of kernel variability. Since for the SMR data sets the convolution data are not saved by default we re-retrieved the convolution data from at least 20 (50) observations that fell into the individual bins (monthly and 20°latitude, see Tab. 3) for the 544 GHz (489 GHz data) set. For those bins where overall fewer observations exist we re-retrieved all of them. From this set we selected as most representative convolution data the one where the averaging kernel minimised the following ~~equation~~quantity:

$$\sum_{j=l_{\text{start}}}^{l_{\text{end}}} \left[\boldsymbol{A}_d(j) - \overline{\boldsymbol{A}_d}(j)\right]^2 \tag{3}$$

Here $\boldsymbol{A}_d$ denotes the averaging kernel diagonal that has been interpolated on a regular altitude grid prior to the analysis. $\overline{\boldsymbol{A}_d}$ is the average averaging kernel diagonal over the entire set of re-retrieved data for a particular bin and j is the index over the altitude levels $l_{\text{start}},...,l_{\text{end}}$ that were considered. For the 544 GHz data set we took into account the altitude range between 10 km and 25 km, while for the 489 GHz data set the altitude range between 15 km and 50 km was considered.

For the remaining data sets averaging kernels are typically not part of their retrieval or could not be provided as for the MIPAS-Oxford V5H and V5R MA data sets. In these cases we generated averaging kernels ourselves based on Gaussian functions, using volume mixing ratio as natural domain (as noted above) and kept the a priori constant at zero. The averaging kernel row $\boldsymbol{A}_r(j)$ for a given altitude index j was calculated as follows:

$$\boldsymbol{A}_r(j) = \frac{\boldsymbol{G}(j)}{\sum_{j=1}^{n_a}\boldsymbol{G}(j)}, \tag{4}$$

with

$$\boldsymbol{G}(j) = \exp\left\{-\frac{4\cdot\ln(2)\cdot[\boldsymbol{z}-\boldsymbol{z}(j)]^2}{\boldsymbol{dz}(j)^2}\right\}. \tag{5}$$

In the equation n_a represents the number of altitudes contained in the altitude vector $\boldsymbol{z}$. Accordingly $\boldsymbol{z}(j)$ is the altitude for which the averaging kernel row is calculated and $\boldsymbol{dz}(j)$ describes the vertical resolution at this altitude. The vertical resolutions that have been used to generate the averaging kernels of the individual data sets are also given in the second column of Tab. 3. For the MIPAS-Oxford V5H and V5R MA data sets the vertical resolutions have been assumed while for the other data sets they are typically based on the field of view. The only exceptions are the GOMOS and the SCIAMACHY solar Onion data sets. For the latter the vertical resolution is based on the smoothing of the absorption profiles while the estimate for the GOMOS data set relied on actual averaging kernels. As altitude vector we considered the altitudes given in the data files for the individual observations. For the ACE-FTS data sets we used the data files with the tangent altitude grid and not those with the interpolated regular 1 km grid. When generating the averaging kernel for a given observation we set rows to zero for those altitudes where data were missing, either due to lacking coverage or screening.

3.3 Derivation of biases between the data sets

The comparisons followed essentially the approach outlined by Dupuy et al. (2009), which compared various ozone data sets. The bias $\bar{b}(t,\phi,z)$ between two coincident data sets for a given ~~bin of time~~ time period t and latitude band ϕ and for a specific altitude z has been calculated as

$$\bar{b}(t,\phi,z) = \frac{1}{n_c(t,\phi,z)}\cdot\sum_{i=1}^{n_c(t,\phi,z)} b_i(t,\phi,z), \tag{6}$$

where $n_c(t,\phi,z)$ denotes the corresponding number of coincident measurements and $b_i(t,\phi,z)$ are the individual differences between those. These differences were considered both in absolute

$$b_i(t,\phi,z) = b_{i,\mathrm{abs}}(t,\phi,z) = x_i(t,\phi,z)_1 - x_i(t,\phi,z)_2 \tag{7}$$

and relative terms

$$b_i(t,\phi,z) = b_{i,\mathrm{rel}}(t,\phi,z) = \frac{x_i(t,\phi,z)_1 - x_i(t,\phi,z)_2}{[x_i(t,\phi,z)_1 + x_i(t,\phi,z)_2]/2}, \tag{8}$$

where $x_i(t,\phi,z)_1$ are the individual water vapour abundances of the first data set and $x_i(t,\phi,z)_2$ correspondingly the abundances of the second data set. As ~~denominator for the relative bias we used the~~ reference several options were possible, like the first data set, the second data set in a comparison or the mean of the two data sets. ~~One common argument for this approach has been convenience as~~ In our work we used the last option. A reason for the decision was that satellite observations can have larger uncertainties ~~(Randall et al., 2003). Here~~and thus the mean may be more appropriate choice (Randall et al., 2003; Dupuy et al., 2009). Another aspect was simply convenience. For a specific comparison there is no need to know which data set acted as reference. Eventuell inconsistencies based on the combination of which data set was chosen to be the first data set in the comparison (see Sect. 3.1) and which one was used as reference can be avoided. Finally, we also wanted to avoid intentionally any preference towards a certain data set as reference~~(as done~~ , but to compare all data sets on equal terms. Accordingly, the relative biases presented here are not comparable to those shown in the first SPARC water vapour assessment ~~, see Introduction) to compare all data sets on equal terms.~~(Kley et al., 2000) where always the HALOE data set was used as reference. In general, any a posteriori attempt to relate the relative bias to the first or the second data set (instead of the mean among the data sets) is not meaningful nor appropriate, because there is some non-intuitive behaviour involved according to Eq. 8.

Before the mean bias $\overline{b}(t,\phi,z)$ was derived we performed an additional screening on the individual biases $b_i(t,\phi,z)$ using the median and median absolute deviation (MAD, e.g. Jones et al., 2012). After screening profiles with data points outside a reasonable abundance range, as described in Sect. 2, this is a second attempt to ensure meaningful bias estimates. We preferred this method over a screening using the mean and standard deviation due to its superior robustness with respect to larger outliers. Individual biases outside the interval $\langle \mathrm{median}[b_i(t,\phi,z)] \pm 10 \cdot \mathrm{MAD}[b_i(t,\phi,z)] \rangle$, with $i = 1,...,n_c(t,\phi,z)$, were discarded. For a normally distributed set of data 10·MAD correspond roughly to 7.5 standard deviations. Hence this has not been a very strict screening, aiming to remove the most prominent outliers of individual biases $b_i(t,\phi,z)$.

As indicated by Eqs. 6 – 8 the biases were calculated for various sets of coincidences covering different ~~times~~ time periods t and latitude bands ϕ as listed below:

- time t: MAM, JJA, SON, DJF and all seasons together
- latitude ϕ: 90°S – 60°S (also referred to as Antarctic), 60°S – 30°S, 30°S – Equator, 15°S – 15°N (also referred to as tropics), Equator – 30°N, 30°N – 60°N, 60°N – 90°N (also referred to as Arctic) and 90°S – 90°N (also referred to as global)

The comparisons were performed on pressure as altitude scale and biases have been derived in the volume mixing ratio space. For this all data sets were interpolated on a common grid with 32 levels per pressure decade. Tropospheric data were intentionally removed using MERRA tropopause information. Comparisons in the troposphere will be presented by Read et al. (in preparation). Due to the finite vertical resolution of the individual data sets the removal of tropospheric data has not been perfect and at the lower boundary volume mixing ratios still remain that are associated with tropospheric conditions. In comparisons where differences in the vertical resolution among the data sets had to be considered the tropospheric data were removed after the convolution to obtain optimal results. In the following figures we show only bias results that are based on at least 20 coincidences to avoid spurious results. This targets primarily the lower and upper vertical limits of the comparisons, where typically the smallest numbers of coincidences tend to occur.

Given the large number of data sets, this work yields a large number of comparisons. Even though every comparison is unique some sort of combination is needed to be able to present the results in a reasonable way. To summarise the bias results for a given data set considering a specific time and latitude band we chose the median over all available comparisons (with an aggregation of the MIPAS results as described later in Sect. 3.5). We tested other approaches but the median appeared to be the optimal choice for multiple reasons. It provides robust statistics in the presence of outliers (avoiding the need for additional screening) and it does not require any assumption of a certain probability distribution nor a specific weighting of the individual comparisons.

3.4 Drift analysis

Besides the bias estimation we also performed an analysis of drifts among the different data sets. Unlike for the bias comparisons, we do not separate the drift comparisons by season. The drift analysis was based on monthly averaged biases derived from a minimum of 5 coincidences. Drifts were only calculated if the overlap period between the two data sets compared was at least 36 months. This period is defined as the time between the first and the last month where sufficient coincidences were found between the two data sets. The estimation of the drifts was done with a regression model that contained an offset, a single linear term for the drift as well as terms for the semi-annual (SAO), annual (AO) and quasi-biennial oscillation (QBO):

$$\begin{aligned}
f(t,\phi,z) =& C_{\text{offset}}(\phi,z) + C_{\text{drift}}(\phi,z)\cdot t\\
&C_{\text{SAO}_1}(\phi,z)\cdot\sin(2\cdot\pi\cdot t/p_{\text{SAO}})+\\
&C_{\text{SAO}_2}(\phi,z)\cdot\cos(2\cdot\pi\cdot t/p_{\text{SAO}})+\\
&C_{\text{AO}_1}(\phi,z)\cdot\sin(2\cdot\pi\cdot t/p_{\text{AO}})+\\
&C_{\text{AO}_2}(\phi,z)\cdot\cos(2\cdot\pi\cdot t/p_{\text{AO}})+\\
&C_{\text{QBO}_1}(\phi,z)\cdot QBO_1(t)+\\
&C_{\text{QBO}_2}(\phi,z)\cdot QBO_2(t).
\end{aligned} \tag{9}$$

In the equation $f(t,\phi,z)$ ~~denotes~~ represents the fit of the regressed bias time series ~~.~~ $\overline{b}(t,\phi,z)$, however here t describes all months where the data sets that are compared have sufficient overlap (i.e. 5 coincidences, see above). C are the regression coefficients of the individual model components and C_{drift} describes the drift that is sought. The SAO and AO are parameterised by orthogonal sine and cosine functions, while for the QBO the normalised winds at 50 hPa (QBO_1) and 30 hPa (QBO_2) observed over Singapore (1°S, 104 °E) are used. These winds are closely orthogonal and have been compiled by Freie Universität Berlin (webpage: http://www.geo.fu-berlin.de/met/ag/strat/produkte/qbo/qbo.dat). p_{SAO} and p_{AO} represent the time periods of the semi-annual (0.5 years) and annual variation (1 year), respectively. The regression coefficients were derived following the method by von Clarmann et al. (2010) using the standard mean error of the monthly averaged biases as statistical weights. In the regression also autocorrelation effects and empirical errors are considered, using the same approach as outlined by Stiller et al. (2012b).

In our work we consider drifts as statistically significant when they exceed the 2σ uncertainty level. σ is defined as the absolute ratio between the drift estimate C_{drift} and its uncertainty $\epsilon_{\mathrm{drift}}$:

$$\sigma = \left| \frac{C_{\mathrm{drift}}}{\epsilon_{\mathrm{drift}}} \right| \tag{10}$$

3.5 Aggregation of the MIPAS results

The previous WAVAS-II papers (Lossow et al., 2017; Nedoluha et al., 2017; Khosrawi et al., 2018) often received comments on the large number of MIPAS data sets (here 13 out of 33, see Tab. 1 for example) included in the assessment. As described in these publications the different MIPAS data sets are based on different measurement modes (with different vertical sampling) and, more prominently, are derived by four different processors with varying retrieval choices, as microwindows, vertical grid regularisation, spectroscopic database or a priori for example. Here, we want to provide general results in the form of percentiles and histograms using all comparison results as well as a summaries of data set specific biases as described at the last paragraph of Sect. 3.3. In general such results will always depend on the data sets that are considered. One of the WAVAS-II goals was to involve as many data sets as possible to provide a rather complete and realistic picture. There are however limits. For example, if all data sets in such assessment would be experimental (i.e. test or research versions), any general result derived from the combination of them would be rather meaningless. Also the large number of MIPAS data sets in our assessment may be such a limit. Accordingly, we asked ourselves if our intended results may be influenced or skewed by the large number of MIPAS data sets. The typical biases among the different MIPAS data sets are significantly smaller than among the non-MIPAS data sets. They amount to roughly $0.1\,\mathrm{ppmv}$ ($0.5\,\mathrm{ppmv}$) for the MIPAS (non-MIPAS) data sets, considering large parts of the stratosphere. A similar picture is found in terms of typical drifts. In the stratosphere they are approximately $0.1\,\mathrm{ppmv}\cdot\mathrm{decade}^{-1}$ for the MIPAS data sets while for the non-MIPAS data sets they correspond to $0.3\,\mathrm{ppmv}\cdot\mathrm{decade}^{-1}$. This indicates a relative similarity among the different MIPAS data sets in contrast to the non-MIPAS data sets. This clearly can affect our intended general results based on all comparison results. In addition, the summary biases (based on the median over all comparisons to the other data sets, see Sect. 3.3) for any randomly picked MIPAS data set will be small because this data set is compared to many relatively similar ones. In contrast, a single non-MIPAS data set has to compare to the bulk of MIPAS data sets. If these comparisons disagree, the summary biases for this non-MIPAS data set will be large. Given these considerations we decided to aggregate the MIPAS results. For percentiles, histograms and full matrix plots the aggregation has been performed as follows:

- all MIPAS comparison results to a given non-MIPAS data set are combined using the median
- comparison results between different MIPAS data sets are not considered ~~any further~~ (in the calculation of the aggregated quantities)

For the summary bias $\overline{b}_S(t,\phi,z)$ of a given data set, described in Sect. 3.3 and shown in Figs. 8 and 9 in the main manuscript as well as in Fig. ~~S8~~ S9 in the Supplement, the following approach has been chosen:

(a) for a non-MIPAS data set, like HALOE

$$\overline{b}_S(t,\phi,z,\mathrm{HALOE}) = \mathrm{median}\langle\overline{b}(t,\phi,z,ds_1),\mathrm{median}[\overline{b}(t,\phi,z,ds_2)]\rangle \tag{11}$$

where $\overline{b}(t,\phi,z,ds_1)$ represents all biases of the HALOE data set to the remaining non-MIPAS data sets and $\overline{b}(t,\phi,z,ds_2)$ describes the HALOE biases relative to all MIPAS data sets

(b) for a given MIPAS data set, like MIPAS-Bologna V5R NOM

$$\overline{b}_S(t,\phi,z,\mathrm{MIPAS-Bologna\ V5R\ NOM}) = \mathrm{median}\langle\overline{b}(t,\phi,z,ds_3),\mathrm{median}[\overline{b}(t,\phi,z,ds_4)]\rangle \tag{12}$$

where $\overline{b}(t,\phi,z,ds_3)$ are all the biases to non-MIPAS data sets and $\overline{b}(t,\phi,z,ds_4)$ represents the biases of the MIPAS-Bologna V5R NOM data set to the remaining MIPAS data sets

In numerous ~~figure~~ figures we supply as auxiliary information the number of comparisons or data points contributing to the results presented. Even, when the MIPAS results are aggregated we still count the contributing results individually and do not condense them into a single contribution. For example in Fig. 9 the bias summaries for the ACE-FTS v3.5 data set are presented. This data set could be compared to all 13 MIPAS data sets if coincidences at all seasons and latitudes are considered. Hence the number of comparisons contributing to these summary biases given in that figure (i.e. 31), includes these 13 comparisons.

We will show some results with and without the aggregation of the MIPAS results for the sake of comparison. In the main manuscript this concerns Figs. 4, 5 and 11. In the Supplement Figs. ~~S1, S4~~S2, S5 and ~~S9~~ S10 show percentiles and histograms without the aggregation of the MIPAS results that correspond respectively to Figs. 6, 7 and 12 in the main manuscript which take this aggregation into account. The two ACE-FTS and SCIAMACHY solar occultation data sets are also based on the same set of measurements. Therefore also an aggregation of these results could be considered. However, due to the small number of the data sets concerned (in relation to the MIPAS data sets), this has not further been pursued.

4 Bias results

The presentation of the bias results is split into three parts. We start with an example to provide a first impression of the analyses. Then, we focus on a general, data set independent, assessment of the biases. This aims to provide a picture of the typical bias characteristics found in the observational database. In the last part of this section, specific results for individual data sets are presented.

The upper triangle of Fig. 2 provides a quick overview which data sets were compared in terms of biases for any of the time-latitude bins considered (see Sect. 3.3). The presentation uses a traffic light system:

(1) green: Comparisons were performed.

(2) yellow: Comparisons were performed. However, the minimum criterion of at least 20 coincidences (as defined in Sect. 3.3) was not met at any considered altitude. This concerns four comparisons, namely the comparisons of the HALOE and SAGE II data sets to SCIAMACHY lunar data set as well as and the comparisons of the MAESTRO data set to both SMILES data sets.

(3) red: No comparison could be performed as the data sets do not overlap.

Complementary to this, Fig. 3 shows the number of coincident observations among the data sets (considering all seasons and latitude bands). The HIRDLS and MLS data sets yield more than 3 million coincidences according to our criteria, the largest number found in our comparisons. The comparisons among the different MIPAS V5R NOM data sets comprise more than 1.7 million coincidences. On the opposite end, less than 100 coincident observations are found in the comparisons of the following data sets: ACE-FTS vs. SMILES, GOMOS vs. SCIAMACHY occultation (both lunar and solar), GOMOS vs. SMILES, HALOE vs. MIPAS V5R MA, ILAS vs. SCIAMACHY lunar, MAESTRO vs. SCIAMACHY lunar as well as SAGE II vs. SCIAMACHY lunar.

4.1 Example

Figure 4 shows exemplarily biases of the SCIAMACHY solar OEM data set, considering coincident observations during all seasons and at all latitudes. The upper row considers biases in absolute terms, while the lower row focuses on biases in relative terms. The left panels show the biases to the individual data sets (i.e. SCIAMACHY solar OEM minus the other data set, see Sect. 3.3). In the right panels the corresponding summary biases are shown. The red profile is based on the median over all comparisons (see Sect. 3.3). The blue profile, additionally, considers the aggregation of MIPAS results as described in Sect. 3.5 and is also used for the summary of the data set specific results presented later in Sect. 4.3 and the Supplement. The legend provides information on the actual temporal and spatial coverage of the individual comparisons as a complement. Even though all latitudes are considered in the analysis, the comparisons are limited to the latitude range between 49°N and 69°N according to the coverage of the SCIAMACHY solar OEM data set.

The comparisons indicate biases of the SCIAMACHY solar OEM data set, that are typically within $\pm 1\,\mathrm{ppmv}$ or $\pm 20\%$ in relative terms. In most cases the biases are positive, but in some comparisons also negative biases are found. These negative biases are visible in the lower (roughly between $100\,\mathrm{hPa}$ and $50\,\mathrm{hPa}$) and upper stratosphere (between $3\,\mathrm{hPa}$ and $1\,\mathrm{hPa}$) as well as in the lower mesosphere (roughly above $0.2\,\mathrm{hPa}$). In the uppermost altitude range this behaviour is systematically observed in comparisons to the MIPAS Bologna data sets derived from the nominal mode observations, i.e. MIPAS-Bologna V5H and MIPAS-Bologna V5R NOM. For the other altitude ranges no such data set specific behaviour is observed. Beyond that, these example biases indicate more issues with specific data sets that will be presented more comprehensively in Sect. 4.3 and the Supplement.

In accordance with the individual bias results presented in the left panels, the summary profiles shown in the right panels indicate generally positive biases for the SCIAMACHY solar OEM data set compared to the other data sets. From the summary biases we find that the results are clearly influenced by the summary approach in the altitude range between $30\,\mathrm{hPa}$ and $0.6\,\mathrm{hPa}$. Here, the median over all comparisons yields consistently lower biases than the median considering the aggregation of the MIPAS results. Differences between these two profiles become as large as $0.4\,\mathrm{ppmv}$, corresponding to 6% in relative terms. This highlights the influence that the large number of MIPAS data sets can have in the comparisons, as discussed in Sect. 3.5. The summary profiles considering the aggregation of the MIPAS results exhibit the smallest biases below $25\,\mathrm{hPa}$ (around $0.25\,\mathrm{ppmv}$ or 5%) and at $0.1\,\mathrm{hPa}$ (about $0.1\,\mathrm{hPa}$ or 2% – 3%). At $10\,\mathrm{hPa}$ and more prominently at $0.25\,\mathrm{hPa}$ the biases maximise. At $10\,\mathrm{hPa}$ the bias amounts to $0.75\,\mathrm{ppmv}$ or 12% while the maximum in the lower mesosphere (also notable in the summary profiles without aggregation) exhibits smaller values ($0.6\,\mathrm{ppmv}$ or 10%). On average, the biases amount to $0.5\,\mathrm{ppmv}$ (about 8%) in the stratosphere.

4.2 General results

The left column of Fig. 5 shows the biases from the full matrix of comparisons. Here, the comparisons that include coincident observations during all seasons and at all latitudes are considered. The upper panel shows the results for the absolute biases, in the lower panel the results for the relative biases are given. Based on our comparison approach (see Sect. 3.1) the results for the full matrix are symmetric around zero. In grey the comparison results without the aggregation of the MIPAS results are shown. With 33 data sets theoretically $33 \cdot 32 = 1056$ comparisons (of which 528 are unique) are possible. But since not all data sets overlap with each other the actual number decreases to 862 comparisons (of which 431 are unique, see Fig. 2). For 8 comparisons (4 unique) the biases are based on less than 20 coincidences at all altitudes and were thus not considered any further (see Sect. 3.3 or description of Fig. 2 in the beginning of this section). Hence, the unaggregated results are effectively based on 854 comparisons (427 unique). In blue the comparison results considering the aggregation of the MIPAS results are shown. As described in Sect. 3.5 the aggregation omits comparisons among the MIPAS data sets, reducing the amount of available comparisons to 770. After combining all MIPAS results in comparisons to non-MIPAS data sets finally 348 comparisons remain for the full matrix.

Overall, the left column of Fig. 5 provides a good first impression of the typical envelope of biases in the observational database. Above $30\,\mathrm{hPa}$ the biases are typically within $\pm 2\,\mathrm{ppmv}$ (or $\pm 40\%$). Below this altitude the biases can get significantly larger and even exceed $\pm 5\,\mathrm{ppmv}$ or $\pm 100\%$ in some occasions.

Based on the positive biases shown in the left panels of Fig. 5 the right panels show the corresponding 50% (i.e. median, blue), 80% (green) and 95% (red) percentiles without (lighter colours) and with (darker colours) the aggregation of the MIPAS results. In general, the 50% and 80% percentiles are quite constant above $70\,\mathrm{hPa}$, while the 95% percentile shows much more variation in this altitude range. At altitudes below there is a distinct increase in the corresponding values. In addition, the percentiles considering the aggregation of the MIPAS results are larger than without this aggregation. At stratospheric altitudes the differences amount to 0.1 ppmv (2%) for the 50% percentile, 0.2 ppmv (5%) for the 80% percentile and 0.5 ppmv (7%) for the 95% percentile, respectively. Prominent exceptions from this behaviour are observed close 0.1 hPa, below 200 hPa (except for 50% percentile of the absolute biases) or between 2 hPa and 1 hPa for the 95% percentile of the absolute biases. In the following description we focus on percentiles considering the aggregation of the MIPAS results. The 50% percentile is around 0.5 ppmv above 100 hPa and minimises at 60 hPa with 0.35 ppmv. Below 200 hPa the 50% percentile exceeds 2 ppmv. In relative terms, the 50% percentile is smaller than 10% around 60 hPa and between 25 hPa and 0.3 hPa. From 100 hPa to 250 hPa the 50% percentile increases from 12% to 40%. Below, the percentile actually decreases again to reach a pronounced minimum of 23% at about 340 hPa. The 80% percentile considering the absolute biases averages to 1.1 ppmv for altitudes above 100 hPa. A distinct minimum is again observed at 60 hPa (0.8 ppmv). Also, in the altitude range between 10 hPa and 3 hPa as well as around 0.5 hPa and 0.1 hPa pronounced minima of about 1 ppmv are visible. At 100 hPa the 80% percentile amounts to 1.5 ppmv. With decreasing altitude it quickly increases and exceeds 5 ppmv slightly below 200 hPa. For the relative biases the 80% percentile varies between 20% and 35% in the altitude range between 100 hPa and 10 hPa. Higher up, it is below 20% with a few exceptions. Below 200 hPa the 80% percentile ranges from 50% to 70%. Again a pronounced minimum is observed close to 370 hPa, similar as observed for the 50% percentile. The 95% percentile is generally smaller than 2 ppmv with three noticeable exceptions. One concerns the altitude range below 70 hPa, in a similar fashion as observed for the other two percentiles. Another exception is observed around 30 hPa where a localised maximum of more than 5 ppmv is found. This behaviour can be attributed to the MAESTRO data set that is close to its upper boundary and exhibits high positive biases at these altitudes. The third exception is visible at 0.7 hPa, primarily attributed to the two SAGE data sets. In relative terms, the 95% percentile ranges from 20% to almost 80% above 70 hPa. Below 100 hPa there are large variations and the values exceed 100% occasionally.

To provide a more quantitative statement how variable these percentiles are we applied a jackknife approach (Efron, 1979) . Randomly we left out five data sets and recalculated the percentiles. We repeated this until every data set had been left out at least once. This approach yields a set of results (typically about 25 for the non-aggregated data and a dozen for the aggregated data) for a given percentile. From this set of results a standard deviation can be calculated. Given our random approach many different sets of results (and corresponding standard deviations) are possible. One characteristic realisation is shown in the Supplement in Fig. S1. Overall, standard deviations are in general around 0.05 ppmv (1%) for the 50% percentile without the aggregation of the MIPAS results. With this aggregation the standard deviations are typically twice as large in the stratosphere. Close to 0.1 hPa standard deviations around 0.25 ppmv (4%) are observed. For the 80% percentile the standard deviations amount roughly to 0.1 ppmv (1% – 5%) and 0.2 ppmv (2% –10%) without and with the aggregation of the MIPAS results, respectively. For the 95% percentile the standard deviations vary typically between 0.05 ppmv and 0.5 ppmv (2% – 10%) when no aggregation of the MIPAS results is considered. If the aggregation is taken into account a larger variation is observed with peak values exceeding 1 ppmv (20%).

In Fig. 6 the characterisation of the typical biases is extended by considering the 50% percentile (median) for different seasons and latitude bands. These results take into account the aggregation of the MIPAS results and are again based on the positive biases only, as the percentile results shown in the previous figure. The left column of the figure considers the absolute biases, the right column focuses on the relative biases. The different rows focus on different seasons or their combination. The results for the different latitude bands are colour-coded. On the right side of the individual panels the number of (unique) comparisons contributing to results are given. As described in Sect. 3.5 the comparisons to the different MIPAS data sets are counted individually. In general, the 50% percentiles exhibit a rather common altitude dependence for the different seasons and latitude bands. Below about 70 hPa the 50% percentiles increase considerably and the highest values are observed in the tropics and subtropics. Below 200 hPa the values are typically beyond the upper limits of the x-axes considered here, i.e. 1 ppmv in absolute terms and 20% in relative terms. The 50% percentiles are typically lowest in the altitude range from roughly 70 hPa to 5 hPa. The values here vary between 0.25 ppmv and 0.5 ppmv in absolute terms and between 5% and 10% in relative terms. In this altitude region, the lowest values generally occur outside the polar regions. Higher up, there is a distinct increase of the 50% percentiles~~within a small altitude range~~, i.e up to about 1 hPa. At this altitude the 50% varies approximately between 0.6 ppmv and 0.8 ppmv (roughly 8% to 12%). In JJA the values are a bit smaller while in DJF there is a much larger variation among the latitude bands (percentiles minimise for the Arctic and maximise for the latitude band from 30°N and 60°N). Higher up, the 50% percentiles vary considerably with altitude and among the latitude bands, comprising values from 0.3 ppmv to 1 ppmv (4% to 20%). The smallest values are typically observed between 0.5 hPa and 0.4 hPa. In MAM, SON and all seasons combined the latitude band from the Equator to 30°N stands for these minimum values, in DJF this occurs prominently in the Arctic. The largest values are observed at 0.1 hPa, with pronounced variations among seasons and latitude bands.

Figure ~~S1~~ S2 in the Supplement shows the results corresponding to Fig. 6 without the aggregation of the MIPAS results. Overall, the altitude dependence is quite similar to the results shown here. However, without the aggregation, the values for the 50% percentiles are smaller (like in Fig. 5), as is the variation among the different latitude bands and seasons (a prominent exception occurs at 0.1 hPa). To further complement Fig. 6 the results for the 80% and 95% percentiles, considering again the aggregation of the MIPAS results, are shown in the Supplement (Figs. ~~S2~~S3 and ~~S3~~S4). For these larger percentiles the altitude dependence is somewhat different, in particular for the 95% percentile where less pronounced differences between stratospheric and lower mesospheric values are visible. Pronounced differences among the latitude bands rather occur in the lower stratosphere than lower mesosphere.

For a last characterisation of the biases in the observational database we use histograms, as shown in Fig. 7. These results use again the positive biases only, consider data from all altitudes and take into account the aggregation of the MIPAS results. The histograms for the absolute biases (left column) use bins of ~~0.05~~0.1 ppmv. For the relative biases (right column) bins of ~~1~~2% are considered. As in the previous figure the different panels consider different seasons or their combination. The different latitude bands are again colour-coded. On the right side of the individual panels the number of data points contributing the results are given (again comparisons to different MIPAS data sets are counted individually, see Sect. 3.5). Overall, the histograms exhibit a rather similar picture for the different seasons and latitude bands. ~~Their shapes are quite close to a Gaussian distribution. Typically, between 5% and 7% of the absolute biases are found~~ The occurrence rates typically maximise within the first bin that ranges from 0 ppmv to ~~0.05~~0.1 ppmv (between 11% and 13%). The decrease in occurrence towards larger biases (up to 0.8 ppmv) is steepest in DJF. For biases around 1 ppmv the occurrence has dropped to ~~1% to 2.5~~2.5% to 4.5%. Biases beyond 3 ppmv occur in 2% to ~~6~~7% of the comparisons. The lowest occurrences for these biases are observed in the Antarctic and tropics. In relative terms the occurrence of biases within the first bin from 0% and ~~1~~2% varies between ~~4% and 7~~10% and 14% depending on season and latitude band. A bias of 10% occurs in ~~3% to 5~~about 6% to 9% of the comparisons. For biases beyond 50% the occurrence is ~~between slightly less~~ typically between than 2% and ~~9~~8%. The lower limit is observed for the latitude band between 30°S and the Equator in JJA. In contrast, the upper limit occurs in the Antarctic in DJF.

As for the previous figure we present the results without the aggregation of the MIPAS results, corresponding to Fig. 7, in the Supplement (Fig. ~~S4~~S5). The results without the aggregation exhibit ~~a larger occurrence rate~~ larger occurrence rates for the smallest biases (between ~~7% and 10~~14% and 19%). Besides that, the variation among the different latitude bands is smaller. In the Supplement we present in addition histograms that focus separately on data in the altitude ranges 100 hPa – 10 hPa, 10 hPa – 1 hPa and 1 hPa – 0.1 hPa (see Figs. ~~S5, S6~~S6, S7 and ~~S7~~S8), again considering the aggregation of the MIPAS results. ~~From these figures we find that for small biases (i.e. up 0.5 or 10%) the occurrence rate is smallest~~ The picture in the altitude range from ~~1~~100 hPa to ~~0.1~~10 hPa ~~. For relative biases the highest occurrence of such biases is observed in the~~ is relatively similar to that observed in Fig. 7. In altitude range from 10 hPa to 1 hPa ~~. In contrast, large biases (>~~the maximum occurrence rates occur over a larger bias range (roughly up to 0.5 ppmv or 10%). Occasionally there are pronounced peaks in the occurrence rate, often involving data in the tropics and subtropics. Biases beyond 3 ppmv or 50% ~~) occur by far most often~~ occur more rarely than in the altitude range from 100 hPa to 10 hPa. ~~The results for~~ This behaviour is even more obvious in the altitude range from ~~10~~1 hPa to ~~1~~0.1 hPa~~deviate to some extent from a Gaussian distribution. In particular, the tropics and subtropics show the maximum occurrence rates for biases of 0.4~~. Here, the histograms exhibit a pronounced variation among the different latitude bands. The smallest biases often show a very high occurrence rates. Within the next bins a steep decrease of the occurrence rates is observed. Pronounced secondary maxima in the occurrence rates occur for biases beyond 0.5 ppmv ~~(7% to 8%). Also, the variations among the latitudebands increase with altitude~~or 10%, depending on season and latitude.

Finally, we want to note that the consideration of differences in the vertical resolution among the data sets, as done in this work (see Sect. 3.2), yields an improvement of the biases in 55% of the comparisons (all data sets, times, latitude bands and altitudes). This primarily concerns altitudes above 70 hPa and pronounced improvements are visible around 30 hPa, the stratopause and above 0.2 hPa. They can reach several tenths of a ppmv (or a few percent) in these altitude regions. Below 70 hPa there are both improvements and deteriorations, however with a clear tendency to the latter and as large as 100% in relative terms. This indicates that differences in the vertical resolution are not the primary cause of the pronounced biases in this altitude region.

4.3 Data set specific results

In this section an overview of data set specific results is presented. Figure 8 shows the summary biases for all data sets, based on the comparisons that consider coincidences during all seasons and at all latitudes. The absolute biases are given in the left column and the relative biases in the ~~columns~~right column. For the sake of better visibility the results have been split into three panels. In the legend this separation is also reflected by the columns. In addition, the legend contains the information on the number of comparisons contributing to the individual summary biases (using the aggregation of the MIPAS results). As described in Sect. 3.5 these results consider the aggregation of the MIPAS results. Overall the smallest biases are observed in the middle and upper stratosphere. The largest biases occur below 100 hPa (larger than ±2 ppmv or ±50%). On occasion also pronounced summary biases are visible in the lower mesosphere close to 0.1 hPa.

The first row comprises the results for the ACE-FTS, GOMOS, HALOE, HIRDLS, ILAS-II, MAESTRO and some MIPAS data sets (Bologna and one from ESA). Here, the biases are relatively small with ±0.4 ppmv, corresponding to a relative biases of ±10%. Larger (negative) biases are found for the GOMOS, HALOE (above 2 hPa) and ILAS-II data sets. Among them, the GOMOS data set shows the absolute largest biases. The GOMOS biases get more negative with increasing altitude above 75 hPa and reach values of −1.4 ppmv at 20 hPa. Up to 2 hPa the biases of the GOMOS data set vary between −1.7 ppmv and −1.1 ppmv (roughly −35% to −25%). Above 2 hPa the biases decrease again in size, however this is close to the upper limit where water vapour information can be retrieved from the GOMOS observations. The biases for the ILAS-II data set generally do not exceed −0.8 ppmv, corresponding to less than −15% in relative terms. For the HALOE data sets the biases vary between −0.5 ppmv and −0.2 ppmv (−5% to −10%) in the altitude range from 70 hPa to 5 hPa. Towards the lower mesosphere the biases increase in size, where they are around −1 ppmv (−15%). At 0.1 hPa the biases for the data sets shown in the first panel range from −0.9 ppmv (−20%) to 0.4 ppmv (10%). Below 100 hPa the absolute biases increase significantly in size. All data sets exhibit biases larger than ±2 ppmv at some altitude. Also, in relative terms a large variation is observed, however the biases for ACE-FTS v2.2 and MAESTRO data sets remain largely within ±10%.

In the second panel results for numerous MIPAS (ESA, IMKIAA and Oxford) data sets are shown, plus those from the MLS and POAM III data sets. For these data sets the biases are generally within −0.3 ppmv to 0.6 ppmv, corresponding roughly to relative biases between −5% and 10%. Larger biases are found for the MIPAS-ESA V5R MA, MIPAS-Oxford V5H and MIPAS-Oxford V5R MA data sets around the stratopause. Some data sets exhibit a pronounced increase in their biases above 0.3 hPa. This concerns the MIPAS-Oxford and the MLS data sets. At 0.1 hPa biases range, overall, from −0.4 to more than 2 ppmv, corresponding to relative biases of −10 to 45%. Below 100 hPa again large biases are visible, with a tendency towards negative values. Data sets for which the biases exceed −50% below 100 hPa are MIPAS-ESA V7R, MIPAS-Oxford V5H, MIPAS-Oxford V5R NOM. The MIPAS-ESA V5R NOM (−25% to 0%), MIPAS-IMKIAA (−20% to 5%), MLS (±20%) and POAM II (5% to 15%) data sets show here typically smaller biases.

The third panel of Fig. 8 presents results for data sets from the following instruments: SAGE, SCIAMACHY, SMILES, SMR and SOFIE. Here, some data sets exhibit quite pronounced biases. This concerns on one hand the experimental SMILES data sets. They cover the altitude range from slightly above 200 hPa to 50 hPa and show good agreement between 70 hPa and 60 hPa. Higher up, distinct positive biases (exceeding 1 ppmv or 20%) are observed while below negative biases of even larger size are visible. The summary biases for the SMR 544 GHz data set are almost entirely negative. Around 30 hPa they amount to −1.8 ppmv (exceeding -50%). Above 15 hPa they get significantly smaller and switch sign at above 10 hPa, close to the upper limit of this data set. The biases for the SMR 489 GHz data set are quite low up to 10 hPa, but start to increase significantly higher up. In the lower mesosphere this data set exhibits biases around −1.2 ppmv in absolute terms and −25% in relative terms. In the lower half of the stratosphere the SAGE II, SAGE III, SCIAMACHY lunar and SOFIE data sets show very good agreement (typically within ±0.2 ppmv or ±5%). Towards higher altitudes biases increases to some extent, most prominently for the SAGE II data set above 3 hPa. The SCIAMACHY solar occultation data sets exhibit low biases in the lower stratosphere (around 5%). Above 30 hPa they vary typically between 0.3 ppmv and 0.7 ppmv (5% to 12%).

Figure 9 shows the summary biases for the ACE-FTS v3.5 data set as function of season and latitude, using the same layout as in Figs. 6 and 7. For all other data sets the corresponding figures are provided in the Supplement (Fig. ~~S8~~S9). The comparisons to the ACE-FTS v3.5 data set show a rather consistent picture above about 100 hPa with relatively small variations among the different seasons and latitude bands. Between about 80 hPa and 5 hPa the biases are typically within ±0.2 ppmv or ±5%, with a clear preference towards negative biases. Towards higher altitudes the biases get more negative. They peak between 2 hPa and 1 hPa with values from -0.8 ppmv (-10%) to -0.2 (-2%), depending on season and latitude. Above 1 hPa, the biases decrease again and switch sign at around 0.4 hPa to 0.3 hPa. At 0.1 hPa there is a larger bias variation with season and latitude band. Here, the biases range between 0 ppmv and 0.9 ppmv (0% to 15%). Below 100 hPa a wide range of biases is observed, occasionally they exceed ±2 ppmv. The vast majority of the biases are negative. In relative terms they vary roughly between -40% and 10%.

5 Drift results

For the presentation of the drift results we choose a similar approach as for the bias results. First an example is shown, followed by a general assessment of the drifts in the observational database. After that we present data set specific drift results. Finally, we compare the drift results to those obtained from the comparisons of monthly zonal mean time series presented in the work by Khosrawi et al. (2018). This aims to quantify how dependent the drift results are upon the actual method to derive them.

As for the biases, the lower triangle of Fig. 2 provides an overview for which data set combinations drift comparisons were possible for any of the time-latitude bins considered in this work. In this context the yellow colour means that the overlap criterion of at least 36 months was not met and thus the drift results were not considered any further (see Sect 3.4). The overlap periods among the different data sets are shown in the lower triangle of Fig. 3. These numbers are based on the comparisons considering coincidences during all seasons and at all latitudes, maximising these periods. The longest overlap period is found between the two SMR data sets and amounts to 153 months. The comparisons of the SMR data sets to the ACE-FTS v3.5, MAESTRO and MLS data sets yield overlap periods periods beyond 120 months. The same is true for the comparisons of the ACE-FTS v3.5 data set to the MAESTRO and MLS data sets. Contrary, overlap periods of less than 40 months are on one hand found in the comparisons to the HIRDLS data set, which itself only comprises 39 months of data. On the other hand, the following comparisons have overlap periods between 36 months and 39 months: GOMOS vs. HALOE, GOMOS vs. SCIAMACHY lunar, HALOE vs. SCIAMACHY limb, POAM III vs. SCIAMACHY solar occultation, SAGE II vs. SCIAMACHY limb and SAGE III vs. SCIAMACHY limb.

5.1 Example

As example we consider the drift of the SMR 489 GHz data relative to other data sets in the latitude range from 30°N to 60°N. The drift estimates are shown in the left panel of Fig. 10. The right panel shows the corresponding significance levels, defined as the absolute ratio between the drift estimates and their associated uncertainties. In the legend for every data set two numbers are provided. The first number indicates the overlap period of the two data sets in months. As described in Sect. 3.4, a minimum overlap period of 36 months was required for a drift to be calculated. The second number shows during how many months the two data sets actually have a sufficient number of coincidences. Since this information is altitude-dependent the legend considers the maximum values over all altitudes. The example indicates mostly positive drifts for the SMR 489 GHz data set, which means that its trends in water vapour are more positive or less negative than the trend estimates derived from the other data sets. The drifts are clearly systematic. Even though the comparisons consider different time periods, and thus the estimates can vary, a very consistent picture of their altitude dependence is obtained. Pronounced drifts are observed around 50 hPa, which is close to the lower altitude limit where water vapour retrievals from SMR observations are possible. The drifts are as large as $2\,\mathrm{ppmv}\cdot\mathrm{decade}^{-1}$ and many of those are also statistically significant at the 2σ uncertainty level. Towards 20 hPa the drift estimates decrease to values smaller than 0.5 $\mathrm{ppmv}\cdot\mathrm{decade}^{-1}$. The comparisons to a few data sets even indicate negative drift estimates for the SMR 489 GHz data set. Above 20 hPa, the drifts increase again and maximise at around 0.5 hPa. Here, the drift estimates typically range from $1\,\mathrm{ppmv}\cdot\mathrm{decade}^{-1}$ to $1.75\,\mathrm{ppmv}\cdot\mathrm{decade}^{-1}$ and are in most cases statistically significant. An exception are HALOE and SAGE II for which drift estimates are even larger than $2\,\mathrm{ppmv}$. Above 0.5 hPa the drift estimates generally decrease again.

5.2 General results

Figure 11 shows the drift estimates from the full matrix of comparisons, similar to the bias results shown in Fig. 5. Again, these results consider the comparisons that incorporate coincidences during all seasons and at all latitudes. The upper panel shows the picture without the aggregation of the MIPAS results, the picture in the lower panel takes this aggregation into account. Overall, from the 862 comparisons (see Sect. 4.2) in the full matrix 470 comparisons yield drift results (see Fig. 2), with the chosen minimum overlap period of 36 months. In 450 comparisons drift estimates that are statistically significant at the 2σ uncertainty level are found. The estimates that are significant are marked in light blue in the figure. The picture without the aggregation of the MIPAS results indicates a wide range of drifts, in particular below 30 hPa and at 0.1 hPa. Some of the extreme values can be assigned to specific data sets. Between 30 hPa and 10 hPa the envelope of the drifts is smallest. Here, they are generally within $\pm 0.4\,\mathrm{ppmv}\cdot\mathrm{decade}^{-1}$. Also median-wise, in this altitude range the smallest drifts are observed. Beyond that, we find that there is some dependence between the overlap period and the absolute drift size. Based on results above 100 hPa, the drift size typically decreases with increasing overlap period for periods up to 70 months. Beyond that overlap period, there is no obvious connection.

The picture with the aggregation of the MIPAS results is clearly sparser than that without the aggregation. Mostly prominently this is visible in the lower mesosphere, similar to the corresponding picture for the biases shown in Fig. 5. In contrast to the unaggregated picture, a notable widening of the drift range at 0.1 hPa is not observed. At lower altitudes the picture is rather similar and the envelope of drifts exhibits a similar minimum region in the middle stratosphere. The typical drift sizes (based on the median) are typically larger for the picture with the aggregation of the MIPAS results, except above 0.2 hPa. Below 30 hPa the difference is of the order of $0.3\,\mathrm{ppmv}\cdot\mathrm{decade}^{-1}$. Above 20 hPa the difference is roughly $0.1\,\mathrm{ppmv}\cdot\mathrm{decade}^{-1}$.

In Fig. 12 drift histograms are shown for the different latitude bands, taking into account the aggregation of the MIPAS results. They consider the positive estimates from all altitudes that are statistically significant at the 2σ uncertainty level. In the upper right corner of the figure the number of available data points is indicated. Bins of ~~0.05~~0.1 ppmv · decade^{-1} are used for the histograms. The smallest drifts ~~occur in less than 1%of comparisons, consistently for all latitudes. Typically such small drifts are not statistically significant. Correspondingly the histograms do not resemble a Gaussian distribution, as typically found for the biases. Considering both statistically significant and non-significant results a more Gaussian-like picture is found (not shown here~~have the lowest occurrence rate in the Antarctic (about 2.5%) and Arctic (4%). In contrast, the largest occurrence rates are observed in the latitude bands from the Equator to 30°N (9.25%) and from 15°S to 15°N (10.25%). Beyond the smallest drift bin, the occurrence rates quickly rise. In fact, the maximum occurrence rates are observed for drifts between ~~0.05~~0.1 ppmv · decade^{-1} and 0.2 ppmv · decade^{-1}~~and vary between 7.5% and 9.5%. In particular, for the latitude bandsfrom 15~~, consistently for all latitude bands. The vary between 12.25% (60°S to ~~15~~30°~~N and from the Equator to~~ S and Antarctic) and 18% (30°S to Equator and 30°N ~~this maximum already occurs in the bin from 0.05 to 0.1~~ to 60°N). Towards larger drifts the occurrence rates generally decrease. However, there are some prominent additional maxima, for example in the Antarctic for drifts between ~~0.45~~0.4 ppmv · decade^{-1} and 0.5 ppmv · decade^{-1} (occurrence rate of ~~more than 7~~12%). For drifts of 1 ppmv · decade^{-1} the occurrence rate is between ~~1% and 2~~2.75% and 4.25%, except for the latitude bands from 15°S to 15°N and from the Equator to 30°N. In those latitude bands again pronounced additional maximum in the occurrence rate (~~between 3%~~ 7% to 7.5% for the bin between 1.0 ppmv · decade^{-1} and ~~4%~~ 1.1 ppmv · decade^{-1}) are visible. For drifts of 2 ppmv · decade^{-1} the occurrence rate is smaller than ~~1~~1.5% and minimises for the ~~latitude band from the Equator to 30N, by a small margin compared to the~~ Antarctic. Drifts larger 3 ppmv · decade^{-1} occur in 2% to 7.5% of the comparisons with the highest occurrence rate for the latitude band from 60°to 30°S and the lowest occurrence rate for the latitude band between 15°S and 15°N.

In the Supplement in Fig. ~~S9~~ S10 the corresponding picture without the aggregation of the MIPAS results is shown. In contrast to Fig. 12, the maximum occurrence rates are ~~a bit~~ larger (between ~~8% and 10~~14.5% and 19.25%). ~~For the Antarctic and Arctic the maximum occurrence rates just occur~~ Prominently, the maximum occurrence rate in the Antarctic is found first for drifts between 0.3 ppmv · decade^{-1} and ~~0.35~~0.4 ppmv · decade^{-1}. ~~For a number of latitude bands a double peak structure is visible, so that the drift range with large occurrence rates (i.e. >5%) is much wider on one hand. On the other hand, the~~ Also, for the latitude band from 30°N to 60°N and the Arctic the maximum occurrence rate is observed at larger drifts than for the aggregated results. Noteworthy secondary maxima in the occurrence rate are not visible in the results without the MIPAS aggregation. The occurrence rates for drifts larger than 1 ppmv · decade^{-1} are ~~much~~ on average smaller than for the picture with the aggregation of the MIPAS results. Also, the variation with increasing drifts and among the latitude bands is smaller in Fig. ~~S9~~S10.

5.3 Data set specific results

In this section we provide summaries of data set specific drift results, focusing on the MIPAS-ESA V7R (Fig. 13) and the MLS data sets (Fig. 14). All remaining results can be found in Fig. ~~S10~~ S11 in the Supplement. No results are available for the

ILAS-II, MIPAS V5H and SMILES data sets. These cover a too short time period for a drift analysis according to our criteria defined in Sect. 3.4. A summary figure for given data set shows all drifts that are statistically significant at the 2σ uncertainty level relative to this data set. For better distinction between the data sets results are only plotted at every second altitude, i.e. with a sampling of $\sim 1\,\mathrm{km}$ (see Sect. 3.3 as well as Figs. 4 and 10). The different panels focus on different latitude bands, as indicated in the upper left. For some of the data sets (e.g. GOMOS, HALOE, POAM III, see Supplement) there are occasionally no results for any of the latitude bands. In these cases there will be information explaining why, in accordance to the list below:

(1) "no comparisons": No comparisons to other data sets could be performed due to missing overlap (at least 20 coincidences, see Sect. 3.3).

(2) "no drift data": Comparisons to other data sets were performed, but yield no drift results. This is because the overlap period is too short or too few data points exist to derive drift estimates.

(3) "no significant results": Drifts were derived, but none of them is statistically significant at the 2σ uncertainty level.

(4) "significant results only outside the plot range": Statistically significant drifts were derived, but those are outside the plot range from $-3\,\mathrm{ppmv}\cdot\mathrm{decade}^{-1}$ to $3\,\mathrm{ppmv}\cdot\mathrm{decade}^{-1}$. This is already a large range that covers of the vast majority of reasonable estimates.

In the legend all possible data sets are listed. A colour-coding is used to convey extra information which data sets contribute results or not (on a global scale):

(1) dark grey: As "no comparisons" in the list above.

(2) light blue: As "no drift data" in the list above.

(3) dark red: As "significant results only outside the plot range" in the list above. This occurs only in a few comparisons (e.g. in the comparison between the GOMOS and SOFIE data sets) and concerns in these cases just a handful of data points. In the figures shown here in the main manuscript no such case occurs.

(4) black: The comparisons to these data sets yield drifts that are significant at the 2σ uncertainty level and, thus, these drift results are visible in the given summary figure.

The comparisons to the MIPAS-ESA V7R data set exhibit predominantly negative drifts as visible in Fig. 13. These negative drifts minimise in size typically around $20\,\mathrm{hPa}$ to $10\,\mathrm{hPa}$ (up to $-0.3\,\mathrm{ppmv}\cdot\mathrm{decade}^{-1}$ to $-0.4\,\mathrm{ppmv}\cdot\mathrm{decade}^{-1}$) and increase towards lower and higher altitudes. Around $50\,\mathrm{hPa}$ large negative drifts (beyond $-1\,\mathrm{ppmv}\cdot\mathrm{decade}^{-1}$) are observed relative to the SMR 489 GHz data set in all latitude bands. Below $100\,\mathrm{hPa}$ drifts of similar size are found more frequently relative to a number of data sets. In the mesosphere again the comparison to SMR 489 GHz data set yield large negative drifts. They often peak in size around $0.5\,\mathrm{hPa}$ (in the polar regions a bit higher up) with values between $-2\,\mathrm{ppmv}\cdot\mathrm{decade}^{-1}$ and $-1.2\,\mathrm{ppmv}\cdot\mathrm{decade}^{-1}$. At $0.1\,\mathrm{hPa}$ the negative drifts vary between $-1.6\,\mathrm{ppmv}\cdot\mathrm{decade}^{-1}$ and $-0.3\,\mathrm{ppmv}\cdot\mathrm{decade}^{-1}$, based on the comparisons to the other MIPAS V5R NOM, MLS and SMR 489 GHz data sets. Notable positive drifts (beyond $1\,\mathrm{ppmv}\cdot\mathrm{decade}^{-1}$) are found below $20\,\mathrm{hPa}$ relative to the HIRDLS, GOMOS, MAESTRO data sets at selected latitudes. Smaller positive drifts occur in the comparisons to the MIPAS V5R NOM data sets derived with the Bologna, IMKIAA and Oxford processors as well as some SCIAMACHY data sets. In the latitude bands from 90°S to 60°S and 60°S to 30°S drifts up to $0.5\,\mathrm{ppmv}\cdot\mathrm{decade}^{-1}$ are observed in the altitude range from $8\,\mathrm{hPa}$ to $1\,\mathrm{hPa}$ in the comparisons to the ACE-FTS, MLS and SCIAMACHY lunar (only Antarctic) data sets. Close to $0.1\,\mathrm{hPa}$ often pronounced positive drifts are found relative to the any of MIPAS-Bologna data sets (except in the latitude from 15°S to 15°N and 60°N to 90°N).

The MIPAS V5 data sets are prone to a small drift since the correction coefficients for the non-linearity in the detector response function have changed over time and this is not accounted for in the V5 calibration (Walker and Stiller, in preparation). In the MIPAS V7 calibration a time dependence of these coefficients is considered and, thus, data sets derived from this calibration are expected to show less drifts. Compared to its predecessor data set, i.e. MIPAS-ESA V5R NOM, the MIPAS-ESA V7R data set exhibits indeed a reduced number of significant drifts. Considering the comparisons to non-MIPAS data sets the number is reduced by 4.6%. If only comparisons to the ACE-FTS v3.5 and MLS data sets are taken into consideration the reduction amounts to 25%. In contrast to the MIPAS-ESA V7R data set, the MIPAS-ESA V5R NOM data set shows a predominance of positive drifts (see Fig. ~~S10~~ S11 in the Supplement). This might be a hint that the correction coefficients used in the MIPAS V7 calibration overcompensate the original issue in the V5 calibration.

The comparisons to the MLS data set (Fig. 14) yield both negative and positive drifts with a slight prevalence of the former. Typically the drift estimates are within $\pm0.5\,\mathrm{ppmv}\cdot\mathrm{decade}^{-1}$. Larger drifts are prominently found in the comparisons to the GOMOS (negative), HIRDLS (primarily positive) and SMR 489 GHz data sets, which highlights rather issues with these data sets than with the MLS data set itself. Positive drifts are consistently found relative to the ACE-FTS data set (around $0.2\,\mathrm{ppmv}\cdot\mathrm{decade}^{-1}$). A similar picture is observed in the comparisons to the SCIAMACHY solar occultation data sets. In the lower stratosphere the comparisons to the MIPAS-ESA V5R NOM (roughly up to about $60\,\mathrm{hPa}$), MIPAS-IMKIAA V5R NOM (up to about $10\,\mathrm{hPa}$) and MIPAS-Oxford V5R NOM (up to about $30\,\mathrm{hPa}$ to $20\,\mathrm{hPa}$) exhibit positive drift estimates. In the lower mesosphere the drifts are positive relative to the MIPAS-Bologna, MIPAS-ESA V7R (not in the Antarctic and from 60°S to 30°S) and the MIPAS-IMKIAA V5R NOM (except in the Antarctic) data sets. In addition, the comparisons to the SOFIE data set indicate positive drifts in the Antarctic (with a gap between $9\,\mathrm{hPa}$ and $1.5\,\mathrm{hPa}$) and the Arctic lower mesosphere. In contrast, negative drifts are found relative to the MIPAS-Bologna data sets below about $1\,\mathrm{hPa}$, the MIPAS-ESA data sets (except those positive drifts mentioned before), the V5R MA data sets derived with the IMKIAA and Oxford processors, the MIPAS-Oxford V5R NOM data set above about $30\,\mathrm{hPa}$ to $20\,\mathrm{hPa}$ as well as the SMR 489 GHz data set.

5.4 Method comparison

In this work we present drift results based on coincident observations. In a preceding WAVAS-II work we presented drift estimates among the different data sets based on the comparison of their zonal mean time series (Khosrawi et al., 2018). The latter approach has the advantage that more data can be used, typically also allowing more comparisons. The disadvantage of the zonal mean time series approach is that it is more prone to sampling errors (in time and space) and does not take into account differences in vertical resolution among the data sets, which, under circumstances, may influence the drift estimates. Here we want to compare the results from these two comparison methods and assess how often the drift estimates differ or not. For that Fig. 15 shows the drift estimates among the different data sets, calculated using the profile-to-profile method, in a matrix form considering data in the latitude band from 80°S to 70°S at 80 hPa, 10 hPa, 3 hPa and 0.1 hPa (from top to bottom). The drift estimates are based on the difference time series between the data sets given at the x-axis and the data sets given at the y-axis. Data sets are only shown if they yield any result at a given altitude to optimise the available space. The drift estimates are colour-coded. In addition to that, different types of auxiliary information are provided in the result boxes. In the upper left the overlap period of the two data sets is given as well as the number of months the data sets actually overlap. A non-significant drift (at the 2σ uncertainty level) is indicated by a slant. For contrast a significant drift is marked by a green frame and the significance level is noted in the lower right corner. As such the figure is directly comparable to Fig. 11 shown in the work of Khosrawi et al. (2018). Both figures exhibit a number of similar patterns. At 0.1 hPa the drift size is the largest among the four altitudes with prominent examples in the comparisons relative to the MIPAS-Bologna V5R MA and SMR 489 GHz data sets. At 3 hPa the large drifts relative to SMR 489 GHz are again a common feature among the two drift estimation methods. Smaller drift sizes are observed both at 10 hPa and 80 hPa with exceptions attributed to the same data sets.

For a more quantitative comparison, Fig. 16 shows in the same style as Fig. 15 the actual drift differences $\Delta C_{\mathrm{drift}}$ between the two approaches, i.e.:

$$\Delta C_{\mathrm{drift}}(\phi, z) = C^{\mathrm{p2p}}_{\mathrm{drift}}(\phi, z) - C^{\mathrm{zmts}}_{\mathrm{drift}}(\phi, z) \tag{13}$$

Here, $C^{\mathrm{p2p}}_{\mathrm{drift}}$ represents the drifts derived from the profile-to-profile comparisons (this work) and $C^{\mathrm{zmts}}_{\mathrm{drift}}$ the drifts based on the comparisons of the zonal mean time series (Khosrawi et al., 2018). The uncertainty of this difference $\varepsilon_{\mathrm{drift}}$ is given by:

$$\varepsilon_{\mathrm{drift}}(\phi, z) = \sqrt{\varepsilon^{\mathrm{p2p}}_{\mathrm{drift}}(z)^2 + \varepsilon^{\mathrm{zmts}}_{\mathrm{drift}}(\phi, z)^2} \tag{14}$$

where $\varepsilon^{\mathrm{p2p}}_{\mathrm{drift}}$ and $\varepsilon^{\mathrm{zmts}}_{\mathrm{drift}}$ are the drift uncertainties from the two approaches and any covariance among them is neglected. The characteristic numbers in the result boxes of Fig. 16 correspond to the profile-to-profile comparisons. Differences not statistically significant at the 2σ uncertainty level are again marked by a slant while for significant differences the significance level is once more provided in the lower right corner. The largest differences between the drift estimates from the two approaches occur at 0.1 hPa and amount to $0.4\,\mathrm{ppmv}\cdot\mathrm{decade}^{-1}$ on average. Prominent examples are visible in comparisons to the ACE-FTS v3.5, SMR 489 GHz and SOFIE data sets. Also, some comparisons among MIPAS data sets exhibit large differences in the drift estimates. ~~However, only for the comparison between the MIPAS-ESA V5R MA and MIPAS-Oxford V5R NOM data sets the difference (2) is statistically significant, however just barely (significance level is 2.01).~~ In contrast, at 3 hPa the drift differences minimise among the four altitudes shown in Fig. 16 (on average $0.15\,\mathrm{ppmv}\cdot\mathrm{decade}^{-1}$). Also, at ~~this altitude there is just one comparison for which the drift estimates obtained from the profile-to-profile and zonal mean time series comparisons differ significantly at the 2σ uncertainty level, namely for that between the MIPAS-IMKIAA V5R NOM and the~~

~~MIPAS-Oxford V5R MA data sets. Again, the significance level is not that large, amounting to 2.1. Larger, non-significant differences are found in comparisons to the ACE-FTS v3.5 and SMR 489 GHz data sets. A similar picture is found at~~ 10 hPa ~~. Comparisons to the SMR 544~~and 80 ~~GHz data set indicate more prominent~~ hPa relatively small differences in the drift estimates from the two approaches ~~. However significant differences are once more restricted to one comparison. In this case it concerns the comparison between the ACE-FTS v3.5 and MLS data sets. The difference is rather small with 0.15 and the significance levels is again just above 2σ, i.e. 2.01. At 80 the comparisons between~~ are found. A few noteworthy exceptions occur in comparisons to the SMR 544 GHz and ~~MIPAS data setsyield significant differences in the drift estimates from the two approaches. They vary between 1 and 2.5 and have significance levels from 2.2 to 4.6. Overall, in just 2.6% of the comparisons shown in Fig. 16 the~~ SOFIE data sets. Even though the drift estimates derived from the profile-to-profile and zonal mean time series comparisons ~~differ significantly~~ occasionally exhibit larger differences, they are only statistically significant (at the 2σ uncertainty level~~.~~

) in 2.6% of the comparisons shown in Fig. 16.

The zonal mean time series comparisons presented by Khosrawi et al. (2018) consider in addition the latitude bands from 15°S to 15°N and from 50°N to 60°N. For these latitude bands the figures corresponding to Figs. 15 and 16 are shown in the Supplement (see Figs. ~~S11~~S12/~~12~~13 and ~~S13~~S14/~~14~~15). In summary, for the tropical band the drift differences maximise on average at 80 hPa, close the top of the highly variable tropical tropopause layer. The minimum differences are observed at 3 hPa, as for the latitude band from 80°S to 70°S. In total, in 6.0% of the comparisons the drift estimates from the two approaches differ significantly. For the latitude band from 50°N to 60°N the differences are largest at 0.1 hPa and smallest at 3 hPa. In 3.8% of the comparisons the drift differences are significant at the 2σ uncertainty level in this latitude band.

For the eight latitude bands primarily considered in this work and altitudes above 100 hPa, overall, in 3.2% of the comparisons the drift estimates derived with the profile-to-profile and zonal mean time series comparisons differ at the 2σ uncertainty level. ~~The~~ On average, the differences in the drift estimates are largest for comparisons among occultation data sets (i.e. ACE-FTS, GOMOS, HALOE MAESTRO, POAM, SAGE, SCIAMACHY occultation and SOFIE). For the remaining data sets with more dense temporal and spatial sampling (i.e. HIRDLS, MIPAS, MLS, SCIAMACHY limb, SMR) the differences are clearly smaller. At the same time the percentage of significant differences in the drift estimates is smallest for comparisons between the occultation data sets and largest for comparisons between more dense data sets. Comparisons between occultation and more dense data sets yield statistics in the middle.

Overall, the differences in the drift estimates from the two approaches minimise in the altitude range between 5 hPa and 2 hPa (typically, based on the median, between 0.05 $\mathrm{ppmv \cdot decade^{-1}}$ and 0.1 $\mathrm{ppmv \cdot decade^{-1}}$). The largest differences are observed towards 100 hPa and 0.1 hPa (typically beyond 0.15 $\mathrm{ppmv \cdot decade^{-1}}$ median-wise). For individual comparisons the differences between the drift estimates derived with the profile-to-profile and zonal mean time series comparisons can be significantly larger, as visible in the example shown in Fig. 16.

6 Conclusions

In this work biases and drifts among 33 data sets of stratospheric and lower mesospheric water vapour, from 15 different satellite instruments, were assessed using profile-to-profile comparisons. Typically, this observational database exhibits the largest biases below 70 hPa, both in absolute and relative terms (see Figs. 5 and 6). In contrast, the lowest biases are generally observed between 70 hPa and 5 hPa. Based on the 50% percentile (median) over the different comparison results the typical biases vary between 0.25 ppmv and 0.5 ppmv (5% to 10%) in this altitude region. The smallest biases occur here at low and mid latitudes. Higher up, the biases generally increase accompanied by considerable variations with altitude and latitude band. Typical bias values range from 0.3 ppmv to 1 ppmv (4% to 20%), again based on the 50% percentile. ~~Bias histograms~~ Histograms considering comparison results from all altitudes ~~have the form of a Gaussian~~ show the largest occurrence rates for biases up to 0.2 ppmv or 5% (see Fig. 7). For other altitude regions ~~this characteristics is not always given~~ (see Figs. ~~S5~~S6 to ~~S7)~~ S8) this behaviour is not is always found, most prominently in the altitude range from 10 hPa to 1 hPa. There is no simple picture which latitude band yields the highest (lowest) occurrences for low (high) biases and vice versa.

~~In our assessment we find a number of noteworthy~~ Besides a general assessment of the biases in the observational database we focused in our work also on data set specific ~~biases~~ issues (see Figs. 8~~ and S8~~, 9 and S9). The most noteworthy data set specific biases are listed below:

- In the upper stratosphere the ACE-FTS data sets show slightly more pronounced negative biases (roughly up to -0.5 ppmv or −10%).

- The GOMOS data set shows clear negative biases (exceeding −1.5 ppmv) above 50 hPa with pronounced variations among the different latitude bands considered in this work as well as season.

- In the lower mesosphere the HALOE data set shows large negative biases of about −1 ppmv (−15%).

- The HIRDLS data set shows distinct positive biases around 100 hPa (roughly around 1 ppmv ~~and~~ or 20%). Towards the upper limit of this data set at 10 hPa its biases also show a pronounced latitudinal dependence.

- In the middle and upper stratosphere the ILAS-II data set exhibits notable negative biases (around −0.8 ppmv).

- For the MAESTRO data set the biases deteriorate at its upper end close to 40 hPa. Already below, the biases in the tropics and subtropics exceed 1 ppmv (20%) on many occasions.

- The MIPAS-Bologna V5R data sets show more pronounced biases around 2 hPa (about 0.4 ppmv or 8%). Close to 0.1 hPa the biases of all Bologna data sets are clearly negative in most seasons and latitude bands (often exceeding −1 ppmv or −25%).

  Similar to the MIPAS-Bologna V5R data sets, the MIPAS-ESA V5R data sets exhibit notable positive biases (peaking roughly about 0.5 ppmv or 10%) in the upper stratosphere. For the MIPAS-ESA V7R data set such biases are observed in the middle stratosphere. The MIPAS-ESA V5H data set shows distinct negative biases close to 0.1 hPa, as noted for the Bologna data sets.

The MIPAS-IMKIAA V5R NOM data set also exhibits distinct negative biases close to 0.1 hPa in numerous seasons and latitude bands (can be as large as -1 ppmv or -25%). Such a behaviour is also visible in the MIPAS-IMKIAA V5R MA data set but not as pronounced.

In the upper stratosphere and lower mesosphere the MIPAS-Oxford V5H data sets shows substantial positive biases, with a pronounced seasonal and latitudinal variation. At 1 hPa the biases vary around 1 ppmv (15%), while at 0.1 hPa they are clearly larger. Similar to a number of MIPAS data sets, the MIPAS-Oxford V5H NOM data set exhibit notable positive biases in the upper stratosphere (also peaking roughly around 0.5 ppmv or 10%). The MIPAS-Oxford V5R MA data set shows prominent positive biases at almost all latitudes. They roughly amount to around 0.5 ppmv (10%), with larger estimates close to 0.1 hPa.

- The biases for the MLS data set are mostly positive and typically smaller than 0.4 ppmv (roughly 8%). Exceptions exist below 100 hPa and close to 0.1 hPa.

- The POAM data set shows a distinct positive bias in the lower stratosphere (around 0.8 ppmv or 15%).

- Around 1 hPa the biases of SAGE II data set are of the order of 1 ppmv (15%).

- Both SMILES data sets show large biases with both signs in the small altitude range where this data data set provides coverage (slightly above 200 hPa to 50 hPa).

- The biases of the SCIAMACHY limb data set are clearly negative (roughly -15%) at the upper end (about 30 hPa) and positive (roughly 25%) at the lower end (somewhat below 200%). The other three data sets derived from the SCIAMACHY observations are mostly positive. Most pronounced they are for the solar occultation data sets in the middle and upper stratosphere (around 0.5 ppmv or 10%).

- In the lower stratosphere the SMR 544 GHz data sets show pronounced negative biases, often in excess of -1.2 ppmv (-35%). Similarly, the other SMR data set in this assessment, based on water vapour emissions at 489 GHz, exhibits notable negative biases in the upper stratosphere and lower mesosphere. These biases occasionally exceed -1 ppmv (-15%).

- In the uppermost stratosphere and lower mesosphere the biases of the SOFIE data set are slightly more pronounced (roughly around -0.5 ppmv or -8%).

For the drift assessment we considered a minimum overlap period of 36 months for the data sets compared with each other. Overall, the observational database shows a wide range of drifts that are statistically significant at the 2σ uncertainty level. In general, the smallest drifts are found between about 30 hPa to 10 hPa. In this altitude region the drifts typically do not exceed 0.25 ppmv $\cdot$ decade^{-1} (0.40 ppmv $\cdot$ decade^{-1}) for the aggregated (unaggregated) global comparisons (see Fig. 11). For other latitude bands the maximum drifts are slightly larger. Histograms considering statistically significant results from all altitudes indicate the largest occurrence for drifts between ~~0.05~~0.1 ppmv $\cdot$ decade^{-1} and ~~0.3~~0.2 ppmv $\cdot$ decade^{-1}.

~~All data sets that allowed a drift assessment drifted significantly with respect to at least one other data set.~~ While the comparison of two data sets does not immediately indicate which data set is responsible for any observed drift, comparisons to a multitude of data sets have the potential to obtain a clearer picture. In our analysis the data sets with the most prominent drifts are~~the GOMOS (primarily negative), HIRDLS (negative), MAESTRO (negative),~~ :

- GOMOS – primarily negative drifts
- HIRDLS – negative drifts
- MAESTRO – negative drifts
- SMR 544 GHz and SMR 489 GHz ~~(positive) data sets.~~ – positive drifts

Other noteworthy results are:

- For the MIPAS V5 data sets a small drift has been expected (Walker and Stiller, in preparation) and is also detected. This can be explained with the calibration of these data sets, which does not account for any time dependence of the correction coefficients for the non-linearity in the detector response. These data sets show primarily positive drifts in the stratosphere, the only exception is the IMKAA V5R NOM data set which exhibits mostly negative drifts. The V7 calibration of the MIPAS data implements a time dependence of the correction coefficients. For the MIPAS-ESA V7R data set the number of significant drifts is indeed reduced compared to the MIPAS-ESA V5R NOM, which is the direct predecessor. The reduction is nearly 5% for the comparisons to non-MIPAS data sets and 25% for the comparisons to the ACE-FTS v3.5 and MLS data sets. The majority of drift estimates for the MIPAS-ESA V7R data set are however negative, in contrast to the predecessor data set. This might suggest that the new correction coefficients implemented in the MIPAS v7 calibration overcompensate the original drift issue. In general, the stratospheric drift estimates for the MIPAS data sets are roughly within $\pm 0.5\,\mathrm{ppmv} \cdot \mathrm{decade}^{-1}$. ~~A similar range can be also reported the~~
- Also for the ACE-FTS, MLS, SCIAMACHY and SOFIE data sets a drift range roughly within $\pm 0.5\,\mathrm{ppmv} \cdot \mathrm{decade}^{-1}$ can be reported. For the MLS data set almost an equivalence of positive and negative drifts is observed. The drift estimates for the data sets from the other three instruments are primarily negative.
- For the HALOE, POAM III, SAGE II, SAGE III data sets only a limited drift assessment is possible. This is because there are only a few data sets which have sufficiently long overlap periods for a drift estimation. Among them are the SMR data sets that have their own issues. Beyond that there is not always consistency in the results which would provide more certainty towards any potential problem for these four data sets.

Finally, we compared our drift estimates to those derived from comparisons of zonal mean time series as presented by Khosrawi et al. (2018). Our profile-to-profile comparisons have the advantage that they minimise sampling errors among the data sets to be compared. Also, differences in the vertical resolution of the data sets can be taken into account. Comparisons of zonal mean time series typically allow more data to be included, potentially yielding more comparisons. ~~For the~~ In our analysis we found that the differences among the drift estimates from the two approaches are in general largest for comparisons among occultation data sets. For comparisons between data sets with more dense temporal and spatial sampling the differences are on average smaller, however the percentage of statistically significant (at 2σ uncertainty level) differences is larger. For the three latitude bands (80°S – 70°S, 15°S – 15°N and 50°N – 60°N) and four altitudes (80 hPa, 10 hPa, 3 hPa and 0.1 hPa) considered in the work of Khosrawi et al. (2018) we found that only in 2.6% to 6.0% of the comparisons the drift estimates derived from the profile-to-profile and zonal mean time series comparisons differed significantly at the 2σ uncertainty level. For the eight latitude bands primarily considered in this work and for altitudes above 100 hPa statistically significant drift differences occurred in 3.2% of the comparisons. Hence, there is largely no need for a specific approach to derive the drift estimates.

In our work consider 13 MIPAS data sets, out 33 data sets in total. Even though, they are based on different measurement modes and processors with different retrieval choices, they exhibit some relative similarity with respect to the remaining data sets. This behaviour has obvious effects on our results and conclusions. Therefore, the general results and the bias summaries of the individual data sets presented in this work consider an aggregation of the results obtained from MIPAS data sets (see Sect. 3.5). With this aggregation the bias percentiles typically exhibit larger values and a smaller occurrence rate for the smallest biases is observed. In addition, the results vary stronger among the different seasons and latitude bands.

Overall, we find that many data sets are useful for scientific analyses, either considering the observational data themselves or in connection with modelling results. For scientific studies where the absolute amount of water vapour is the key the data sets listed above with bias issues should be used with caution. Likewise, those data sets mentioned with drift issues should be treated with care if variability beyond 36 months is of interest. Combining the bias and drift characteristics found in this work the altitude range between 50 hPa and 5 hPa shows the least number of issues in the observational database, making it most optimal place for scientific analyses regarding stratospheric and lower mesospheric water vapour.

Data availability. Results from WAVAS-II activity can be found on the following website: https://zenodo.org/communities/wavas-ii/

Competing interests. The authors declare that they have no conflict of interest.

Acknowledgements. The Atmospheric Chemistry Experiment (ACE), also known as SCISAT, is a Canadian-led mission mainly supported by the Canadian Space Agency and the Natural Sciences and Engineering Research Council of Canada. We appreciate the HALOE Science Team and the many members of the HALOE project for producing and characterising the high quality HALOE data set. We would like to thank the European Space Agency for making the MIPAS level-1b data set available. MLS data were obtained from the NASA Goddard Earth Sciences and Information Center. Work at the Jet Propulsion Laboratory, California Institute of Technology, was done under contract with the National Aeronautics and Space Administration. SCIAMACHY spectral data have been provided by ESA. M. García-Comas was financially supported by the MINECO under its “Ramon y Cajal" subprogramme, project ESP2014-54362-P and EC FEDER funds. S. Lossow was funded by the

“Stratospheric Change and its Role for Climate Prediction” (SHARP) under contract STI 210/9-2. Thanks to Hauke Schmidt for providing the HAMMONIA data used for the convolution of higher vertically resolved data sets. We would like to thank two anonymous referees for their helpful comments on the paper. We want to express our gratitude to SPARC and WCRP (World Climate Research Programme) for their guidance, sponsorship and support of the WAVAS-II programme.

The article processing charges for this open-access publication were covered by a Research Centre of the Helmholtz Association.

References

Azam, F., Bramstedt, K., Rozanov, A., Weigel, K., Bovensmann, H., Stiller, G. P., and Burrows, J. P.: SCIAMACHY lunar occultation water vapor measurements: retrieval and validation results, Atmospheric Measurement Techniques, 5, 2499 – 2513, https://doi.org/10.5194/amt-5-2499-2012, 2012.

Baron, P., Urban, J., Sagawa, H., Möller, J., Murtagh, D. P., Mendrok, J., Dupuy, E., Sato, T. O., Ochiai, S., Suzuki, K., Manabe, T., Nishibori, T., Kikuchi, K., Sato, R., Takayanagi, M., Murayama, Y., Shiotani, M., and Kasai, Y.: The Level 2 research product algorithms for the Superconducting Submillimeter-Wave Limb-Emission Sounder (SMILES), Atmospheric Measurement Techniques, 4, 2105 – 2124, https://doi.org/10.5194/amt-4-2105-2011, 2011.

Bevilacqua, R. M., Kriebel, D. L., Pauls, T. A., Aellig, C. P., Siskind, D. E., Daehler, M., Olivero, J. J., Puliafito, S. E., Hartmann, G. K., Kämpfer, N., Berg, A., and Croskey, C. L.: MAS measurements of the latitudinal distribution of water vapor and ozone in the mesosphere and lower thermosphere, Geophysical Research Letters, 23, 2317 – 2320, https://doi.org/10.1029/96GL01119, 1996.

Brasseur, G. and Solomon, S.: Aeronomy of the middle atmosphere, Springer, ISBN-10 1-4020-3284-6, P.O. Box 17, 3300 AA Dordrecht, The Netherlands, 2005.

Brewer, A. W.: Evidence for a world circulation provided by the measurements of helium and water vapour distribution in the stratosphere, Quarterly Journal of the Royal Meteorological Society, 75, 351 – 363, https://doi.org/10.1002/qj.49707532603, 1949.

Carleer, M. R., Boone, C. D., Walker, K. A., Bernath, P. F., Strong, K., Sica, R. J., Randall, C. E., Vömel, H., Kar, J., Höpfner, M., Milz, M., von Clarmann, T., Kivi, R., Valverde-Canossa, J., Sioris, C. E., Izawa, M. R. M., Dupuy, E., McElroy, C. T., Drummond, J. R., Nowlan, C. R., Zou, J., Nichitiu, F., Lossow, S., Urban, J., Murtagh, D. P., and Dufour, D. G.: Validation of water vapour profiles from the Atmospheric Chemistry Experiment (ACE), Atmospheric Chemistry & Physics Discussions, 8, 4499 – 4559, 2008.

Connor, B. J., Siskind, D. E., Tsou, J. J., Parrish, A., and Remsberg, E. E.: Ground-based microwave observations of ozone in the upper stratosphere and mesosphere, Journal of Geophysical Research, 99, 16 757 – 16 770, https://doi.org/10.1029/94JD01153, 1994.

Dessler, A. E., Schoeberl, M. R., Wang, T., Davis, S. M., and Rosenlof, K. H.: Stratospheric water vapor feedback, Proceedings of the National Academy of Science, 110, 18 087 – 18 091, https://doi.org/10.1073/pnas.1310344110, 2013.

Dupuy, E., Walker, K. A., Kar, J., Boone, C. D., McElroy, C. T., Bernath, P. F., Drummond, J. R., Skelton, R., McLeod, S. D., Hughes, R. C., Nowlan, C. R., Dufour, D. G., Zou, J., Nichitiu, F., Strong, K., Baron, P., Bevilacqua, R. M., Blumenstock, T., Bodeker, G. E., Borsdorff, T., Bourassa, A. E., Bovensmann, H., Boyd, I. S., Bracher, A., Brogniez, C., Burrows, J. P., Catoire, V., Ceccherini, S., Chabrillat, S., Christensen, T., Coffey, M. T., Cortesi, U., Davies, J., de Clercq, C., Degenstein, D. A., de Mazière, M., Demoulin, P., Dodion, J., Firanski, B., Fischer, H., Forbes, G., Froidevaux, L., Fussen, D., Gerard, P., Godin-Beekmann, S., Goutail, F., Granville, J., Griffith, D., Haley, C. S., Hannigan, J. W., Höpfner, M., Jin, J. J., Jones, A., Jones, N. B., Jucks, K., Kagawa, A., Kasai, Y., Kerzenmacher, T. E., Kleinböhl, A., Klekociuk, A. R., Kramer, I., Küllmann, H., Kuttippurath, J., Kyrölä, E., Lambert, J., Livesey, N. J., Llewellyn, E. J., Lloyd, N. D., Mahieu, E., Manney, G. L., Marshall, B. T., McConnell, J. C., McCormick, M. P., McDermid, I. S., McHugh, M., McLinden, C. A., Mellqvist, J., Mizutani, K., Murayama, Y., Murtagh, D. P., Oelhaf, H., Parrish, A., Petelina, S. V., Piccolo, C., Pommereau, J., Randall, C. E., Robert, C., Roth, C., Schneider, M., Senten, C., Steck, T., Strandberg, A., Strawbridge, K. B., Sussmann, R., Swart, D. P. J., Tarasick, D. W., Taylor, J. R., Tétard, C., Thomason, L. W., Thompson, A. M., Tully, M. B., Urban, J., Vanhellemont, F., Vigouroux, C., von Clarmann, T., von der Gathen, P., von Savigny, C., Waters, J. W., Witte, J. C., Wolff, M., and Zawodny, J. M.: Validation of ozone measurements from the Atmospheric Chemistry Experiment (ACE), Atmospheric Chemistry & Physics, 9, 287 – 343, https://doi.org/10.5194/acp-9-287-2009, 2009.

Efron, B.: Bootstrap methods: Another look at the jackknife, The Annals of Statistics, 7, 1 – 26, 1979.

Fahey, D. W., Kelly, K. K., Kawa, S. R., Tuck, A. F., and Loewenstein, M.: Observations of denitrification and dehydration in the winter polar stratospheres, Nature, 344, 321 – 324, https://doi.org/10.1038/344321a0, 1990.

Feofilov, A. G., Kutepov, A. A., Pesnell, W. D., Goldberg, R. A., Marshall, B. T., Gordley, L. L., García-Comas, M., López-Puertas, M., Manuilova, R. O., Yankovsky, V. A., Petelina, S. V., and Russell, J. M.: Daytime SABER/TIMED observations of water vapor in the mesosphere: retrieval approach and first results, Atmospheric Chemistry & Physics, 9, 8139 – 8158, 2009.

Frank, F., Jöckel, P., Gromov, S., and Dameris, M.: Investigating the yield of H_2O and H_2 from methane oxidation in the stratosphere, Atmospheric Chemistry & Physics, 18, 9955 – 9973, https://doi.org/10.5194/acp-18-9955-2018, 2018.

Fueglistaler, S., Dessler, A. E., Dunkerton, T. J., Folkins, I., Fu, Q., and Mote, P. W.: Tropical tropopause layer, Reviews of Geophysics, 47, RG1004, https://doi.org/10.1029/2008RG000267, 2009.

Gille, J., Grey, L., Cavanaugh, C., Coffey, M., Dean, V., Halvorson, C., Karol, S., Khosravi, R., Kinnison, D., Massie, S., Nardi, B., Rivas, M. B., , Smith, L., Torpy, B., Waterfall, A., and Wright, C.: HIRDLS data description and quality version 7, http://docserver.gesdisc.eosdis.nasa.gov/repository/Mission/HIRDLS/3.3_Product_Documentation/3.3.5_Product_Quality/HIRDLS-DQD_V7.pdf, Last access: 17 January 2018, 2013.

Goss-Custard, M., Remedios, J. J., Lambert, A., Taylor, F. W., Rodgers, C. D., Lopez-Puertas, M., Zaragoza, G., Gunson, M. R., Suttie, M. R., Harries, J. E., and Russell, J. M.: Measurements of water vapor distributions by the improved stratospheric and mesospheric sounder: Retrieval and validation, Journal of Geophysical Research, 101, 9907 – 9928, https://doi.org/10.1029/95JD02032, 1996.

Griesfeller, A., von Clarmann, T., Griesfeller, J., Höpfner, M., Milz, M., Nakajima, H., Steck, T., Sugita, T., Tanaka, T., and Yokota, T.: Intercomparison of ILAS-II version 1.4 and version 2 target parameters with MIPAS-Envisat measurements, Atmospheric Chemistry & Physics, 8, 825 – 843, 2008.

Gunson, M. R., Farmer, C. B., Norton, R. H., Zander, R., and Rinsland, C. P.: Measurements of CH_4, N_2O, CO, H_2O, and O_3 in the middle atmosphere by the Atmospheric Trace Molecule Spectroscopy experiment on Spacelab 3, Journal of Geophysical Research, 95, 13 867 – 13 882, https://doi.org/10.1029/JD095iD09p13867, 1990.

Haefele, A., Hocke, K., Kämpfer, N., Keckhut, P., Marchand, M., Bekki, S., Morel, B., Egorova, T., and Rozanov, E.: Diurnal changes in middle atmospheric H_2O and O_3: Observations in the Alpine region and climate models, Journal of Geophysical Research, 113, D17 303, https://doi.org/10.1029/2008JD009892, 2008.

Harries, J. E., Russell, J. M., Tuck, A. F., Gordley, L. L., Purcell, P., Stone, K., Bevilacqua, R. M., Gunson, M., Nedoluha, G., and Traub, W. A.: Validation of measurements of water vapor from the Halogen Occultation Experiment (HALOE), Journal of Geophysical Research, 101, 10 205 – 10 216, https://doi.org/10.1029/95JD02933, 1996.

Hegglin, M. I., Tegtmeier, S., Anderson, J., Froidevaux, L., Fuller, R., Funke, B., Jones, A., Lingenfelser, G., Lumpe, J., Pendlebury, D., Remsberg, E., Rozanov, A., Toohey, M., Urban, J., Clarmann, T., Walker, K. A., Wang, R., and Weigel, K.: SPARC Data Initiative: Comparison of water vapor climatologies from international satellite limb sounders, Journal of Geophysical Research, 118, 11 824, https://doi.org/10.1002/jgrd.50752, 2013.

Holton, J. R., Haynes, P. H., McIntyre, M. E., Douglass, A. R., Rood, R. B., and Pfister, L.: Stratosphere-troposphere exchange, Reviews of Geophysics, 33, 403 – 439, https://doi.org/10.1029/95RG02097, 1995.

Jones, A., Walker, K. A., Jin, J. J., Taylor, J. R., Boone, C. D., Bernath, P. F., Brohede, S., Manney, G. L., McLeod, S., Hughes, R., and Daffer, W. H.: Technical Note: A trace gas climatology derived from the Atmospheric Chemistry Experiment Fourier Transform Spectrometer (ACE-FTS) data set, Atmospheric Chemistry & Physics, 12, 5207 – 5220, https://doi.org/10.5194/acp-12-5207-2012, 2012.

Kanzawa, H., Schiller, C., Ovarlez, J., Camy-Peyret, C., Payan, S., Jeseck, P., Oelhaf, H., Stowasser, M., Traub, W. A., Jucks, K. W., Johnson, D. G., Toon, G. C., Sen, B., Blavier, J.-F., Park, J. H., Bodeker, G. E., Pan, L. L., Sugita, T., Nakajima, H., Yokota, T., Suzuki, M., Shiotani, M., and Sasano, Y.: Validation and data characteristics of water vapor profiles observed by the Improved Limb Atmospheric Spectrometer (ILAS) and processed with the version 5.20 algorithm, Journal of Geophysical Research, 107, 8217, https://doi.org/10.1029/2001JD000881, 2002.

Kelly, K. K., Tuck, A. F., Murphy, D. M., Proffitt, M. H., Fahey, D. W., Jones, R. L., McKenna, D. S., Loewenstein, M., Podolske, J. R., Strahan, S. E., Ferry, G. V., Chan, K. R., Vedder, J. F., Gregory, G. L., Hypes, W. D., McCormick, M. P., Browell, E. V., and Heidt, L. E.: Dehydration in the lower Antarctic stratosphere during late winter and early spring, 1987, Journal of Geophysical Research, 94, 11 317 – 11 357, https://doi.org/10.1029/JD094iD09p11317, 1989.

Khosrawi, F., Lossow, S., Stiller, G. P., Rosenlof, K. H., Urban, J., Burrows, J. P., Damadeo, R. P., Eriksson, P., García-Comas, M., Gille, J. C., Kasai, Y., Kiefer, M., Nedoluha, G. E., Noël, S., Raspollini, P., Read, W. G., Rozanov, A., Sioris, C. E., Walker, K. A., and Weigel, K.: The SPARC water vapour assessment II: comparison of stratospheric and lower mesospheric water vapour time series observed from satellites, Atmospheric Measurement Techniques, 11, 4435 – 4463, https://doi.org/10.5194/amt-11-4435-2018, 2018.

Kley, D., Russell, J. M., and Philips, C.: Stratospheric Processes and their Role in Climate (SPARC) - Assessment of upper tropospheric and stratospheric water vapour, SPARC Report 2, WMO/ICSU/IOC World Climate Research Programme, Geneva, 2000.

Lahoz, W. A., O'Neill, A., Carr, E. S., Harwood, R. S., Froidevaux, L., Read, W. G., Waters, J. W., Kumer, J. B., Mergenthaler, J. L., Roche, A. E., Peckham, G. E., and Swinbank, R.: Three-Dimensional Evolution of Water Vapor Distributions in the Northern Hemisphere Stratosphere as Observed by the MLS., Journal of the Atmospheric Sciences, 51, 2914 – 2930, https://doi.org/10.1175/1520-0469(1994)051<2914:TDEOWV>2.0.CO;2, 1994.

Le Texier, H., Solomon, S., and Garcia, R. R.: The role of molecular hydrogen and methane oxidation in the water vapour budget of the stratosphere, Quarterly Journal of the Royal Meteorological Society, 114, 281 – 295, https://doi.org/10.1002/qj.49711448002, 1988.

Lossow, S., Khosrawi, F., Nedoluha, G. E., Azam, F., Bramstedt, K., Burrows, J. P., Dinelli, B. M., Eriksson, P., Espy, P. J., García-Comas, M., Gille, J. C., Kiefer, M., Noël, S., Raspollini, P., Read, W. G., Rosenlof, K. H., Rozanov, A., Sioris, C. E., Stiller, G. P., Walker, K. A., and Weigel, K.: The SPARC water vapour assessment II: comparison of annual, semi-annual and quasi-biennial variations in stratospheric and lower mesospheric water vapour observed from satellites, Atmospheric Measurement Techniques, 10, 1111 – 1137, https://doi.org/10.5194/amt-10-1111-2017, 2017.

Milz, M., Clarmann, T. V., Bernath, P., Boone, C., Buehler, S. A., Chauhan, S., Deuber, B., Feist, D. G., Funke, B., Glatthor, N., Grabowski, U., Griesfeller, A., Haefele, A., Höpfner, M., Kämpfer, N., Kellmann, S., Linden, A., Müller, S., Nakajima, H., Oelhaf, H., Remsberg, E., Rohs, S., Russell, J. M., Schiller, C., Stiller, G. P., Sugita, T., Tanaka, T., Vömel, H., Walker, K., Wetzel, G., Yokota, T., Yushkov, V., and Zhang, G.: Validation of water vapour profiles (version 13) retrieved by the IMK/IAA scientific retrieval processor based on full resolution spectra measured by MIPAS on board Envisat, Atmospheric Measurement Techniques, 2, 379 – 399, 2009.

Montoux, N., Hauchecorne, A., Pommereau, J.-P., Lefèvre, F., Durry, G., Jones, R. L., Rozanov, A., Dhomse, S., Burrows, J. P., Morel, B., and Bencherif, H.: Evaluation of balloon and satellite water vapour measurements in the Southern tropical and subtropical UTLS during the HIBISCUS campaign, Atmospheric Chemistry & Physics, 9, 5299 – 5319, 2009.

Mote, P. W., Rosenlof, K. H., McIntyre, M. E., Carr, E. S., Gille, J. C., Holton, J. R., Kinnersley, J. S., Pumphrey, H. C., Russell, J. M., and Waters, J. W.: An atmospheric tape recorder: The imprint of tropical tropopause temperatures on stratospheric water vapor, Journal of Geophysical Research, 101, 3989 – 4006, https://doi.org/10.1029/95JD03422, 1996.

Moyer, E. J., Irion, F. W., Yung, Y. L., and Gunson, M. R.: ATMOS stratospheric deuterated water and implications for troposphere-stratosphere transport, Geophysical Research Letters, 23, 2385 – 2388, https://doi.org/10.1029/96GL01489, 1996.

Munro, R. and Rodgers, C. D.: Latitudinal and season variations of water vapour in the middle atmosphere, Geophysical Research Letters, 21, 661 – 664, https://doi.org/10.1029/94GL00183, 1994.

Nassar, R., Bernath, P. F., Boone, C. D., Manney, G. L., McLeod, S. D., Rinsland, C. P., Skelton, R., and Walker, K. A.: Stratospheric abundances of water and methane based on ACE-FTS measurements, Geophysical Research Letters, 32, L15S05, https://doi.org/10.1029/2005GL022383, 2005.

Nedoluha, G. E., Bevilacqua, R. M., and Hoppel, K. W.: POAM III measurements of dehydration in the Antarctic and comparisons with the Arctic, Journal of Geophysical Research, 107, 8290, https://doi.org/10.1029/2001JD001184, 2002.

Nedoluha, G. E., Kiefer, M., Lossow, S., Gomez, R. M., Kämpfer, N., Lainer, M., Forkman, P., Christensen, O. M., Oh, J. J., Hartogh, P., Anderson, J., Bramstedt, K., Dinelli, B. M., Garcia-Comas, M., Hervig, M., Murtagh, D., Raspollini, P., Read, W. G., Rosenlof, K., Stiller, G. P., and Walker, K. A.: The SPARC water vapor assessment II: intercomparison of satellite and ground-based microwave measurements, Atmospheric Chemistry & Physics, 17, 14 543 – 14 558, https://doi.org/10.5194/acp-17-14543-2017, 2017.

Noël, S., Bramstedt, K., Rozanov, A., Bovensmann, H., and Burrows, J. P.: Water vapour profiles from SCIAMACHY solar occultation measurements derived with an onion peeling approach, Atmospheric Measurement Techniques, 3, 523 – 535, 2010.

Offermann, D., Schaeler, B., Riese, M., Langfermann, M., Jarisch, M., Eidmann, G., Schiller, C., Smit, H. G. J., and Read, W. G.: Water vapor at the tropopause during the CRISTA 2 mission, Journal of Geophysical Research, 107, 8176, https://doi.org/10.1029/2001JD000700, 2002.

Payne, V. H., Noone, D., Dudhia, A., Piccolo, C., and Grainger, R. G.: Global satellite measurements of HDO and implications for understanding the transport of water vapour into the stratosphere, Quarterly Journal of the Royal Meteorological Society, 133, 1459 – 1471, https://doi.org/10.1002/qj.127, 2007.

Pumphrey, H. C. and Harwood, R. S.: Water vapour and ozone in the mesosphere as measured by UARS MLS, Geophysical Research Letters, 24, 1399 – 1402, https://doi.org/10.1029/97GL01158, 1997.

Randall, C. E., Rusch, D. W., Bevilacqua, R. M., Hoppel, K. W., Lumpe, J. D., Shettle, E., Thompson, E., Deaver, L., Zawodny, J., Kyrö, E., Johnson, B., Kelder, H., Dorokhov, V. M., König-Langlo, G., and Gil, M.: Validation of POAM III ozone: Comparisons with ozonesonde and satellite data, Journal of Geophysical Research, 108, 4367, https://doi.org/10.1029/2002JD002944, 2003.

Read et al., W. G.: The SPARC water vapour assessment II: Comparisons of water vapour observed in the upper troposphere, in preparation.

Remsberg, E., Russell, J. M., Gordley, L. L., Gille, J. C., and Bailey, P. L.: Implications of the stratospheric water vapor distribution as determined from the Nimbus 7 LIMS experiment, Journal of the Atmospheric Sciences, 41, 2934 – 2948, 1984.

Rienecker, M. M., Suarez, M. J., Gelaro, R., Todling, R., Bacmeister, J., Liu, E., Bosilovich, M. G., Schubert, S. D., Takacs, L., Kim, G.-K., Bloom, S., Chen, J., Collins, D., Conaty, A., da Silva, A., Gu, W., Joiner, J., Koster, R. D., Lucchesi, R., Molod, A., Owens, T., Pawson, S., Pegion, P., Redder, C. R., Reichle, R., Robertson, F. R., Ruddick, A. G., Sienkiewicz, M., and Woollen, J.: MERRA: NASA's Modern-Era Retrospective Analysis for Research and Applications, Journal of Climate, 24, 3624 – 3648, https://doi.org/10.1175/JCLI-D-11-00015.1, 2011.

Riese, M., Ploeger, F., Rap, A., Vogel, B., Konopka, P., Dameris, M., and Forster, P.: Impact of uncertainties in atmospheric mixing on simulated UTLS composition and related radiative effects, Journal of Geophysical Research, 117, D16 305, https://doi.org/10.1029/2012JD017751, 2012.

Rind, D., Chiou, E.-W., Chu, W., Oltmans, S., Lerner, J., Larsen, J., McCormick, M. P., and McMaster, L.: Overview of the Stratospheric Aerosol and Gas Experiment II water vapor observations: Method, validation, and data characteristics, Journal of Geophysical Research, 98, 4835 – 4856, https://doi.org/10.1029/92JD01174, 1993.

Roche, A. E., Kumer, J. B., Mergenthaler, J. L., Ely, G. A., Uplinger, W. G., Potter, J. F., James, T. C., and Sterritt, L. W.: The Cryogenic Limb Array Etalon Spectrometer (CLAES) on UARS: Experiment description and performance, Journal of Geophysical Research, 98, 10 763 – 10 776, 1993.

Rong, P., Russell, J. M., Gordley, L. L., Hervig, M. E., Deaver, L., Bernath, P. F., and Walker, K. A.: Validation of v1.022 mesospheric water vapor observed by the SOFIE instrument on the AIM Satellite, Journal of Geophysical Research, 115, D16 209, https://doi.org/10.1029/2010JD013852, 2010.

Schmidt, H., Brasseur, G. P., Charron, M., Manzini, E., Giorgetta, M. A., Diehl, T., Fomichev, V. I., Kinnison, D., Marsh, D., and Walters, S.: The HAMMONIA chemistry climate model: Sensitivity of the mesopause region to the 11-year solar cycle and CO_2 doubling, Journal of Climate, 19, 3903 – 3931, https://doi.org/10.1175/JCLI3829.1, 2006.

Seele, C. and Hartogh, P.: Water vapor of the polar middle atmosphere: Annual variation and summer mesosphere conditions as observed by ground-based microwave spectroscopy, Geophysical Research Letters, 26, 1517 – 1520, https://doi.org/10.1029/1999GL900315, 1999.

Sioris, C. E., Zou, J., McElroy, C. T., McLinden, C. A., and Vömel, H.: High vertical resolution water vapour profiles in the upper troposphere and lower stratosphere retrieved from MAESTRO solar occultation spectra, Advances in Space Research, 46, 642 – 650, https://doi.org/10.1016/j.asr.2010.04.040, 2010.

Sioris, C. E., Malo, A., McLinden, C. A., and D'Amours, R.: Direct injection of water vapor into the stratosphere by volcanic eruptions, Geophysical Research Letters, 43, 7694 – 7700, https://doi.org/10.1002/2016GL069918, 2016.

Solomon, S.: Stratospheric ozone depletion: A review of concepts and history, Reviews of Geophysics, 37, 275 – 316, https://doi.org/10.1029/1999RG900008, 1999.

Sonnemann, G. R., Grygalashvyly, M., and Berger, U.: Autocatalytic water vapor production as a source of large mixing ratios within the middle to upper mesosphere, Journal of Geophysical Research, 110, D15 303, https://doi.org/10.1029/2004JD005593, 2005.

Stiller, G. P., Kiefer, M., Eckert, E., von Clarmann, T., Kellmann, S., García-Comas, M., Funke, B., Leblanc, T., Fetzer, E., Froidevaux, L., Gomez, M., Hall, E., Hurst, D., Jordan, A., Kämpfer, N., Lambert, A., McDermid, I. S., McGee, T., Miloshevich, L., Nedoluha, G., Read, W., Schneider, M., Schwartz, M., Straub, C., Toon, G., Twigg, L. W., Walker, K., and Whiteman, D. N.: Validation of MIPAS IMK/IAA temperature, water vapor, and ozone profiles with MOHAVE-2009 campaign measurements, Atmospheric Measurement Techniques, 5, 289 – 320, https://doi.org/10.5194/amt-5-289-2012, 2012a.

Stiller, G. P., von Clarmann, T., Haenel, F., Funke, B., Glatthor, N., Grabowski, U., Kellmann, S., Kiefer, M., Linden, A., Lossow, S., and López-Puertas, M.: Observed temporal evolution of global mean age of stratospheric air for the 2002 to 2010 period, Atmospheric Chemistry & Physics, 12, 3311 – 3331, https://doi.org/10.5194/acp-12-3311-2012, 2012b.

Summers, M. E., Gordley, L. L., and McHugh, M. J.: Discovery of a water vapor layer in the Arctic summer mesosphere: Implications for polar mesospheric clouds, Geophysical Research Letters, 28, 3601 – 3604, https://doi.org/10.1029/2001GL013217, 2001.

Taha, G., Thomason, L. W., and Burton, S. P.: Comparison of Stratospheric Aerosol and Gas Experiment (SAGE) II version 6.2 water vapor with balloon-borne and space-based instruments, Journal of Geophysical Research, 109, D18 313, https://doi.org/10.1029/2004JD004859, 2004.

Thomason, L. W., Moore, J. R., Pitts, M. C., Zawodny, J. M., and Chiou, E. W.: An evaluation of the SAGE III version 4 aerosol extinction coefficient and water vapor data products, Atmospheric Chemistry & Physics, 10, 2159 – 2173, 2010.

Urban, J., Lautié, N., Murtagh, D. P., Eriksson, P., Kasai, Y., Lossow, S., Dupuy, E., de La Noë, J., Frisk, U., Olberg, M., Le Flochmoën, E., and Ricaud, P.: Global observations of middle atmospheric water vapour by the Odin satellite: An overview, Planetary and Space Science, 55, 1093 – 1102, https://doi.org/10.1016/j.pss.2006.11.021, 2007.

von Clarmann, T., Höpfner, M., Kellmann, S., Linden, A., Chauhan, S., Funke, B., Grabowski, U., Glatthor, N., Kiefer, M., Schieferdecker, T., Stiller, G. P., and Versick, S.: Retrieval of temperature, H_2O, O_3, HNO_3, CH_4, N_2O, $ClONO_2$ and ClO from MIPAS reduced resolution nominal mode limb emission measurements, Atmospheric Measurement Techniques, 2, 159 – 175, 2009.

von Clarmann, T., Stiller, G., Grabowski, U., Eckert, E., and Orphal, J.: Technical Note: Trend estimation from irregularly sampled, correlated data, Atmospheric Chemistry & Physics, 10, 6737 – 6747, 2010.

Walker, K. A. and Stiller, G. P.: The SPARC water vapour assessment II: Data set overview, in preparation.

Waters, J. W., Froidevaux, L., Harwood, R. S., Jarnot, R. F., Pickett, H. M., Read, W. G., Siegel, P. H., Cofield, R. E., Filipiak, M. J., Flower, D. A., Holden, J. R., Lau, G. K., Livesey, N. J., Manney, G. L., Pumphrey, H. C., Santee, M. L., Wu, D. L., Cuddy, D. T., Lay, R. R., Loo, M. S., Perun, V. S., Schwartz, M. J., Stek, P. C., Thurstans, R. P., Boyles, M. A., Chandra, K. M., Chavez, M. C., Chen, G.-S., Chudasama, B. V., Dodge, R., Fuller, R. A., Girard, M. A., Jiang, J. H., Jiang, Y., Knosp, B. W., Labelle, R. C., Lam, J. C., Lee, A. K., Miller, D., Oswald, J. E., Patel, N. C., Pukala, D. M., Quintero, O., Scaff, D. M., Vansnyder, W., Tope, M. C., Wagner, P. A., and Walch, M. J.: The Earth Observing System Microwave Limb Sounder (EOS MLS) on the Aura Satellite, IEEE Transactions on Geoscience and Remote Sensing, 44, 1075 – 1092, https://doi.org/10.1109/TGRS.2006.873771, 2006.

Weigel, K., Rozanov, A., Azam, F., Bramstedt, K., Damadeo, R., Eichmann, K.-U., Gebhardt, C., Hurst, D., Kraemer, M., Lossow, S., Read, W., Spelten, N., Stiller, G. P., Walker, K. A., Weber, M., Bovensmann, H., and Burrows, J. P.: UTLS water vapour from SCIAMACHY limb measurements V3.01 (2002-2012), Atmospheric Measurement Techniques, 9, 133 – 158, https://doi.org/10.5194/amt-9-133-2016, 2016.

Wetzel, G., Oelhaf, H., Berthet, G., Bracher, A., Cornacchia, C., Feist, D. G., Fischer, H., Fix, A., Iarlori, M., Kleinert, A., Lengel, A., Milz, M., Mona, L., Müller, S. C., Ovarlez, J., Pappalardo, G., Piccolo, C., Raspollini, P., Renard, J.-B., Rizi, V., Rohs, S., Schiller, C., Stiller, G., Weber, M., and Zhang, G.: Validation of MIPAS-ENVISAT H_2O operational data collected between July 2002 and March 2004, Atmospheric Chemistry & Physics, 13, 5791 – 5811, https://doi.org/10.5194/acp-13-5791-2013, 2013.

Wrotny, J. E., Nedoluha, G. E., Boone, C., Stiller, G. P., and McCormack, J. P.: Total hydrogen budget of the equatorial upper stratosphere, Journal of Geophysical Research, 115, D04 302, https://doi.org/10.1029/2009JD012135, 2010.

Table 1. Overview over the water vapour data sets from satellites used in this study.

Instrument	Data set	Label	Number
ACE-FTS	v2.2	ACE-FTS v2.2	1
	v3.5	ACE-FTS v3.5	2
GOMOS	LATMOS v6	GOMOS	3
HALOE	v19	HALOE	4
HIRDLS	v7	HIRDLS	5
ILAS-II	v3/3.01	ILAS-II	6
MAESTRO	Research	MAESTRO	7
MIPAS	Bologna V5H v2.3 NOM	MIPAS-Bologna V5H	8
	Bologna V5R v2.3 NOM	MIPAS-Bologna V5R NOM	9
	Bologna V5R v2.3 MA	MIPAS-Bologna V5R MA	10
	ESA V5H v6 NOM	MIPAS-ESA V5H	11
	ESA V5R v6 NOM	MIPAS-ESA V5R NOM	12
	ESA V5R v6 MA	MIPAS-ESA V5R MA	13
	ESA V7R v7 NOM	MIPAS-ESA V7R	14
	IMKIAA V5H v20 NOM	MIPAS-IMKIAA V5H	15
	IMKIAA V5R v220/221 NOM	MIPAS-IMKIAA V5R NOM	16
	IMKIAA V5R v522 MA	MIPAS-IMKIAA V5R MA	17
	Oxford V5H v1.30 NOM	MIPAS-Oxford V5H	18
	Oxford V5R v1.30 NOM	MIPAS-Oxford V5R NOM	19
	Oxford V5R v1.30 MA	MIPAS-Oxford V5R MA	20
MLS	v4.2	MLS	21
POAM III	v4	POAM III	22
SAGE II	v7.00	SAGE II	23
SAGE III	Solar occultation v4	SAGE III	24
SCIAMACHY	Limb v3.01	SCIAMACHY limb	25
	Lunar occultation v1.0	SCIAMACHY lunar	26
	Solar occultation - OEM v1.0	SCIAMACHY solar OEM	27
	Solar occultation - Onion peeling v4.2.1	SCIAMACHY solar Onion	28
SMILES	NICT v2.9.2 band A	SMILES-NICT band A	29
	NICT v2.9.2 band B	SMILES-NICT band B	30
SMR	v2.0 544 GHz	SMR 544 GHz	31
	v2.1 489 GHz	SMR 489 GHz	32
SOFIE	v1.3	SOFIE	33

Table 2. The convolution classes. Based on these differences in the vertical resolution were considered in the comparisons of the data sets. The first four classes consider resolution differences around the hygropause while class V addresses differences at the stratopause and lower mesosphere. Data sets marked by a asterisk have a limited coverage of the hygropause. The consideration of differences in the vertical resolution in comparisons to these data sets may be not necessary, but has been performed just in case.

class I **data sets**	**class II** **data sets**	**class III** **data sets**	**class IV** **data sets**	**class V** **data sets**
$\mathrm{dz} \leq 1.6\,\mathrm{km}$	$1.6\,\mathrm{km} < \mathrm{dz} \leq 3.0\,\mathrm{km}$	$3.0\,\mathrm{km} < \mathrm{dz} \leq 4.5\,\mathrm{km}$	$\mathrm{dz} > 4.5\,\mathrm{km}$	$\mathrm{dz} > 6.0\,\mathrm{km}$ (above $1\,\mathrm{hPa}$)
HIRDLS	GOMOS	ACE-FTS v2.2	SCIAMACHY limb	MIPAS-Bologna V5H
ILAS-II	HALOE	ACE-FTS v3.5	SCIAMACHY lunar*	MIPAS-Bologna V5R NOM
MAESTRO	MIPAS-ESA V5R NOM	MIPAS-Bologna V5H	SMILES-NICT band A	MIPAS-Bologna V5R MA
POAM III	MIPAS-ESA V5R MA*	MIPAS-Bologna V5R NOM	SMILES-NICT band B	MIPAS-ESA V5H
SAGE II	MLS	MIPAS-Bologna V5R MA*	SMR 544 GHz	MIPAS-ESA V7R
SAGE III		MIPAS-ESA V5H	SMR 489 GHz*	MIPAS-IMKIAA V5H
SOFIE*		MIPAS-ESA V7R		MIPAS-IMKIAA V5R NOM
		MIPAS-IMKIAA V5H		MIPAS-Oxford V5H
		MIPAS-IMKIAA V5R NOM		MIPAS-Oxford V5R NOM
		MIPAS-IMKIAA V5R MA*		SCIAMACHY solar OEM
		MIPAS-Oxford V5H		
		MIPAS-Oxford V5R NOM		
		MIPAS-Oxford V5R MA*		
		SCIAMACHY solar OEM		
		SCIAMACHY solar Onion		

Table 3: Sources and characteristics of the convolution data used in the comparisons.

Data set	Source of convolution data	log space	vmr or density	zero a priori
ACE-FTS v2.2	set of generated kernels and a priori data vertical resolution of 3.5 km	no	vmr	yes
ACE-FTS v3.5	set of generated kernels and a priori data vertical resolution of 3.5 km	no	vmr	yes
GOMOS-LATMOS	set of generated kernels and a priori data vertical resolution: z $\leq$ 20 km: 2 km, z $\geq$ 30 km: 4 km	no	vmr	yes
HALOE	set of generated kernels and a priori data vertical resolution of 2.5 km	no	vmr	yes
MIPAS-Bologna V5H	complete set of original kernels and a priori data	no	vmr	no
MIPAS-Bologna V5R NOM	complete set of original kernels and a priori data	no	vmr	no
MIPAS-Bologna V5R MA	complete set of original kernels and a priori data	no	vmr	no
MIPAS-ESA V5H	complete set of original kernels and a priori data	no	vmr	yes
MIPAS-ESA V5R NOM	complete set of original kernels and a priori data	no	vmr	yes
MIPAS-ESA V5R MA	complete set of original kernels and a priori data	no	vmr	yes
MIPAS-ESA V7R	complete set of original kernels and a priori data	no	vmr	yes
MIPAS-IMKIAA V5H	complete set of original kernels and a priori data	yes	vmr	yes
MIPAS-IMKIAA V5R NOM	complete set of original kernels and a priori data	yes	vmr	yes
MIPAS-IMKIAA V5R MA	complete set of original kernels and a priori data	yes	vmr	no
MIPAS-Oxford V5H	set of generated kernels and a priori data vertical resolution: p$\geq$ 425 hPa: 2 km, p = 200 hPa: 4 km, p = 3 hPa: 4 km, p = 0.1 hPa: 10 km, p $\leq$ 0.01 hPa: 15 km	no	vmr	yes
MIPAS-Oxford V5R NOM	set of characteristic kernels and corresponding a priori data one kernel per 3 months and 5 latitude bands (90°S – 60°S, 60°S – 20°S, 20°S – 20°N, 20°N – 60°N, 60°N – 90°N)	yes	vmr	no
MIPAS-Oxford V5R MA	set of generated kernels and a priori data vertical resolution: p$\geq$ 250 hPa: 3 km, p = 100 hPa: 4 km, p = 1 hPa: 4 km, p = 0.1 hPa: 5 km, p $\leq$ 0.01 hPa: 6 km	no	vmr	yes
MLS	one characteristic kernel, complete set of a priori data	yes	vmr	no

SCIAMACHY limb	complete set of original kernels and a priori data	yes	density	no
SCIAMACHY lunar	one characteristic kernel, complete set of a priori data	yes	density	no
SCIAMACHY solar OEM	one characteristic kernel, complete set of a priori data	yes	density	no
SCIAMACHY solar Onion	set of generated kernels and a priori data vertical resolution of 4.1 km	no	vmr	yes
SMILES-NICT band A	set of generated kernels and a priori data vertical resolution varies, given in the data files	no	vmr	yes
SMILES-NICT band B	set of generated kernels and a priori data vertical resolution varies, given in the data files	no	vmr	yes
SMR 544 GHz	set of characteristic kernels and corresponding a priori data one kernel per month, 20°latitude band and 1 km tropopause height interval	yes	vmr	no
SMR 489 GHz	set of characteristic kernels and corresponding a priori data one kernel per month and 20°latitude band	no	vmr	no

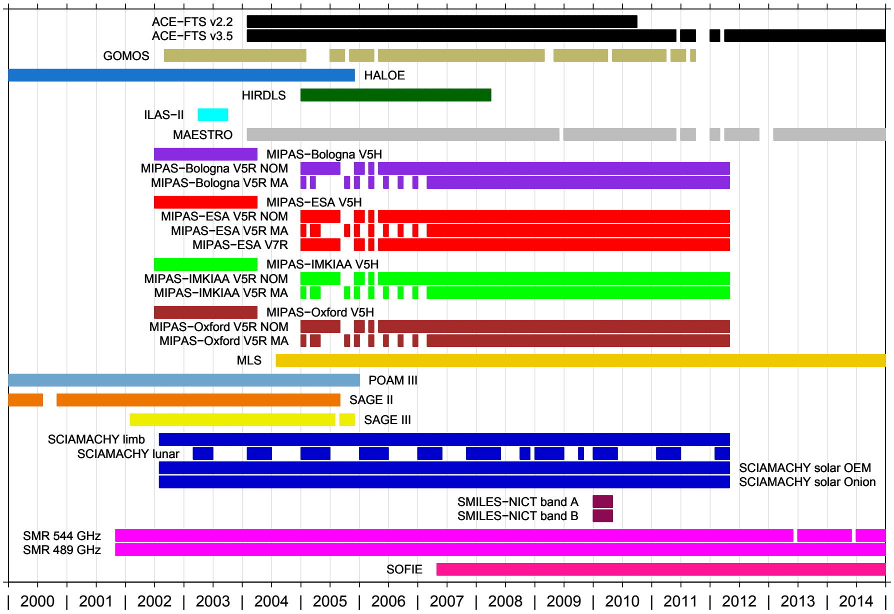

Figure 1. The data sets that were included in the comparisons and their corresponding time coverage on a monthly basis. Only data obtained since 2000 are considered.

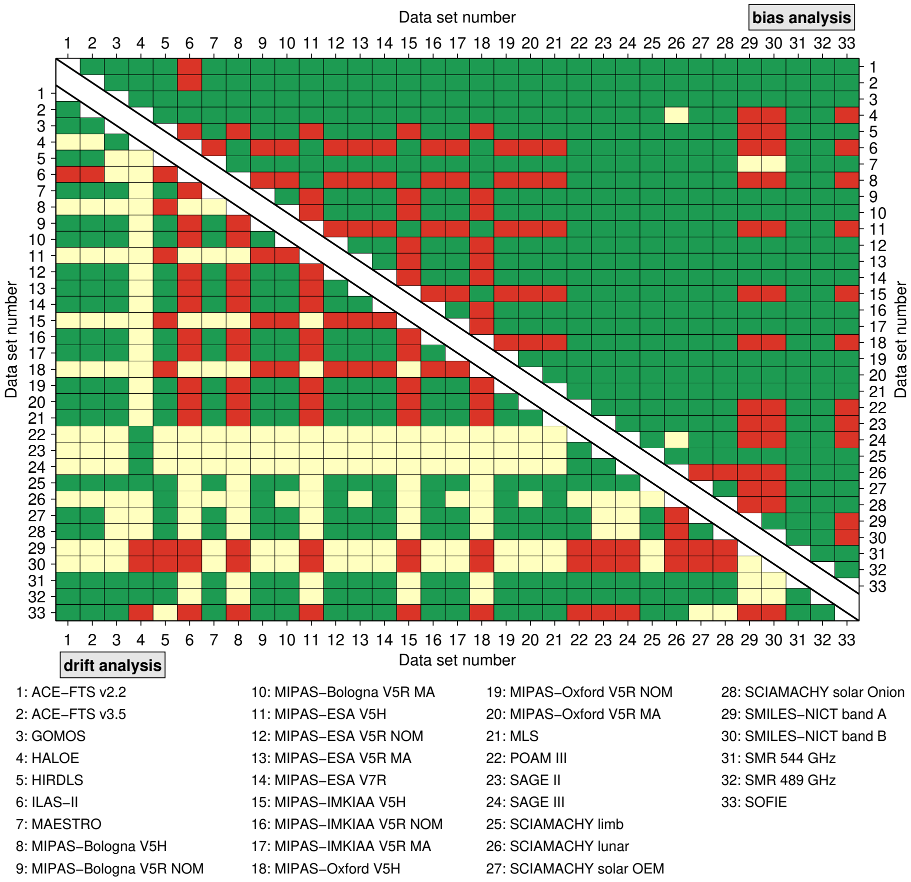

Figure 2. Overview which data sets where compared with each other in terms of biases (upper triangle) and drifts (lower triangle). Green means that comparisons were performed while red indicates that this was not the case. Yellow means that comparisons were performed but the results were not considered any further since they did not meet the minimum criteria we defined in Sect. 3. For the bias comparisons this concerns the minimum number of coincidences (i.e. 20, see Sect. 3.3), while for the drift comparisons this involves the minimum overlap period (i.e. 36 months, see Sect. 3.4).

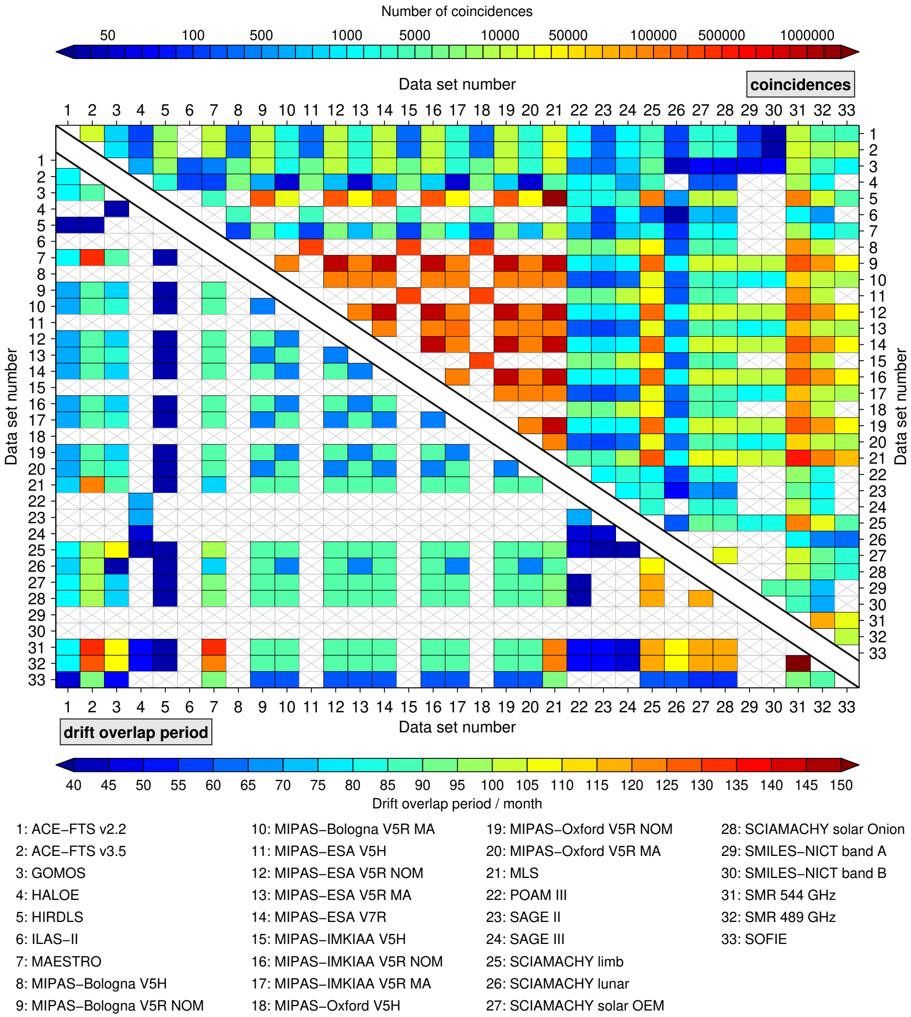

Figure 3. Overview on the number of coincidences (upper triangle) and the drift overlap period (lower triangle) between the compared data sets. All numbers consider the comparisons that take into account coincidences during all seasons and at all latitudes. White boxes with grey crosses indicate that no comparison results are available (either yellow or red in Fig. 2).

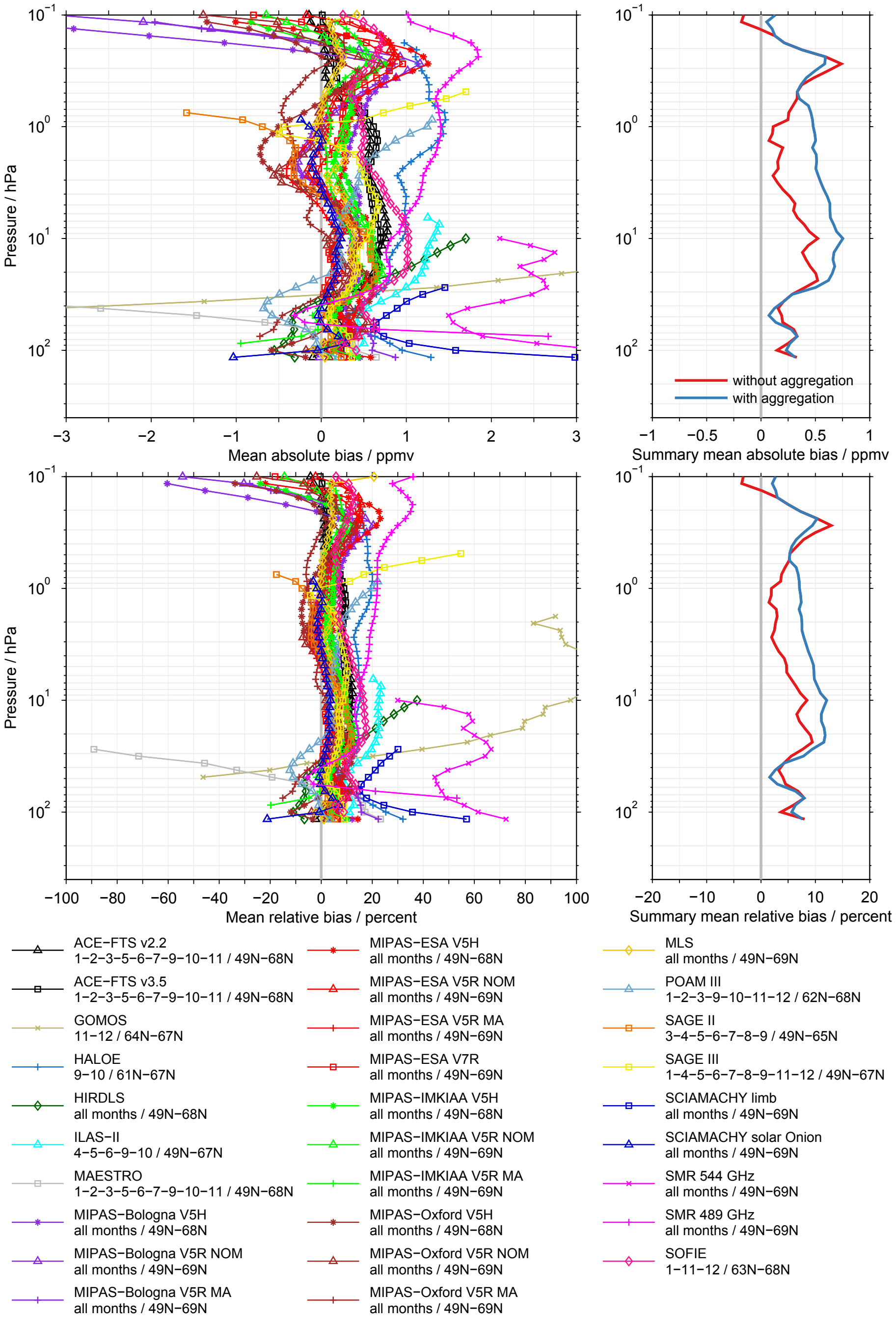

Figure 4. Biases of the SCIAMACHY solar OEM data set in absolute (upper panel) and relative terms (lower panel). These example results are based on coincident observations during all seasons and at all latitudes. The left panel shows the mean biases to the individual data sets, as listed in the legend. In addition, the legend provides information on the temporal and spatial coverage of the individual comparisons. The right panels provides a summary of the bias results shown in the left panels. The red profile is based on the median over all comparisons, while the blue profile considers the aggregation of MIPAS results as described in Sect. 3.5. The latter profile is used in Sect 4.3 and in the Supplement to summarise the bias results for the individual data sets. For better visibility only results at every second altitude are plotted (see Sect. 3.3).

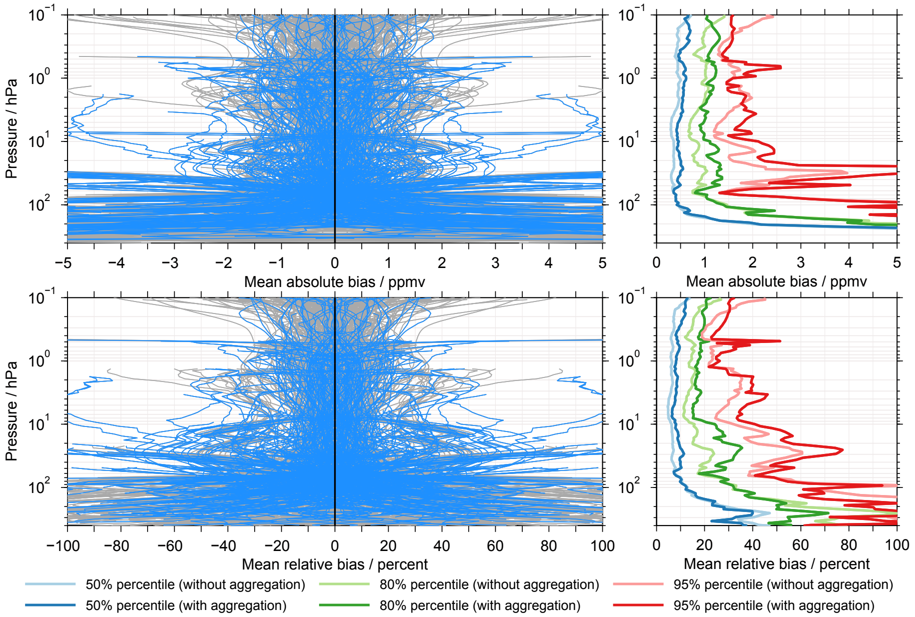

Figure 5. Left ~~panel~~panels: Bias results for the full matrix of comparisons considering coincidences during all seasons and at all latitudes. The upper panel shows the absolute biases, the lower panel the relative biases. The grey profiles do not consider the aggregation of the MIPAS results while the light blue profiles do. Right ~~panel~~panels: The 50% (median), 80% and 95% percentiles derived from the positive part of the biases shown in the left panels, with and without the aggregation of the MIPAS results.

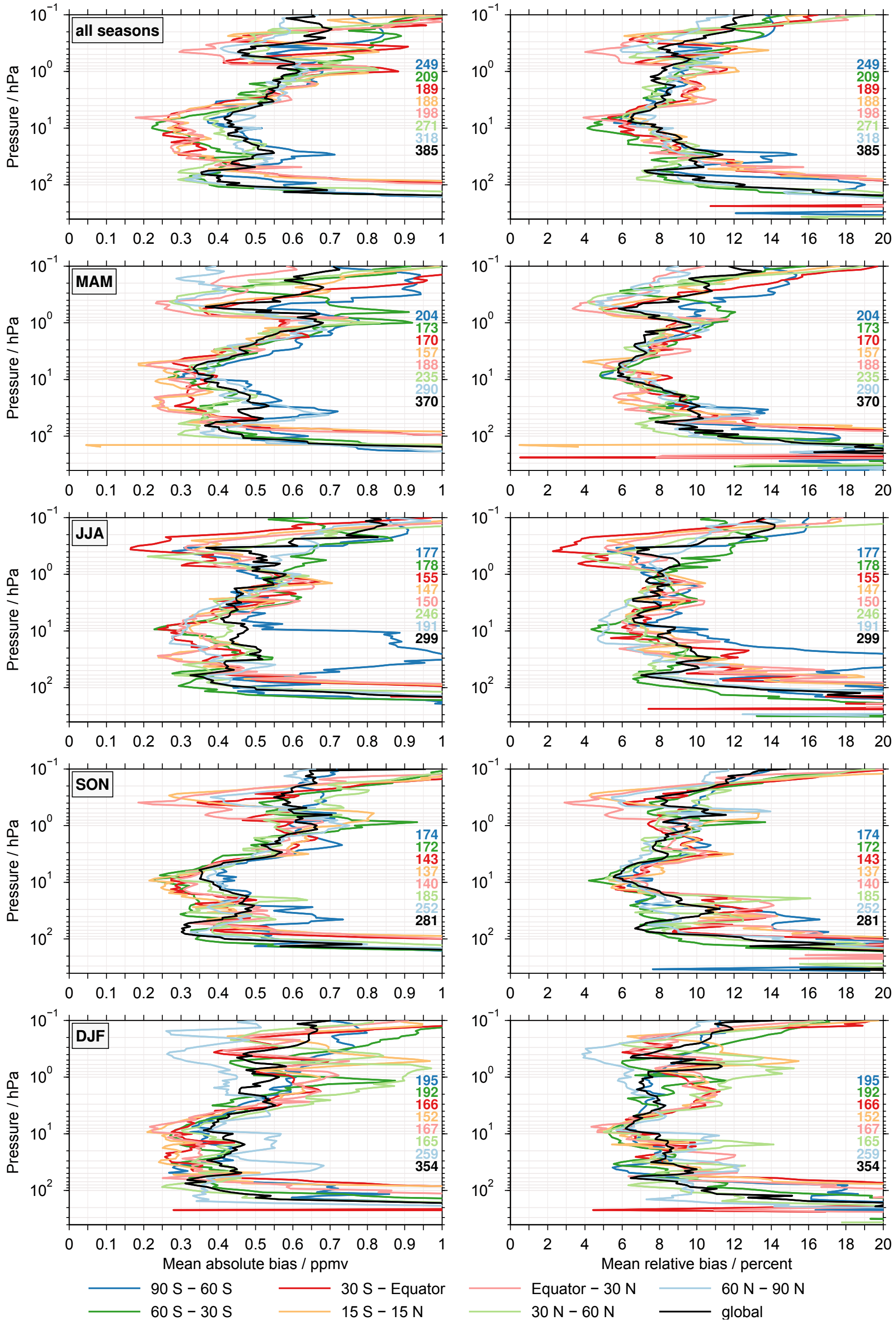

Figure 6. The 50% percentile (median) of the biases from all available comparisons for different times and latitude bands, considering the aggregation of the MIPAS results. The left column considers the absolute biases, the right column the relative biases. The different rows focus on individual seasons or their combination. The results for the different latitude bands are colour-coded. On the right-hand side of the individual panels the number of comparisons contributing to the results are indicated. Here, the comparisons to the different MIPAS data sets are counted individually and not combined into a single comparison.

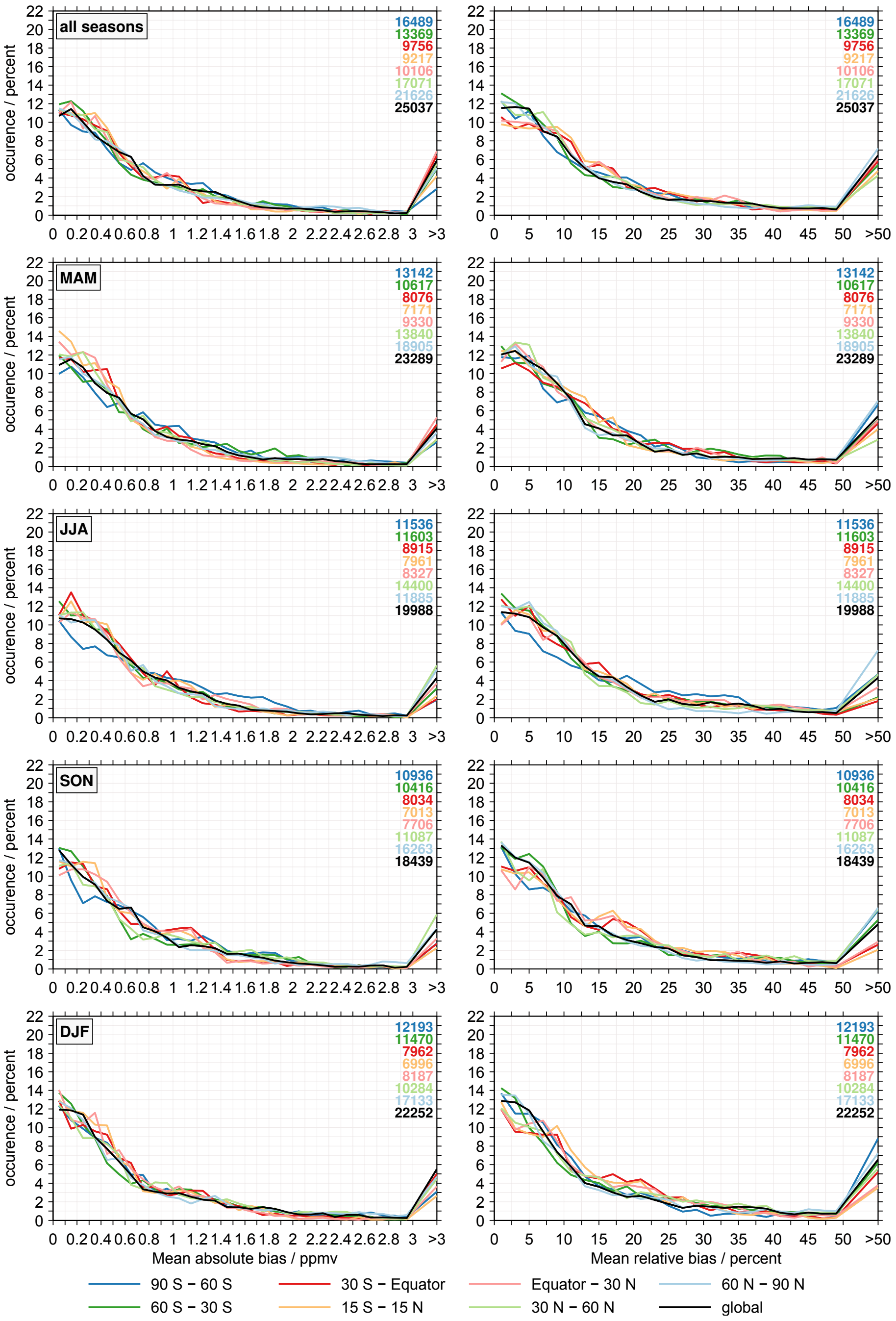

Figure 7. Histograms of the absolute (left column) and relative biases (right column) considering results from the entire altitude range. As in the previous figure the different rows consider different seasons while the different latitude bands are colour-coded in the individual panels. Also, these histograms take into consideration the aggregation of the MIPAS results. The increase at the right end of the panes comes from the integration over all biases larger than 3 ppmv and 50%, respectively.

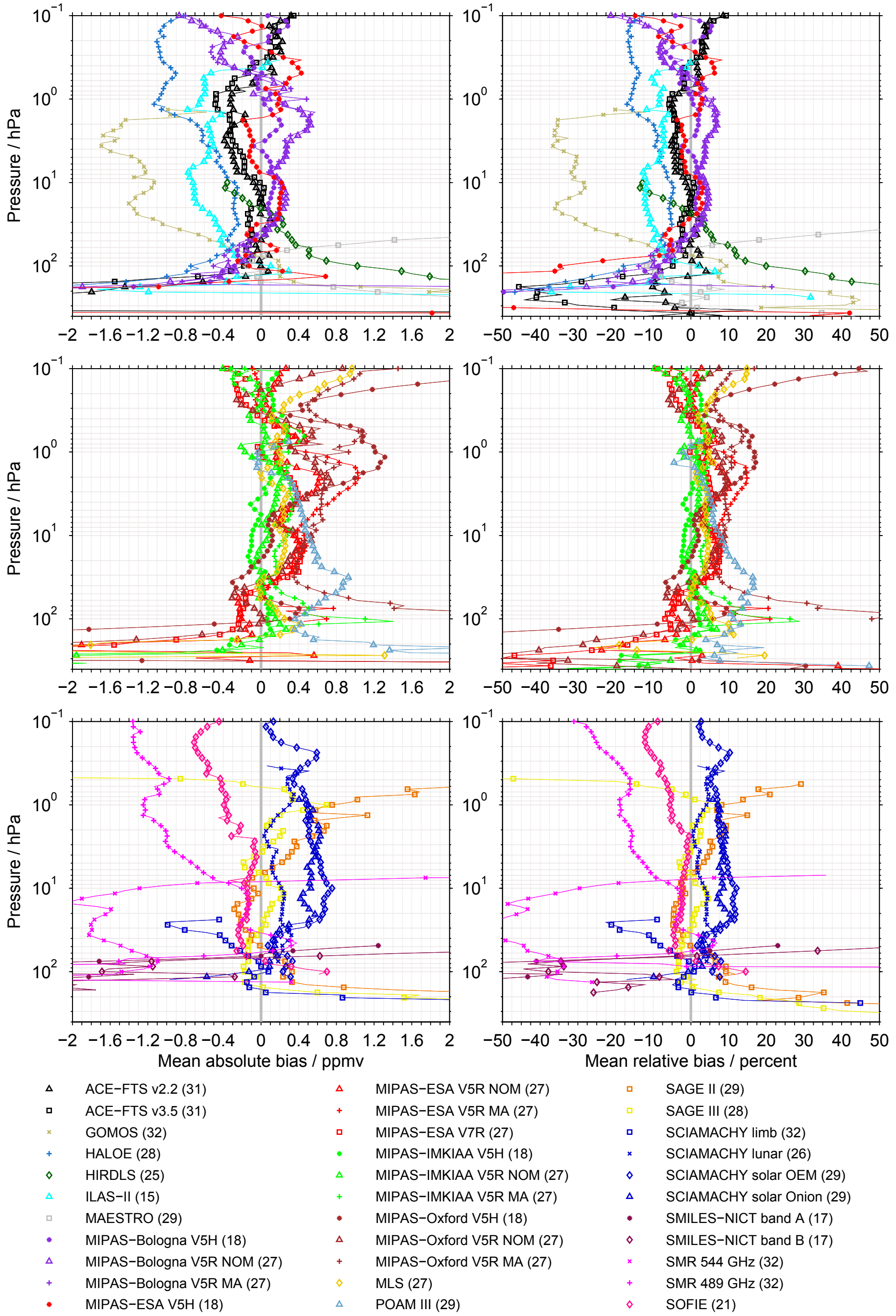

Figure 8. A bias summary for all data sets. This summary is based on the comparisons that considers coincidences during all seasons and at all latitudes and takes into account the aggregation of the MIPAS results (see Sect. 3.5). Absolute biases are shown in the left column, relative biases in the right column. For the sake of better visibility the results have been split among three rows. The separation is also reflected by the legend columns. In the legend also the number of comparisons contributing to the summary for the individual data sets is indicated.

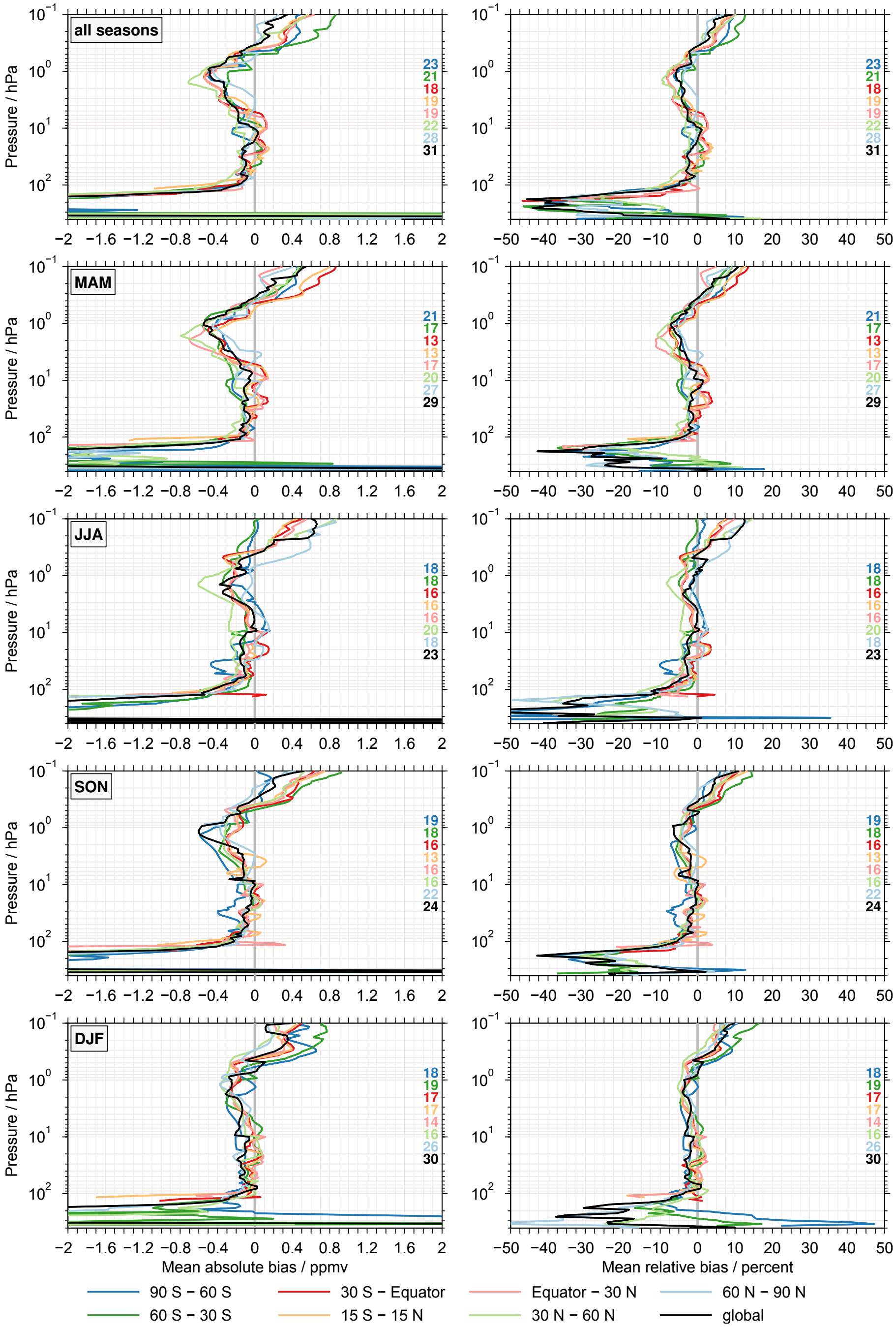

Figure 9. Bias summary for the ACE-FTS v3.5 data set. The left column considers the absolute biases and the right column the relative biases. As in Fig. 6 and 7 the different rows focus on the results for different seasons or their combination. In the individual panels on the right the number of comparisons contributing to the summary are indicated. As described in Sect. 3.5 the number of comparisons to the different MIPAS data sets are counted individually, even though these results are aggregated.

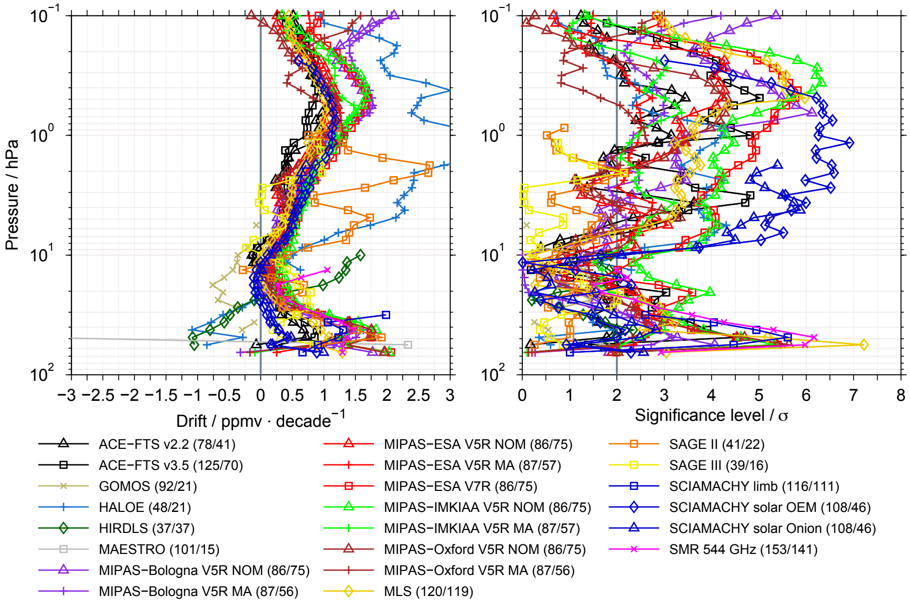

Figure 10. The left panel shows the drift of the SMR 489 GHz data set relative to other data sets. In the right panel the corresponding significance level of the drift estimates are shown. This example considers the latitude band between 30°N and 60 °N. In the legend the first number indicates the maximum overlap period in terms of months (over all altitudes) of the two data sets compared, i.e. the time between the first and the last month sufficient coincidences were found between the two data sets. The second number indicates during how many months both data sets actually yield sufficient coincidences, again represented by the maximum over all altitudes. As in Fig. 4 only results at every second altitude are plotted for better visibility.

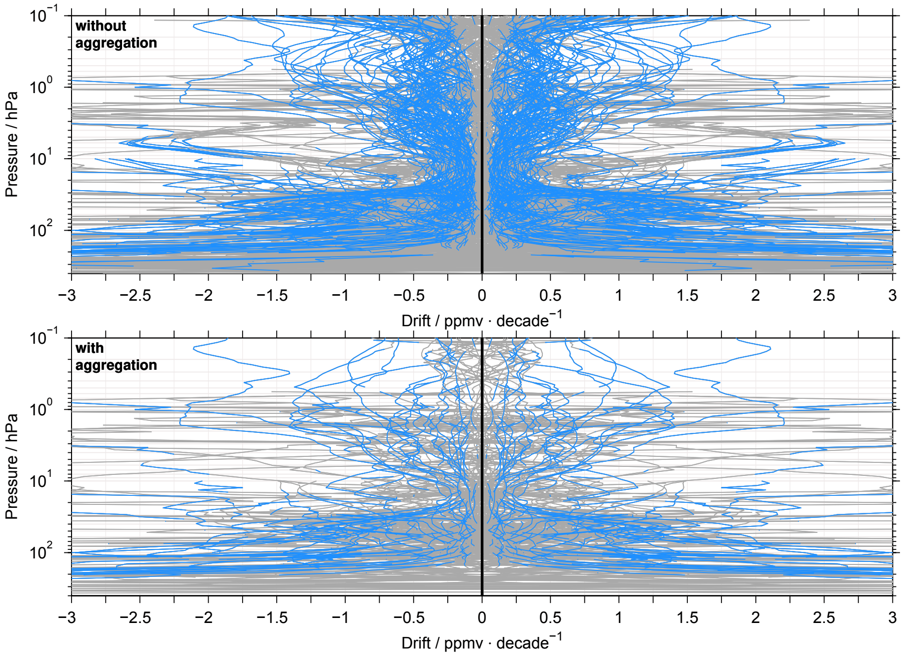

Figure 11. Drift results for the full matrix of comparisons considering coincident observations during all seasons and at all latitudes. Drifts that are statistically significant at the 2σ uncertainty level are marked in light blue. The upper panel shows the picture without the aggregation of the MIPAS results while the lower panel considers this aggregation.

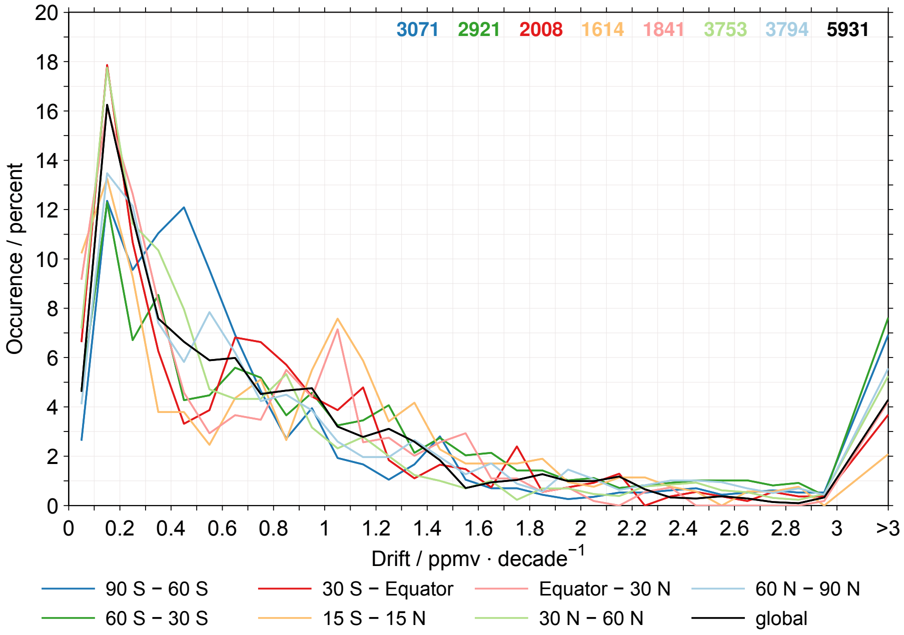

Figure 12. Drift histograms using estimates from all altitudes and taking into account the aggregation of the MIPAS results. Only positive drifts and those that are statistically significant at the 2σ uncertainty level are considered in the calculation. The results for the different latitude bands are given by the different colours. In the upper right corner the number of available data points is indicated, counting comparisons to different MIPAS data sets individually.

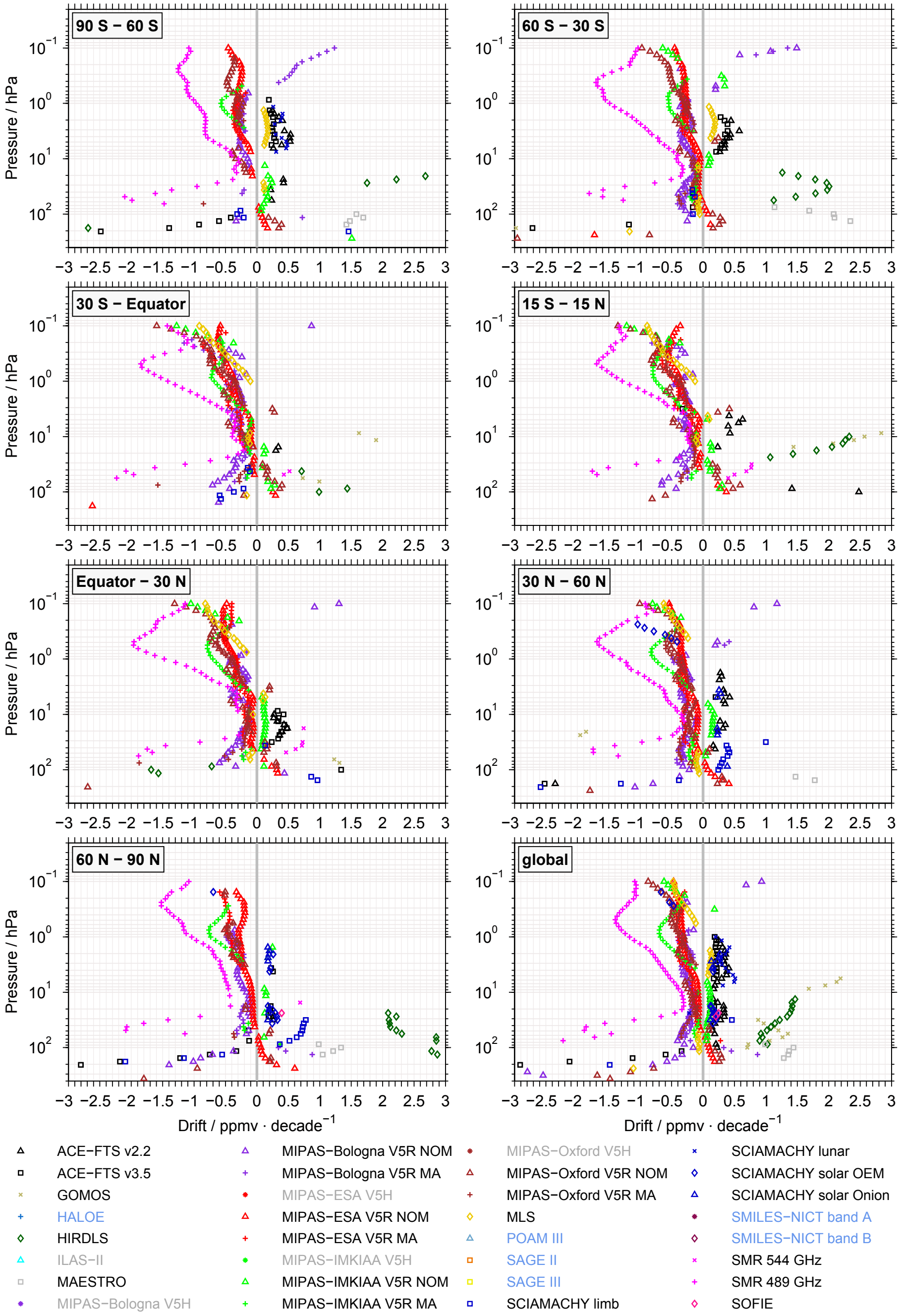

Figure 13. Drift summary for the MIPAS-ESA v7 data set. The summary shows only drifts that are statistically significant at the 2σ uncertainty level and only results at every second altitude are plotted (as in Figs. 4 and 10). The different panels consider the results for different latitude bands.The legend lists all possible data sets. Different colours convey additional information which results the different data sets contribute, as described in Sect. 5.3.

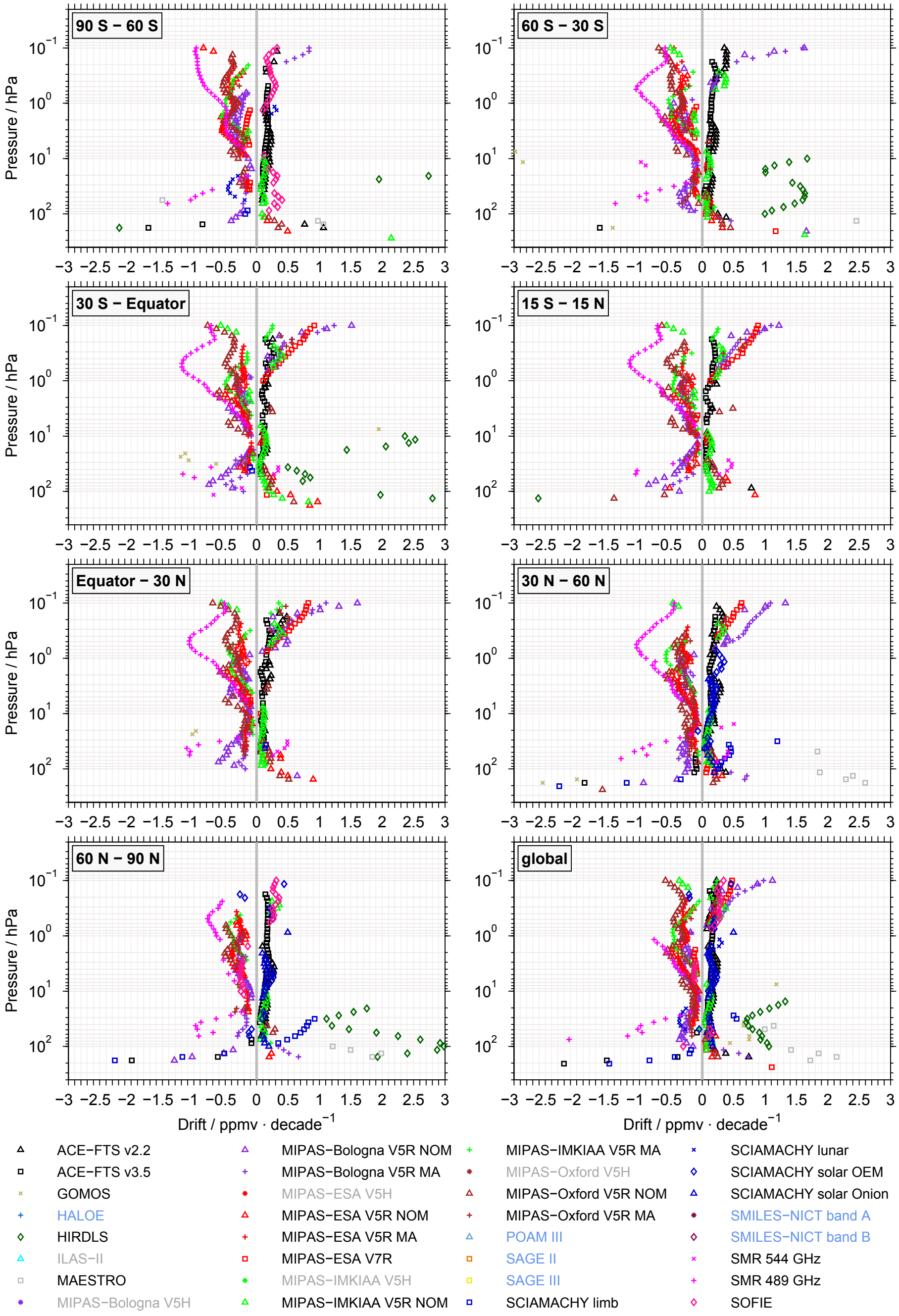

Figure 14. As Fig. 13 but here considering the MLS data set.

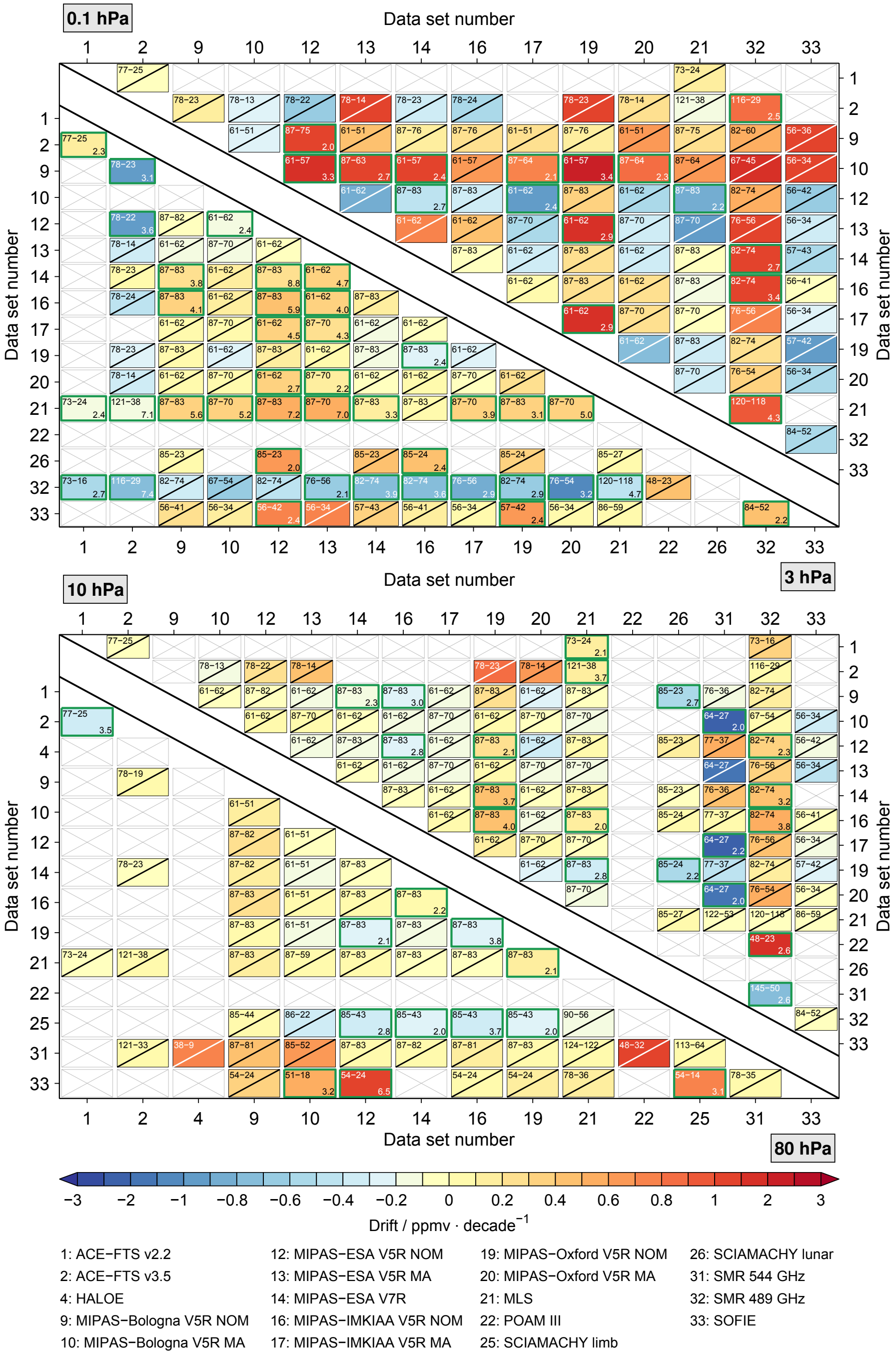

Figure 15. Drifts between the different data sets in the latitude band between 80°S and 70°S at 80 hPa, 10 hPa, 3 hPa and 0.1 hPa. The drift estimates are based on the difference time series between the data sets given at the x-axis and the data sets given at the y-axis. Data sets are only shown if they yield any result at a given altitude. Besides the colour-coded drift estimates the result boxes contain additional information. In the upper left the overlap period of the two data sets is given first. The second number indicates how many months the data sets actually overlap. If a drift is not significant at the 2σ uncertainty level this is marked by a slant. In contrast, if a drift is significant this is marked by a green frame and the significance level is noted in the lower right corner.

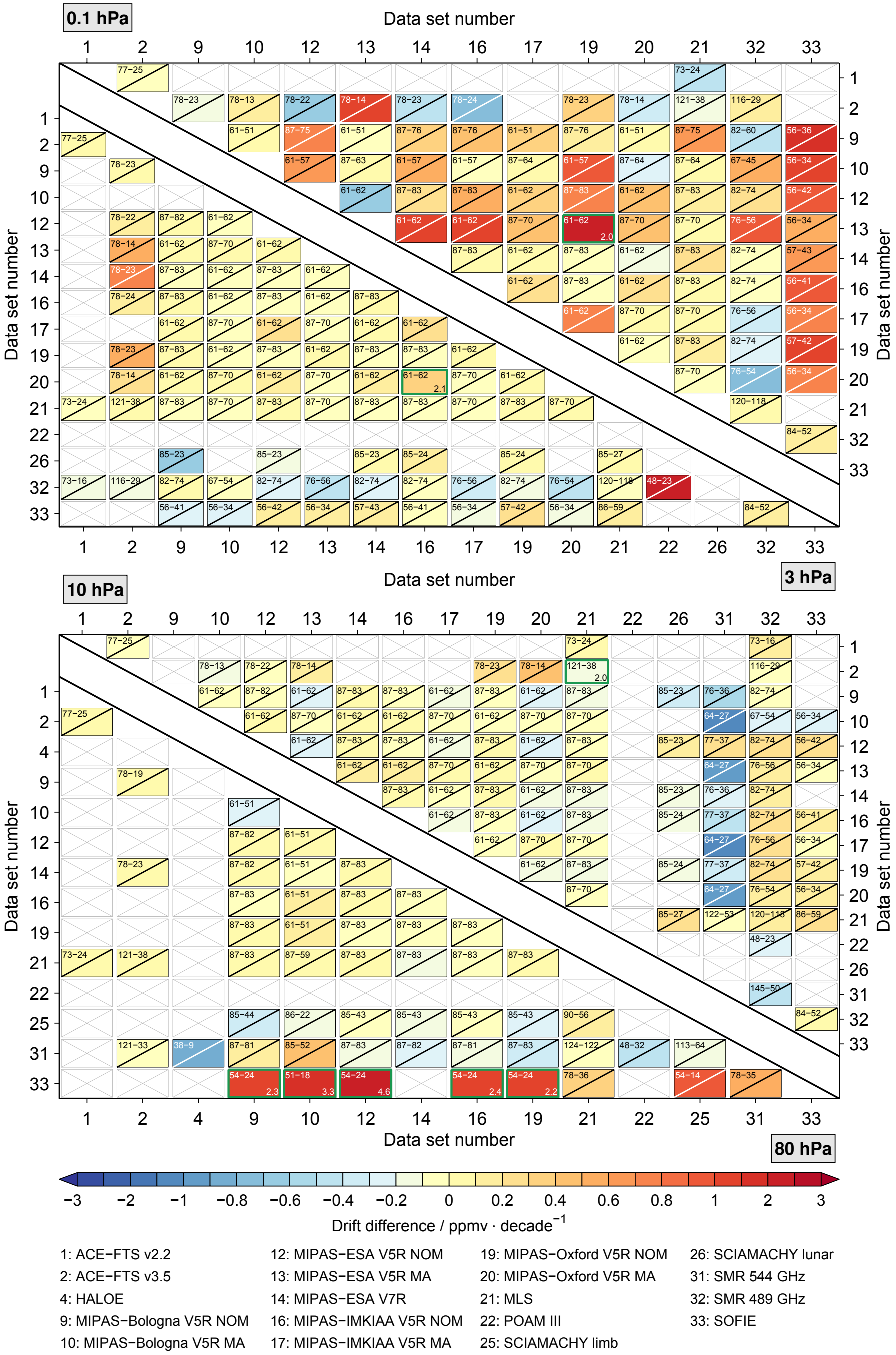

Figure 16. As Fig. 15, but here the differences between the drift estimates derived from the profile-to-profile comparisons and those obtained from the comparisons of zonal mean time series (see Eq. 13) are shown. The characteristic numbers in the result boxes correspond to the profile-to-profile comparisons. Typically they are not the same for the comparisons of zonal mean time series and, thus, are just displayed for guidance. Differences not statistically significant at the 2σ uncertainty level (see Eq. 14) are marked by a slant, otherwise the significance level is again indicated in the lower right corner.